Arctic sea ice altimetry - advances and current uncertainties

Marta Ewa Zygmuntowska

Dissertation for the degree philosophiae doctor (PhD)
at the University of Bergen

2014

Dissertation date: June 11

Dla
Mamy i Taty

Acknowledgements

I would like to thank my supervisors Stein Sandven and Frank Nilsen for giving me the opportunity to do this work in the first place. Thanks are also due to Lars Henrik Smedsrud who took the lead in my supervisor team after two years, speeded up my work when this was urgently needed and was a great support through the rest of the time! I would also like to express my sincere gratitude to my co-supervisor Kirill Khvorostovsky, who was in particularly a big help in the beginning, when I didn't know how to start this work and at the end, when I didn't know how to finish.
In addition, I would particularly like to thank Pierre Rampal: Pierre, it was a real pleasure working and learning from you. This work would not have been possible without your advice and encouragement!
I am also grateful to my colleagues at the Nansen Center, particularly Laurent Bertino for his advice on my statistical methods, Natalia Ivanova for all her support and discussions (all of them :-)), Hanne Sagen (and Frank again!) for bringing me along on her cruises, Tim and Richard for language corrections, Mohamed for his wise words and my office mates Linling and particularly Svetlana for supporting me in the last months and weeks. And Torge, thanks for reminding me about the joy in life every single day.

Scientific environment

The work in this PhD study has been carried out at the Nansen Environmental and Remote Sensing Center, Bergen. The work was funded by the Norwegian Research Council through the CISAR project 'CryoSat land and sea ice studies in the Arctic' no. 202313/V30 and by the Trond Mohn donation (from January 2014).

Besides the work on sea ice altimetry, which is highlighted in this thesis, I contributed to several field campaigns on Arctic sea ice with the Norwegian Polar Institute (2011/3, PRODEX project), the Nansen Environmental and Remote Sensing Center (2011/9, 8/2012, ACOBAR and WIFAR projects) and University Center in Svalbard (2012/3, 2012/9, supervision of fieldwork during bachelor/master courses 'Air-Sea-Ice-inetraction I&II'). Additionally, cooperation was established with the University in Hamburg, where I spend 4 weeks in June 2013 to work on the synergy of sea ice thickness retrievals from SMOS and CryoSat-2. The research stay was funded by the Norwegian Research School in Climate Dynamics (ResClim).

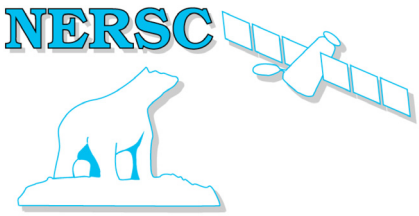

Abstract

One of the most prominent features of global climate change is the reduction in Arctic sea ice thickness. The main tool to derive sea ice thickness on an Arctic wide scale is altimetry from satellites, yet current estimates are associated with high uncertainties. In this thesis we present a new quantification of uncertainties in Arctic sea ice thickness and volume and identify the main sources of uncertainty. Furthermore, we explore the possibility for sea ice classification based on data from radar altimeters, which can be used to improve current estimates of sea ice thickness.

We quantify uncertainties in Arctic sea ice thickness and volume using freeboard retrievals from ICESat and investigate different assumptions on snow depth, sea ice density and area. These geophysical parameters are needed when converting freeboard measurements from altimeters in estimates of sea ice thickness and volume. We show that these parameters have an influence on the overall mean, the year-to-year variability, and the longterm trends. The overall uncertainties appear larger than previous studies suggest, and the recent dramatic ice loss appears smaller. We find the total uncertainty in sea ice volume to be around 13% during the cold season. Uncertainties in ice area are of minor importance for the estimates of sea ice volume and thickness. The uncertainty in snow depth contributes up to 70% of the total uncertainty, and the ice density up to 30–35%.

We analyze radar altimeter data over different Arctic sea ice regimes to develop a method for sea ice classification for CryoSat-2. Information about sea ice type is needed to be able to use ice type dependent values for snow and ice properties while converting freeboard into thickness. CryoSat's payload instrument is the SAR/Interferometric Radar Altimeter (SIRAL), which uses the synthetic aperture radar (SAR) technique to enhance the resolution along track. First we present a case study based on data from the airborne synthetic aperture radar ASIRAS, which is a replica of SIRAL on-board CryoSat-2. We analyze different parameters that characterize the radar signal waveforms and identify parameters that are most sensitive to sea ice type. With a bayesian based method we are able to classify more than 80% of the signal waveforms correctly as First- or Multi-Year-Ice. In the final step we analyze signal waveforms from CryoSat-2 on an Arctic wide scale. We find several of the waveform parameters to be significantly different over First- and Multi-Year-Ice. Analyzing the spatial distribution, some discrepancies occur compared to other retrievals of sea ice type. CryoSat-2 waveform parameters have values typical for Multi-Year-Ice over large areas of First-Year-Ice. These areas of First-Year-Ice contain strong gradients in drift speed, indicating that the radar signal is mainly sensitive to surface roughness. The information about surface roughness can potentially be used to remove biases in current freeboard retrievals from CryoSat-2.

Contents

Chapter 1

Scientific background and motivation for this study

This chapter is divided in four sections. In the first two sections I present a general overview about the role of Arctic sea ice in the climate system and about changes in Arctic sea ice during the last decades. The third section briefly describes the concept of sea ice altimetry and its limitations. In the last section I give further technical details on the processing of radar altimeter signals.

1.1 Role of sea ice in the climate system

Arctic sea ice is an important component of the global climate system as it keeps the Arctic region cool and helps moderate global temperatures. During the dark cold winter it insulates the warm ocean from the cold atmosphere and therefore reduces the release of heat from the ocean to the atmosphere. By keeping the Arctic atmosphere cool it drives the temperature gradient and the exchange of heat between the high and mid-latitudes. In boreal summer, when the sun never sets, the high albedo of sea ice significantly reduces the absorption of incoming solar radiation and prevents a heating of the Arctic ocean (Serreze and Barry, 2005).

In the last decades, however, observations show that Arctic sea ice cover has become smaller (Cavalieri et al., 1997; Parkinson and Comiso, 2013; Serreze et al., 2007), thinner (Kwok and Untersteiner, 2011; Kwok et al., 2009; Laxon et al., 2013) and younger (Fowler et al., 2004; Maslanik et al., 2011, 2007). These changes have been found to be caused by a combination of natural climate variability and external forcing (Stroeve et al., 2012b). Natural variability that can influence Arctic sea ice has been observed in surface temperatures (e.g. Kay et al., 2011) as well as in atmospheric (Ogi and Wallace, 2007) and oceanic circulation and heat transport (Morison et al., 2012; Polyakov et al., 2011; Shimada et al., 2006). Changes in external forcing are mainly man-made by rising concentrations of atmospheric greenhouse gases. These changes in the concentration of greenhouse gases lead to a warming of the atmosphere (Arrhenius, 1896; Stern and Kaufmann, 2014), which has been found to be particularly pronounced in the Arctic (AICA, 2005; Manabe and Stouffer, 1980).

This so called 'Arctic Amplification' is in part caused by the ice-albedo feedback over

the Arctic ocean (e.g. Screen and Simmonds, 2010; Serreze and Francis, 2006, see also Pithan and Mauritsen (2014) for a recent contribition to the discussion on Arctic Amplification). The ice albedo feedback is a well known positive feedback (Curry et al., 1995; Perovich et al., 2007): reduced sea ice extent enhances absorption of radiation, causes warming of the ocean and a further reduction of the sea ice cover (and vice versa). Many other feedbacks such as the influence of clouds on, and response to, sea ice loss are in turn, only partly quantified (Kay and Gettelman, 2009; Kay et al., 2008; Liu et al., 2012; Schweiger et al., 2008), mainly due to a lack of reliable data sources (Kay and L'Ecuyer, 2013; Zygmuntowska et al., 2012). Changes in sea ice can also influence other components of the climate system: larger areas of open water may influence European weather patterns (Francis and Vavrus, 2012; Outten and Esau, 2012; Overland and Wang, 2010) and the freshwater input from melting ice influences the water masses in the adjacent seas and the ocean circulation (e.g Aagaard and Carmack, 1989; McPhee et al., 2009, 1998). A recent review about effects of Arctic sea ice decline on weather and climate is given in Vihma (2014).

Sea ice is considered to be one of the main indicators of global climate change (Stocker et al., 2013). Since the early 90's, it has been an important component in the climate change debate, both in the scientific community (Chapman and Walsh, 1993; Johannessen et al., 2004) but also in public media (e.g. www.bbc.com - Climate Change, www.nytimes.com). The changes also cause new economical possibilities and political disputes. Smaller sea ice extent and longer ice free summers over large areas of the Arctic ocean allow for new shipping routes through the Arctic (Stephenson et al., 2013), and stimulate new plans for exploration of oil and gas in the Arctic region (www.bbc.com - North Pole, www.arctic-council.org).

1.2 Observed changes in Arctic sea ice

Scientific interest concerning the change of Arctic sea ice started in the late 19th century. A modern basis of Arctic science, including many international cooperations, was already established during the first International Polar Year (IPY) 1882-1883 (Weeks and Ackley, 1986; Wood and Overland, 2006). Since then many famous expeditions, such as *Fram* and *Maud* (Nansen, 1897), provided new insight into the Arctic climate system. In the 1930s the first Soviet Union Arctic Ocean drifting stations were established. This program was continued until the beginning of the 1990s and provides the most continuous measurements of the Arctic climate system (the program was re-established after a few years by the Russian federation 2003, www.aari.ru). The last apex of scientific research concerning the Arctic was the International Polar Year 2007 to 2009 (www.ipy.org).

On an Arctic wide scale sea ice and the observed changes can only be monitored with satellites. Already from the beginning of the satellite era in the 1970s, passive microwave measurements have been used to derive information about the sea ice concentration (Cavalieri et al., 1984; Comiso et al., 2007; Meier et al., 2012). For the last decades significant negative trends have been found, which have accelerated in the most recent years (see Figure 1.1). The largest decline is observed in September when the annual sea ice minimum is reached. Meier et al. (2012) observed a decline of -84100 $\pm$ 9600 km^2/yr in

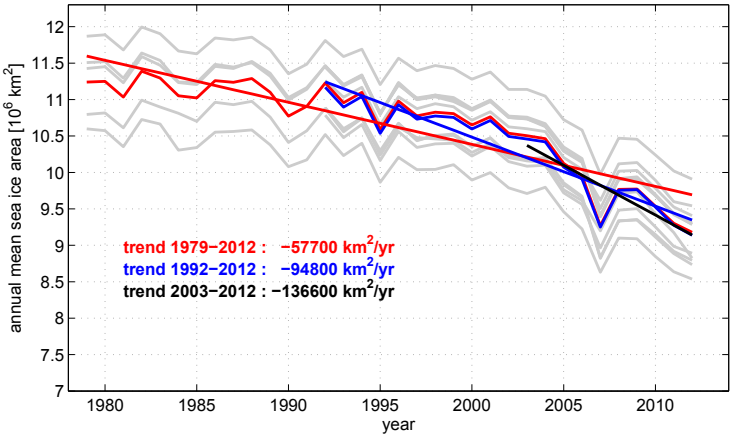

Figure 1.1: Annual mean of Arctic sea ice area based on different algorithms. Trends are calculated for the mean of these algorithms for three different time periods 1979-2012 (five algorithms), 1992-2012 (11 algorithms as used in paper I) and 2003-2012. Data for sea ice area provided by N. Ivanova (see Ivanova et al., 2014, and paper I of this thesis for more information about algorithms).

September for the period 1979-2011. Despite this long time period of measurements, absolute values of sea ice area still have high uncertainties. Uncertainties in sea ice concentration are particularly large in summer, where in some areas uncertainties of more than 20% are reached (Meier and Notz, 2010). The spread in annual mean sea ice area, caused by the use of different algorithms, is shown in Figure 1.1 (see e.g. Andersen et al., 2007; Ivanova et al., 2014; Kattsov et al., 2010, for more information about algorithm uncertainties).

Sea ice thickness can be monitored on an Arctic wide scale with altimeters on-board satellites (Kwok et al., 2006; Laxon, 1994a,b; Zwally et al., 2002). The first Arctic wide estimate of sea ice thickness was published by Laxon et al. (2003, see Figure 1.2). Exploring radar altimeter measurements from ERS-1/2 and Envisat from the 1990s, they

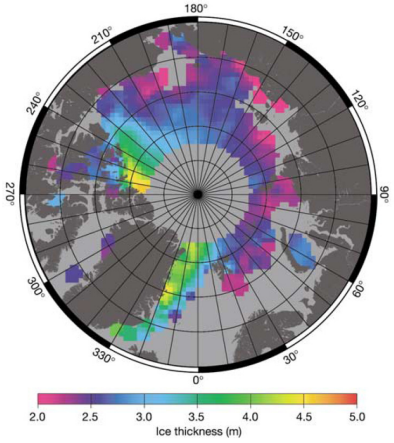

Figure 1.2: First ever published figure showing Arctic wide (circumpolar) sea ice thickness. Average winter (October to March) Arctic sea ice thickness from October 1993 to March 2001 is shown. Results are based on Envisat/ERS satellite altimeter measurements of ice freeboard. Data are only available south of 81.58 N and not in the marginal ice zone. Figure from Laxon et al. (2003).

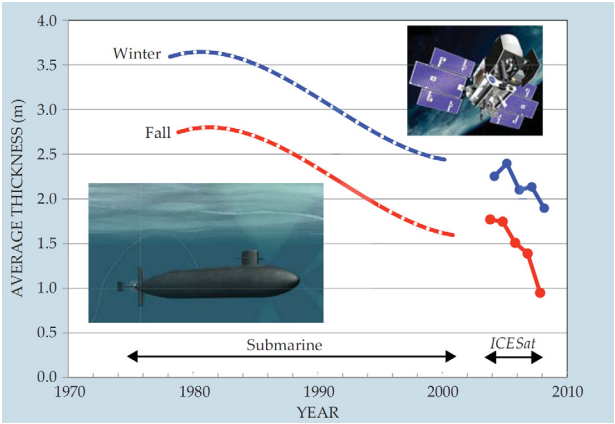

Figure 1.3: The thinning of Arctic sea ice from 1978 to 2008. From 1978 to 2001 results are based on measurements from upward looking sonars mounted on submarines. From 2003 till 2008 data is based on NASA's Ice, Cloud and Land Elevation Satellite (ICESat). The overall mean winter thickness in the 80's of 3.64 m is 1.75 m higher than at the end of the ICESat period, when it was 1.89 m. The rate of decline has also increased. Figure from Kwok and Untersteiner (2011).

found a strong inter-annual variability in sea ice thickness (Laxon et al., 2003), and circumpolar thinning of Arctic sea ice following the 2007 record ice extent minimum (Giles et al., 2008). In addition, laser altimeter measurements from NASA's Ice, Cloud, and land Elevation Satellite ICESat are available for the last decade. Analysing these measurements from ICESat, Kwok et al. (2009) found a decline in Arctic sea ice thickness of 0.18 m/yr between 2003 and 2008. At the end of the ICESat period in 2008, a winter thickness of 1.89 m has been found, which is 1.75 m lower than found in the 80's based on submarine data in the central Arctic (Kwok and Untersteiner, 2011, see also Figure 1.3). In 2010 CryoSat-2 was launched, providing information about sea ice thickness up to high latitudes of 88°N (see section 1.4 for detailed information on CryoSat-2). Preliminary results, using unvalidated data available from the Alfred-Wegener-Institute (www.meereisportal.de, see also Hendricks et al. (2013) for more details), show a mean sea ice thickness of 1.87 m in the central Arctic in winter 2012/2013 (October - March).

Additionally to these changes in sea ice thickness, sea ice has also become younger within the Multi-Year-Ice pack. Fowler et al. (2004) calculated the sea ice age back to 1979, based on passive microwave retrievals of sea ice drift. Following this apparoach, Maslanik et al. (2007) found a clear decline in the fraction of the oldest ice north of Greenland and the Canadian Archipelago. The strongest decline of 0.19×10^6 km^2/yr has been observed for the ice older than 5 years from 2004 to 2011 (Maslanik et al., 2011). However, their approach has some limitations, and I will discussed the accuracy of these results in chapter 3.

Changes in sea ice concentration and thickness eventually influence the large-scale drift pattern of sea ice. This main drift pattern has been well known for decades: ice circulates in the Beaufort Sea Gyre and is transported out of the Arctic through Fram Strait by the Transpolar Drift Stream (e.g. Colony and Thorndike, 1984). In the last years, however, an increase in deformation and drift speed has been observed (Rampal et al., 2009). While several studies focused mainly on the wind speed as possible forcing (Kwok et al., 2013; Spreen et al., 2011; Vihma et al., 2012), more recently Olason and Notz (manuscript submitted to JGR 2014, personal comunication) analyzed the influence of sea ice concentration and thickness. They found changes in sea ice concentration

to be the main driver for changes in drift speed for areas with low ice concentration in the summer months, while changes in sea ice thickness are found to be the main driver in winter, when concentrations are above 90%. A general overview about sea ice dynamics and it's kinematics is further given in Kwok (2011).

Decline in sea ice area and thickness also result in a reduction of sea ice volume. Based on data from the laser altimeter on board ICESat, Kwok et al. (2009) found a net loss of 5400 km^3 in October-November and 3500 km^3 in February-March during the ICESat period from 2003 to 2008. Recent results, exploring new data from the radar altimeter on-board CryoSat-2, report a further decline in Arctic sea ice volume (Laxon et al., 2013). The average sea ice volume in October-November for 2010 and 2011 was estimated to be 7560 km^3, i.e. 64% of the 2003-2008 mean value estimated from ICESat (Kwok et al., 2009). However, all these findings are associated with large uncertainties. Paper I presents a detailed analysis of the uncertainties in sea ice thickness and volume as well as their implications for trends between the ICESat and CryoSat period. More information about the concept of sea ice altimetry is given in section 1.3.

Debates are still ongoing as to whether we have already reached a 'tipping point' and sea ice will disappear very soon (Holland et al., 2006; Lenton, 2012; Wadhams, 2012) or if recovery mechanisms may largely outbalance the abrupt decline (Notz, 2009; Tietsche et al., 2011, see also (Serreze, 2011) for more discussions). However, in the last years the discussion about the future of Arctic sea ice and its disappearance in summer has generally shifted: it is no longer a question whether we will have a 'blue' ice free Arctic in the future, but rather when this event will occur. Overland and Wang (2013) categorized the recent contributions to this discussion as coming from *trendsetters*, *modelers* and *stochasters*. While *trendsetters* extrapolate sea ice volume data to calculate the first occurrence of a 'blue' Arctic (e.g. Maslowski et al., 2012; Schweiger et al., 2011), *modelers* use climate model ensemble projections (e.g. Massonnet et al., 2012; Stroeve et al., 2007, 2012a; Wang and Overland, 2009). *Stochasters* assume several more rapid ice loss events (so called RILEs) such as 2007 and 2012 that will lead to an ice free Arctic (e.g. Holland et al., 2006; Kay et al., 2011; Vavrus et al., 2012). Based on these studies, the Arctic could be ice free in summer by the end of this decade or latest by the end of the first half of this century.

1.3 Concept of sea ice altimetry

The primary objective of altimetry is to measure the elevation of a target or a surface below the instrument. The principle is that the instrument emits a signal in nadir direction and measures the echo reflected from the surface. The time the signal takes is proportional to the altitude (range) of the satellite over the surface (Fetterer, 1992), and can be used to retrieve the surface elevation. Sea ice altimetry relies further on the ability to discriminate accurately between return signals originating from leads (cracks in the sea ice) and signals originating from ice floes (Laxon, 1994a,b). For radar altimetry this is done by looking at the strength and shape of the returned signal: For smooth surfaces, such as leads, the signal is strong and specular while over rougher surfaces, such as sea ice and ridges, the signal becomes weaker and more diffuse (see Figure 1.4 for ex-

Figure 1.4: Typical waveform shapes over sea ice and leads from the radar altimeter SIRAL on-board CryoSat-2. The return signal from leads is specular while over sea ice the echo signal is diffuse.

ample of radar altimeter waveforms). More information about the signal processing of radar altimeters is given in Section 1.4 and information about the signal processing from laser altimeters can be found in Kwok et al. (2006).

The freeboard, the part of the ice above the water level, can be obtained by using the elevation over leads as the instantaneous sea surface height and calculating the difference between the sea surface height and ice floes (see Section 1.4 or Hendricks et al., 2013; Kwok et al., 2007; Zwally et al., 2002, for more details). For radar altimeters the signal is assumed to be reflected from the snow and ice interface (Beaven et al., 1995), thus provides the ice freeboard, while the laser signal is reflected from the air-snow interface, and provides the snow-plus-ice freeboard. Assuming hydrostatic equilibrium, the freeboard can be converted into an estimate of sea ice thickness (see Figure 1.5).

The following formula can be used to convert ice freeboard into sea ice thickness:

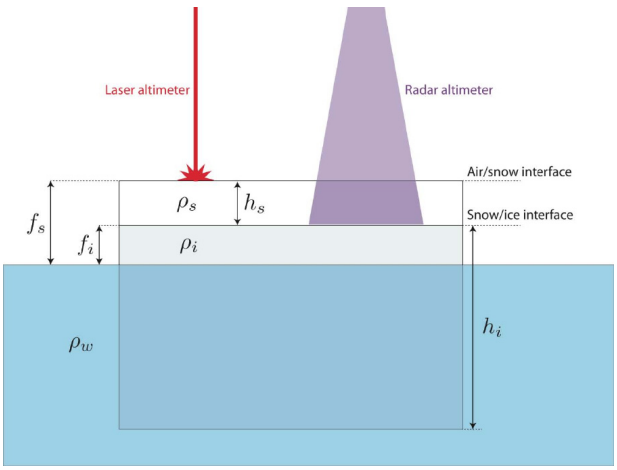

Figure 1.5: Schematic illustration of sea ice measurements from altimetry. The signal from laser altimeters is reflected from the snow-air interface, and thus gives information about the snow-plus-ice freeboard f_s (e.g. ICESat). Radar altimeters have a wider footprint compared to laser altimeters. For dry snow conditions the signal is reflected from the snow-ice interface giving information about the ice freeboard f_i (e.g. CryoSat-2). To estimate ice thickness h_i, hydrostatic equilibrium is assumed, and the density of water ρ_w, ice ρ_i and snow ρ_s as well as the snow depth h_s have to be known.

$$h_i = \frac{f_i \rho_w}{(\rho_w - \rho_i)} + \frac{h_s \rho_s}{(\rho_w - \rho_i)} \qquad \text{(radar)}$$

where f_i is the ice freeboard as retrieved from radar altimeters, h_s is the snow depth, and ρ_w, ρ_s, and ρ_i are the densities of water, snow and ice, respectively.

To convert the snow-plus-ice freeboard into sea ice thickness, the following formula can be used:

$$h_i = \frac{f_s \rho_w}{(\rho_w - \rho_i)} + \frac{h_s (\rho_s - \rho_w)}{(\rho_w - \rho_i)} \qquad \text{(laser)}$$

where f_s is the snow-plus-ice freeboard.

Limitations and uncertainties of the conversion of freeboard into sea ice thickness by this method are discussed in detail in paper I.

1.4 CryoSat-2 and the concept of synthetic aperture radar altimeters

CryoSat-2 was launched in 2010 and is ESA's first satellite mission specifically designed to measure changes in the Earth's cryosphere. The advantage of CryoSat-2, compared to previous satellite radar altimeter missions, is the high inclination of the satellite orbit of 92°N and the increased resolution of the measurements. The satellite has an orbit repeat cycle of 369 days, but sub-cycles every 30 days, which allows to monitor the Arctic ocean on a regular grid on a monthly basis.

CryoSat's payload instrument is the SAR/Interferometric Radar Altimeter (SIRAL). It has a center frequency of 13.575 GHz and a receive bandwidth of 320 MHz. The instrument operates in three different modes: Low Resolution Mode (LRM), Synthetic Aperture Radar mode (SAR), and the SAR/Interferometric mode (SARIn). LRM mode,

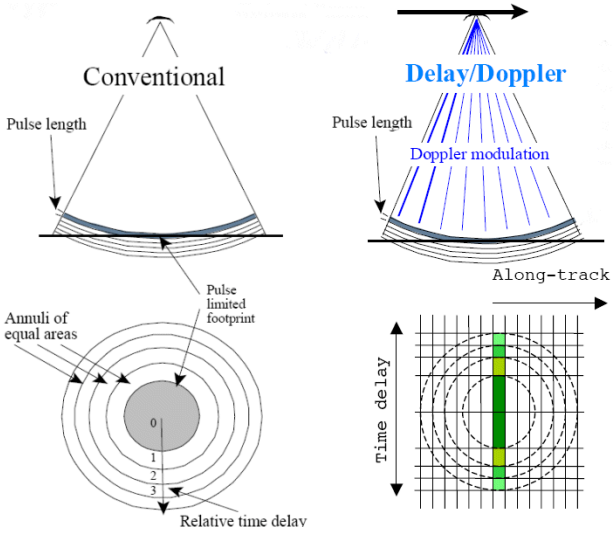

Figure 1.6: Comparison between sampling of conventional radar altimeter (left) and Delay Doppler/SAR (right) as used by CryoSat-2 in SAR mode. The along track processing increases the resolution and offers a multi-look processing with two independent dimensions: along-track and across-track (range). The resulting smaller footprint size is visualized in the lower figures. Figure adapted from Raney (1998).

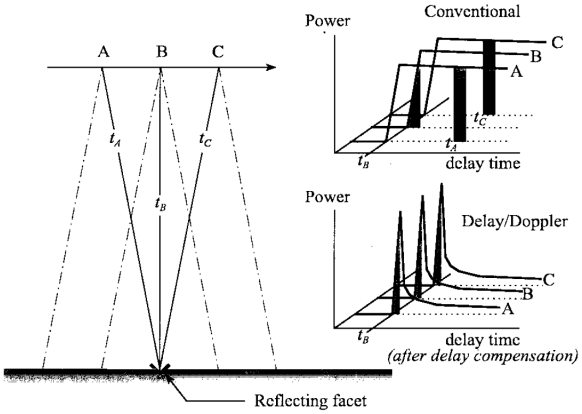

Figure 1.7: Concept of multi-looking and the resulting radar altimeter echo waveforms. The delay time is always longer for all surface locations that are not at minimum range position. For conventional altimeters this results in the step function. The delay/doppler altimeter or synthetic aperture radar altimeter compensates for this extra delay, resulting in much sharper waveforms. Figure from Raney (1998).

which is equivalent to conventional altimeters, is used over oceans and glacier interiors. In SAR mode the synthetic aperture radar technique is used to enhance the resolution along-track over sea ice. In SARIn mode two receiving antennas are used, and from interferometry in across-track direction information about surface slopes, i.e. over ice caps and ice sheet margins, can be derived.

The application of the synthetic aperture technique to conventional radar altimeters was first introduced by Raney (1998). Figures 1.6 and 1.7 illustrate the formation of the return signal. For conventional altimeters the footprint is very large, i.e. between 2 to 10 km for Envisat, depending on surface roughness. For CryoSat-2, operating in it's SAR mode, the nominal footprint is reduced to around 300 m in along-track and 1700 m in across-track direction. For SIRAL, the radar altimeter on-board CryoSat-2, 64 bursts of phase-coherent pulses are transmitted and the corresponding received echoes are processed to form 64 beams in along track direction (see strips arranged across the track in Figure 1.6), by looking at the frequency shift (doppler effect). Echoes from forward and backward looking parts of the beams are corrected to account for the additional travel time ('slant-range' correction). As subsequent bursts are transmitted and received along the satellite path, all of the echoes from beams directed at individual along track locations are superimposed (multi-looked) to reduce radar speckle noise (see Figure 1.7). For CryoSat-2 these beams are separated by approximately 300 m. The returning echos are sampled in 128 bins each 1.563 ns resulting in a range resolution of 0.486 m. The final processed return signal is usually referred to as waveform (see Figure 1.7 and 1.4), and can be interpreted to get information about the surface elevation and the surface properties. More information about the signal processing from CryoSat-2 can be found in the paper by Wingham et al. (2006). The advantages of the SAR approach are the decreased footprint size (finer resolution, see also Figure 1.6) and the more efficient use of the instrument's energy. The increased resolution means that the instrument can resolve smaller ice floes, resulting in a better retrieval of sea ice freeboard.

For accurate retrieval of surface elevation, further geophysical and re-tracking corrections have to be applied. Geophysical corrections include the ionospheric delay time, wet and dry tropospheric delay, inverse barometric effect, dynamic atmospheric correc-

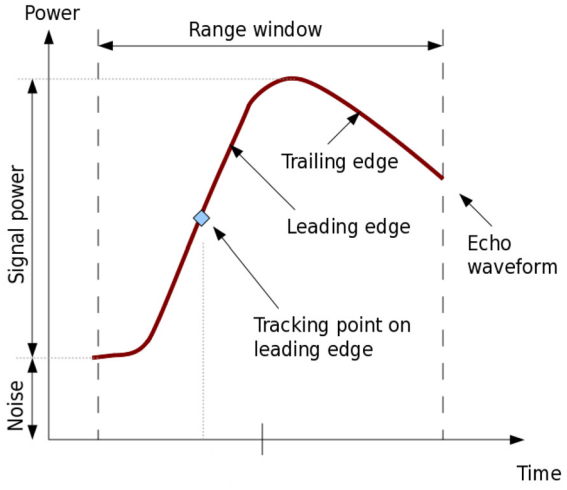

Figure 1.8: Idealized response waveform for delay/doppler altimeter as recorded in the instruments range window. To find the surface elevation the waveform has to be 're-tracked' to retrieve the position along the leading edge which belongs to the surface (diamond). Often a fixed threshold is used such as e.g. 50% of the maximum power (common value used for conventional altimeters).

tions, ocean equilibrium tide, and solid earth tide. Re-tracking refers to the process of identifying the point along the leading edge of the signal waveform which belongs to the surface (see Figure 1.8). Currently, over sea ice different approaches are used: fitting a simple spline function to the measurement points in combination with a fixed threshold (Hendricks et al., 2013), fitting idealized waveforms to the measurements in combination with a fixed threshold (Giles et al., 2007) or using a semi-empirical model, taking into account surface roughness and incidence angle (Kurtz et al., 2014).

Additionally to surface elevation, the magnitude and shape of the signal waveform contain information about the characteristics of the surface e.g. significant wave height over oceans or wind speed (e.g. Fedor and Brown, 1982; Gourrion et al., 2002). For sea ice the waveform shape is generally used to identify leads between the ice floes. This distinction is done by looking at the 'pulse peakiness' factor, the ratio of the accumulated power to the power maximum (Laxon, 1994b). For CryoSat-2 also the 'stack standard' deviation is used, i.e. the variability of the multi-looked signals at one location (Hendricks et al., 2013; Laxon et al., 2013). How the signal shape can additionally be used to obtain information about sea ice type, is presented in paper II and paper III.

Chapter 2

Objectives and summary of the papers

The observed changes in Arctic sea ice thickness and volume are two of the main indicators of global climate change. Yet remotely sensed estimates of these parameters are associated with high uncertainties. The first objective of this thesis was thus to quantify the current uncertainties in sea ice thickness and volume and to identify the main sources of uncertainty. The second objective was to develop a sea ice classification method based on the shape of radar altimeter signal waveforms. This method could be used to convert freeboard into thickness more accurately and to improve the estimates of sea ice thickness and volume.

Below I will briefly summarize the scientific results of each paper:

PAPER I:

Uncertainties in Arctic sea ice thickness and volume: New estimates and implications for trends, Zygmuntowska, M.; Rampall, P.; Ivanova, N. ; Smedsrud, L.H., in press, accepted for publication in *The Cryosphere*, March 2014.

In paper I we provide a new quantification of uncertainties in remotely sensed estimates of sea ice thickness and volume and identify the main sources of uncertainty. To quantify these uncertainties we use freeboard retrievals from NASA's Ice, Cloud, and land Elevation Satellite ICESat and investigate different assumptions on snow depth, sea ice density and area. Uncertainties in sea ice thickness and volume are calculated with a Monte-Carlo-approach based on probability distribution functions for these three parameters. Our approach is different to earlier methods as we take into account the spatial auto-correlation of uncertainties.

We show that these geophysical parameters have influence on the overall mean, the year-to-year variability, and the longterm trends. The mean total sea ice volume and its uncertainty are 10120 $\pm$ 1280 km ^{3} in October/November and 13250 $\pm$ 1860 km^3 in February/March for the time period 2005–2007. Based on the found uncertainties we obtain trends in sea ice volume of -1450$\pm$530 km ^{3}/yr in October/November and -880$\pm$260 km ^{3}/yr in February/March over the ICESat period (2003–2008). Taking into account the uncertainties, our results further indicate that the decline in sea ice volume in the Arctic between the ICESat (2003–2008)

and CryoSat-2 (2010–2012) periods may have been less dramatic than reported in previous studies. However, more work and validation is required to quantify these changes and analyse possible unresolved biases in the freeboard retrievals.

PAPER II:

Waveform classification of synthetic aperture radar altimeter over Arctic sea ice, Zygmuntowska, M.; Khvorostovsky, K.; Helm, V. and Sandven, S., The Cryosphere, 7, 1315 - 1324, 2013.

Paper II presents a method to derive sea ice type based on the shape of the return signal waveform from radar altimeters. The shape of the radar signal waveform is known to be dependent on surface properties, but so far no method exists to identify the sea ice type based on the waveform alone. Information about sea ice type, however, is needed to be able to use ice type dependent values for snow and ice properties while converting freeboard into thickness. For our study we use data from the Airborne Synthetic Aperture Radar and Interferometric Radar Altimeter System ASIRAS, which is a replica of the radar altimeter on-board ESAs satellite CryoSat-2.

We present a first case study, analyzing data from validation campaigns performed mainly north of Greenland and Canada in late winter 2007 and 2008. We parametrize the waveform shape and identify parameters most suitable for sea ice classification. We show that the waveform maximum and the width of the trailing edge are the best parameters to distinguish between Multi-Year-Ice and First-Year-Ice. By applying a bayesian based method to these parameters we are able to detect 80% of the waveforms correctly. We also show that the false classification rate of leads can be reduced by using the waveform maximum instead of the widely used Pulse Peakiness parameter. For the Pulse Peakiness the rate of false classification of leads is 13%, but is reduced to 6% when using the power maximum.

How our method can be used for CryoSat-2 is presented in paper III.

PAPER III:

Analysis of CryoSat's radar altimeter waveforms over different Arctic sea ice regimes, Zygmuntowska, M. and Khvorostovsky, K. manuscript to be submitted, 2014.

Paper III presents an analysis of CryoSat's radar altimeter waveforms over different surface regimes. Encouraged by the positive results based on airborne data presented in paper II, in this study we analyze signal waveforms from satellite based radar altimeters. The difference between the two instruments is mainly the increased footprint size for CryoSat-2 as well as the increased sampling interval compared to the ASIRAS data used in paper II.

We define several parameters to account for the difference in the shape of radar altimeter waveforms over different sea ice regimes. The parameters with the largest difference between the two ice types are the Pulse Peakiness, Stack Standard Deviation and Leading Edge Width. These waveform parameters can thus be used to classify First- and Multi-Year-Ice over large areas of the Arctic Ocean. However, analyzing the spatial distribution we find some discrepancies to other retrievals of sea ice type. CryoSat-2 waveform parameters have values typical for Multi-Year-Ice over large areas of First-Year-Ice. These areas are co-located with strong gradients in drift speed, indicating, that the radar signal is mainly sensitive to surface roughness. Potentially this information could be used to reduce biases in the freeboard retrievals and to improve estimates of sea ice thickness.

Chapter 3

Discussion and future perspectives

Aside from the findings mentioned in chapter 2, and discussed in detail in the respective papers, a number of general lessons, implications, and questions have arisen from our work. Below I will first highlight the importance of snow for the radar altimeter measurements over Arctic sea ice. Then I briefly outline the planned, or already ongoing, work to address the unresolved questions from the three presented papers.

Currently the main barrier to deriving accurate information about sea ice thickness from radar altimetry is a lack of information about snow depth, it's properties and it's influence on the radar signal. The lack of information about snow is mentioned in all three studies, but herein I will explain in more detail how snow influences the estimates of range, freeboard and thickness. Where possible I describe how the resulting problems should be addressed in the future.

1. The snow on sea ice influences the speed of the radar signal and thus the estimates of range and freeboard (fb). Current operational algorithms do not, however, account for this bias, h_c ($fb=fb_{radar}+h_c$). h_c can be described as $h_c=h_s(1-\frac{c_{snow}}{c})$, where c is the speed of the radar signal through vacuum, h_s is the snow depth and c_{snow} the speed through the snow. Following Tiuri et al. (1984), c_{snow} can be described as $c_{snow} = \frac{c}{1+1.7\rho_s+0.7\rho_s^2}$ (with ρ_s being the density of snow in g cm^{-3}). Given typical values for snow density and snow depth for the Arctic, this introduces a bias of several centimeters to the estimates of sea ice thickness (see also Kurtz et al., 2014, for more discussions). To derive correct information about sea ice thickness and its changes, this correction has to be applied in the future.

2. Ice layers within the snow after refreezing can act as scattering surfaces and thus influence the estimates of range and freeboard. In ideal conditions, with cold and dry snow, the radar signal penetrates through the snow and is reflected from the snow ice interface (Beaven et al., 1995). In warmer conditions, however, this is not always the case, and the signal has been found to be reflected within the snow layer (Willat et al., 2011). Hendricks et al. (2013) thus assumed a maximal penetration depth of 23 cm into the snow layer in mid winter. More work is required to test this assumption and improve this simple parametrization.

3. Wrong assumptions on snow depth introduce a bias into the estimates of sea ice thickness. The majority of studies, in which sea ice thickness is estimated from radar altimetry, assume a snow depth taken from the climatology from Warren

et al. (1999). The use of this climatology does introduce biases, as 1) these values overestimate snow depth in the recent years, both over First-Year-Ice (Kurtz and Farrell, 2011b) and Multi-Year-Ice (Zygmuntowska et. al, 2014; paper I of this thesis) and 2) the climatology does not capture the year-to-year variability. This is particularly important when analyzing short term changes in sea ice thickness. Such year-to-year changes in sea ice thickness, estimated from CryoSat-2 measurements (preliminary results presented at the AGU Fall meeting 2013 Tilling et al., 2013), recently caught a lot of media attention (www.bbc.com - CryoSat). However, these findings are not necessarily real changes in sea ice thickness but can - at least partly - be explained by an over- or underestimation of snow depth. To derive accurate estimates of sea ice thickness real-time data should be used. Such measurements are already available from the Advanced Microwave Scanning Radiometer AMSR-E over First-Year-Ice (Brucker and Markus, 2013; Markus and Cavalieri, 1998, 2008) and methods are being developed for Multi-Year-Ice based on measurements from the Soil Moisture Ocean Salinity satellite SMOS (Maaß et al., 2013).

In the three presented studies a few questions remained open, which still deserve some closer attention. These are in particular the unresolved biases in the freeboard retrievals (paper I) and the discrepancies in existing retrievals of sea ice type and age (paper III). While it was clearly beyond the scope of the respective studies to analyze these issues, I will describe below how they can, or will, be addressed in the future.

1. In paper I we found potential biases in the freeboard retrievals from ICESat and CryoSat-2. In the presented study we primarily analyze uncertainties in sea ice thickness and volume stemming from geophysical parameters such as snow depth, ice density and sea ice area. Using consistent choices for these parameters we obtain a decline in sea ice volume in the Arctic between the ICESat (2003–2008) and CryoSat-2 (2010–2012) periods that is less dramatic than reported in a previous study by Laxon et al. (2013). On the one hand our findings are consistent with synoptic airborne measurements showing little change in sea ice thickness in this period (Haas et al., 2010; Richter-Menge and Farrell, 2013), but on the other hand, the underlying thickness estimates used by Laxon et al. (2013) have been evaluated and agree well with independent in-situ data. Consequently an alternative interpretation of our findings is that there are biases in the freeboard retrievals and these biases are mitigated by the choices made for sea ice density and snow depth. In paper I, we did not analyze these uncertainties and biases stemming from freeboard estimates as this analysis was beyond the scope of our study. At present we try to quantify and resolve potential biases, and below I will briefly outline our approach:

   (a) To quantify uncertainties and biases in the freeboard retrievals from ICESat we currently reproduce the two main existing algorithms developed by Kwok et al. (2009) and Yi et al. (2011). Many studies already exist, analyzing the freeboard uncertainties arising from lead detection algorithms (e.g. Kwok et al., 2007) or the sampling size (e.g. Connor et al., 2013; Farrell et al., 2011).

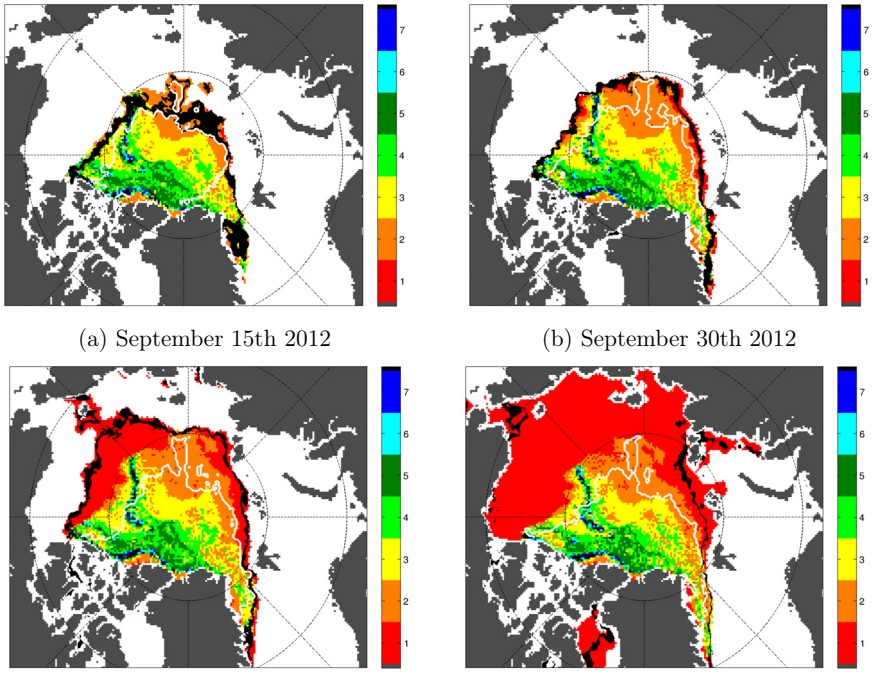

(a) September 15th 2012 (b) September 30th 2012

(c) October 15th 2012 (d) November 15th 2012

Figure 3.1: Comparison of sea ice age (in years) based on the algorithm outlined in Fowler et al. (2004) and the retrieval from the EUMETSAT Ocean and Sea Ice Satellite Application Facility on ice type and ice edge for autumn 2012 (see paper III for more information about the data product). The colored pattern shows the sea ice age, the white contour line shows the border between First- and Multi-Year-Ice and the black contour line indicates the ice edge.

Yet a detailed comparison of the two main ICESat data sets available from JPL (Kwok et al., 2009) and NSIDC (Yi et al., 2011) is so far missing.

(b) In paper III we outline a potential method how biases in freeboard retrievals from CrySat-2 can be reduced by using information about surface roughness. Biases in freeboard retrievals have been reported in several studies: Armitage and Davidson (2013) found a potential bias in the freeboard retrievals due to off-nadir reflection from leads, Tonboe et al. (2010) found a bias due to preferential sampling of thin ice, Hendricks et al. (2013) found a bias due to an incomplete penetration of the radar signal through the snow (see above for more detailed discussion) and Kurtz et al. (2014) show a bias due to the use of a fixed threshold while re-tracking the surface elevation from the radar altimeter waveforms. With our method we are potentially able to resolve this last bias. While Kurtz et al. (2014) suggest the use an empirical model for waveform simulation to remove this bias, we suggest the use of information about surface roughness to correct existing re-trackers that are using a fixed threshold (also see paper III for a detailed discussion). A similar ad-hoc correction has been used for freeboard retrievals from ICESat, e.g. to account for unresolved biases due to snow accumulations on refrozen

leads (Kwok and Cunningham, 2008) and the width of leads (Kwok et al., 2009). To develop this correction, freeboard estimates from CryoSat-2 could be validated against data from airborne instruments, and differences could be compared to waveform parameters, as described in paper III. Potential airborne measurements are, for example, laser altimeter measurements from Operation IceBridge (Kurtz et al., 2013), snow-plus-ice measurements with electromagnetic induction ('EMBird' Haas et al., 1997, 2011; Renner et al., 2013, see also ESA CryoVex blog, 2014) and radar and laser altimeter data from CryoSat's validation campaigns (see e.g ASIRAS, CryoVex blog 2014 for current campaign)

2. In paper III we found large discrepancies between the age of sea ice, as derived from Lagrangian tracking (e.g. described in Fowler et al., 2004), and the sea ice type retrieval based on instantaneous passive and active microwave measurements (Eastwood, 2012, obtained from the EUMETSAT Ocean and Sea Ice Satellite Application Facility). In Figure 3.1 both datasets are compared for autumn 2012, from the minimum ice extent in September to the freeze-up of the entire Arctic ocean in November. The discrepancy between the two data sets increases at the beginning of the freeze-up in September and then remains at this high level throughout large parts of the winter. While Figure 3.1 only briefly illustrates the problem, a detailed analysis should be performed, quantifying the discrepancy of the retrievals with respect to ice area, ice edge and its dynamic behavior over several years.

3.1 Conclusions

The main conclusions of this study are the following:

1. Assumptions on geophysical parameters such as snow depth, ice density and area introduce an uncertainty in sea ice volume of around 13%. The uncertainty in snow depth contributes up to 70% of the total uncertainty and the ice density up to 30%. Uncertainties in ice area are of minor importance for the estimates of sea ice volume and thickness. The assumptions made further influence the estimated year-to-year variability, and longterm trends.

2. Parameters which describe the radar altimeter signal waveform from CryoSat-2 are significantly different over First- and Multi-Year-Ice over large areas of the Arctic Ocean. However, the radar signal is mainly sensitive to surface roughness and areas of strongly deformed First-Year-Ice can be falsely classified as Multi-Year-Ice. Potentially the information about surface roughness can be used to reduce biases in the freeboard retrievals and to improve estimates of sea ice thickness.

Chapter 4

Scientific papers

Paper I:

Uncertainties in Arctic sea ice thickness and volume: New estimates and implications for trends, Zygmuntowska, M.; Rampall, P.; Ivanova, N. ; Smedsrud, L.H., in press, accepted for publication in *The Cryosphere*, March 2014.

Paper II:

Waveform classification of synthetic aperture radar altimeter over Arctic sea ice, Zygmuntowska, M.; Khvorostovsky, K.; Helm, V. and Sandven, S., *The Cryosphere*, 7, 1315 - 1324, 2013.

Paper III:

Analysis of CryoSat's radar altimeter waveforms over different Arctic sea ice regimes, Zygmuntowska, M. and Khvorostovsky, K. manuscript to be submitted.

I

Paper I

Uncertainties in Arctic sea ice thickness and volume: New estimates and implications for trend

Zygmuntowska, M.; Rampall, P.; Ivanova, N. ; Smedsrud, L.H.

in press, accepted for publication in *The Cryosphere*, March 2014

Manuscript prepared for The Cryosphere
with version 4.2 of the LaTeX class copernicus.cls.
in press, accepted for publication March 2014.

Uncertainties in Arctic sea ice thickness and volume: new estimates and implications for trends

M. Zygmuntowska[1,2], **P. Rampal**[1], **N. Ivanova**[1], **and L. H. Smedsrud**[2]

[1]Nansen Environmental and Remote Sensing Center, Bergen, Norway
[2]Geophysical Institute, University of Bergen, Norway

Abstract. Sea ice volume has decreased in the last decades, evoked by changes in sea ice area and thickness. Estimates of sea ice area and thickness rely on a number of geophysical parameters which introduce large uncertainties. To quantify these uncertainties we use freeboard retrievals from ICESat and investigate different assumptions on snow depth, sea ice density and area. We find that uncertainties in ice area are of minor importance for the estimates of sea ice volume during the cold season in the Arctic basin. The choice of mean ice density used when converting sea ice freeboard into thickness mainly influences the resulting mean sea ice thickness, while snow depth on top of the ice is the main driver for the year-to-year variability, particularly in late winter. The absolute uncertainty in the mean sea ice thickness is $0.28\,\mathrm{m}$ in February/March and $0.21\,\mathrm{m}$ in October/November. The uncertainty in snow depth contributes up to 70 % of the total uncertainty and the ice density 30–35 %, with higher values in October/November. We find large uncertainties in the total sea ice volume and trend. The mean total sea ice volume is $10120 \pm 1280\,\mathrm{km}^3$ in October/November and $13250 \pm 1860\,\mathrm{km}^3$ in February/March for the time period 2005–2007. Based on these uncertainties we obtain trends in sea ice volume of $-1450 \pm 530\,\mathrm{km}^3\mathrm{a}^{-1}$ in October/November and $-880 \pm 260\,\mathrm{km}^3\mathrm{a}^{-1}$ in February/March over the ICESat period (2003–2008). Our results indicate that, taking into account the uncertainties, the decline in sea ice volume in the Arctic between the ICESat (2003–2008) and CryoSat-2 (2010–2012) periods may have been less dramatic than reported in previous studies. However, more work and validation is required to quantify these changes and analyse possible unresolved biases in the freeboard retrievals.

Correspondence to: M. Zygmuntowska (marta.zygmuntowska@nersc.no)

1 Introduction

Remotely sensed estimates of sea ice area and thickness reveal a dramatic decline in Arctic sea ice volume in the last decades (Kwok et al., 2009b; Laxon et al., 2013). This decline mirrors changes in the Arctic heat budget (e.g. Kurtz et al., 2011b; Perovich et al., 2011) and alters the exchange of freshwater between sea ice and the ocean (e.g. Aagaard and Carmack, 1989; McPhee et al., 2009). As they are of primary importance for the Arctic (Screen and Simmonds, 2010) and the global climate system (Outten and Esau, 2012) these remotely sensed data have been analysed in many studies. Unfortunately, many of the studies lack a detailed estimate of uncertainties. We fill this gap and quantify total uncertainties in sea ice thickness and volume in the Arctic basin. We further identify the main factors contributing to the uncertainties, analysing snow depth, sea ice density and area. We provide uncertainties averaged over the Arctic basin and analyse the spatial and seasonal variability.

Arctic sea ice area has been observed from satellites over the last $40\,\mathrm{yr}$ starting with the Nimbus 5 electrically scanning microwave radiometer (ESMR) in 1972. A decrease in sea ice area was detected in the early 1990's (Serreze et al., 1995; Parkinson et al., 1999) and has continued at an increased rate in the last decade (Cavalieri and Parkinson, 2012). The average difference in daily sea ice extent among the most known algorithms can reach up to ± 1 million km^2 , but it seems difficult to get a grip on which algorithm produces the most correct estimates.

Until the 1990s, our knowledge of Arctic sea ice thickness was determined by sparse field campaigns or submarine measurements giving only limited insight into the overall Arctic sea ice thickness. Based on submarine data from the central Arctic region Rothrock et al. (1999) found a decline in Arctic sea ice draft, the part of the ice below the water level, of $1.3\,\mathrm{m}$ from the 1960's to 1980's. Over the last decade both laser and radar altimeters have been used to estimate

sea ice thickness on a basin wide scale (Laxon et al., 2003; Kwok et al., 2004b). Analysing measurements from the laser altimeter on-board ICESat Kwok et al. (2009b) found a decline in Arctic sea ice thickness of $0.18\,\mathrm{ma}^{-1}$ between 2003 and 2008. Spatially the strongest decline was found in the region covered by Multi-Year-Ice between Greenland and the North Pole. These results were consistent with sea ice thickness estimates from ERS and EnviSat radar altimeters reporting strong inter-annual variability in sea ice thickness (Laxon et al., 2003), and circumpolar thinning of Arctic sea ice following the 2007 record ice extent minimum (Giles et al., 2008). Combining sea ice thickness estimates from satellites and submarines, Kwok and Rothrock (2009a) determined that, in the central Arctic where submarine data was released, the mean ice thickness in fall declined from $3.02\,\mathrm{m}$ in the 1960's to $1.92\,\mathrm{m}$ in the 1990's, and then to $1.43\,\mathrm{m}$ during the ICESat period 2003–2007.

Sea ice thickness is a quantity that cannot be measured directly by satellite based instruments. Altimeters on board satellites measure the elevation of the Earth surface and by identifying leads between the ice floes, the freeboard (the height of the ice above the water level) can be derived. The thickness is calculated by assuming hydrostatic equilibrium and estimating the density of sea ice and snow and the snow depth on top of the ice. These quantities may vary both in space and time and introduce large uncertainties in the sea ice thickness estimates.

Decline in sea ice area and thickness results in a reduction of sea ice volume. Based on data from the laser altimeter on board ICESat, Kwok et al. (2009b) found a net loss of $5400\,\mathrm{km}^3$ in October/November and $3500\,\mathrm{km}^3$ in February/March during the ICESat record from 2003 to 2008. Recent results, exploring new data from the radar altimeter onboard CryoSat-2, report a further decline in Arctic sea ice volume (Laxon et al., 2013). The average sea ice volume in October/November for 2010 and 2011 was estimated to be $7560\,\mathrm{km}^3$, i.e. 64 % of the 2003–2008 mean value estimated from ICESat (Kwok et al., 2009b). For the maximum annual value in February/March, the sea ice volume was estimated to be $14\,819\,\mathrm{km}^3$, i.e. 91 % of the previous ICESat value (Laxon et al., 2013).

To investigate the influence of snow depth, sea ice density, and area on sea ice thickness and volume estimates we use freeboard retrievals from ICESat, together with different assumptions on snow and ice properties, and sea ice concentration derived from different algorithms. Uncertainties are calculated with a Monte-Carlo-approach based on probability distribution functions for the three parameters. Our approach is different to earlier methods as we take into account the spatial auto-correlation of uncertainties. We also provide, for the first time on an Arctic-wide scale, contributions of each of the analysed parameters to the total volume uncertainty. Our paper is outlined as follows: In Sect. 2 we describe the data sets used for ice sea freeboard, area, type and snow depth. In Sect. 3 we describe how sea ice thickness is estimated and provide a description of the Monte-Carlo approach used to calculate uncertainties in sea ice thickness and volume. Results on the uncertainties in sea ice thickness and volume are given in Sect. 4 and a detailed discussion, including implications on the trend in sea ice volume, is given in Sect. 5.

2 Data

To calculate sea ice thickness and volume, we combine satellite based retrievals of sea ice freeboard, type and area. In this section we will describe the data sets and the processing steps used to derive the necessary parameters for our analysis.

2.1 Sea ice freeboard

The starting point of this paper is the ICESat freeboard retrieval. The Geoscience Laser Altimeter System (GLAS) on ICESat is using a $1064\,\mathrm{nm}$ laser channel for surface altimetry, with an expected accuracy of $15\,\mathrm{cm}$. The satellite orbit has an inclination of 94°, measurements have a resolution of $70\,\mathrm{m}$ and the surface was sampled every $170\,\mathrm{m}$ (Zwally et al., 2002). ICESat was in orbit for almost six years from 2003 to 2009 but was generally operating only for two separated periods each year in February/March and October/November. The laser measures the top of the snow on the ice, if snow is present, and the freeboard value retrieved is thus the combined value for sea ice and snow.

The data set mainly used in our study is available from NSIDC (Yi and Zwally, 2009) and based on the original data processing described by Zwally et al. (2002). The data set is only available for the campaigns from October/November 2005 to 2007 (see Table 1 for more information) and provides sea ice freeboard information along track. Sea ice thickness is also available in this data set but has not been used in our analysis. In this algorithm the freeboard has been obtained by defining leads as the lowest 1% of elevation along a 50 km running mean. Further detail on the original processing and the freeboard retrieval are provided in Zwally et al. (2002) and at NSIDC (http://nsidc.org/data/docs/daac/nsidc0393_arctic_seaice_freeboard/index.html).

For comparison we also use the gridded sea ice thickness data set from JPL (available at http://rkwok.jpl.nasa.gov/icesat/download.html). To get information about sea ice freeboard a slightly different approach has been used for this data set. Kwok et al. (2007) used the standard deviation of surface elevation together with values of reflectivity to identify leads. Additionally, Kwok et al. (2009b) included two corrections to account for possible unresolved biases, such as due to the size of leads and snow accumulation on refrozen leads. A detailed description of this data set can be found in Kwok and Cunningham (2008) and Kwok et al. (2009b).

As no freeboard data are available from JPL, we did not perform an analysis of freeboard uncertainties. In our study

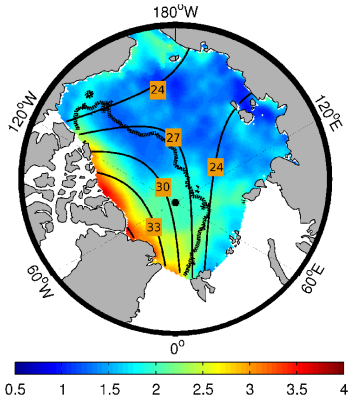

Fig. 1: Arctic sea ice properties and the Arctic sea ice area as defined in this study. Annual mean sea ice thickness from ICESat is shown in color [m]. The line of 50% Multi-Year-Ice fraction is plotted as thick contour line. Both parameters are given as the average during the ICESat campaigns 2005 to 2007. Climatological winter (October-April) snow depth from Warren (1999) from 1954 to 1991 is given as the labeled thin contour lines in centimeter.

we focus on how snow depth, sea ice density, and area influence sea ice thickness estimate. In this way the word "uncertainty" as used in this study covers the "geophysical assumptions" of the sea ice thickness estimate and not instrumental "errors". A detailed analysis of the freeboard retrievals and its associated uncertainties for each algorithm were described in a clear and concise manner by Zwally et al. (2002), Kwok et al. (2007) and Kwok and Cunningham (2008).

2.2 Sea ice type

Information about sea ice type is derived from QuikSCAT scatterometer data. QuikSCAT provides normalized radar cross section ($sigma_0$) measurements of the Earth's surface. In this study we use daily averaged gridded QuikSCAT data processed at the Brigham Young University (BYU) for each mid-day of the evaluated periods (ftp://ftp.scp.byu.edu/data/qscat/SigBrw). The small hole around the North Pole (0.5° N) is filled with a nearest neighbor interpolation. Backscatter is converted into Multi-Year-Ice (MYI) fraction using the method described in Kwok (2004a). This method is based on a relationship between the MYI fraction from high resolution RADARSAT/RGPS images and $sigma_0$ backscatter from QuikSCAT (see Fig. 6 in Kwok, 2004a). We checked that our results are consistent with the fields published in Kwok (2004a) and Polyakov et al. (2011) for 1 January from 2000 to 2008.

Table 1: ICESat campaigns as used in this study.

Survey	Period
ON05	21 Oct to 24 Nov 2005
FM06	22 Feb to 27 Mar 2006
ON06	25 Oct to 27 Nov 2006
MA07	12 Mar to 14 Apr 2007
ON07	2 Oct to 5 Nov 2007

The backscatter from scatterometers is sensitive to the physical properties of sea ice that change after sea ice has survived the melting season. Thus the term MYI, as defined in this study, refers to sea ice that survived one summer, but may actually be younger than one year. However as scatterometers only capture the surface properties, this method does not allow us to account for the part of (First-Year-Ice) FYI growing from the bottom during winter freezing, and therefore underestimates the volume fraction of FYI.

In this study we use two different approaches to define the sea ice type: a fraction of the ice type per pixel, as described above, and a binary classification. To get the binary sea ice classification between FYI and MYI for each pixel we used a threshold of 50 % for the sea ice type. This binary classification has been used in previous studies, e.g. Kwok et al. (2009b).

2.3 Sea ice area

Sea ice area is derived from sea ice concentration estimates based on brightness temperatures from DMSP SSM/I (Special Sensor Microwave Imager). In this study, we use gridded brightness temperatures in polar stereographic projection available from NSIDC (Maslanik and Stroeve, 2004, updated 2012). Various algorithms exist to derive sea ice concentration from this type of measurements. The underlying theory behind the algorithms is that sea ice and open water emit differently across the frequency spectrum and polarisations. The measured brightness temperatures are therefore a linear combination of these two temperatures, with weights according to the concentration of sea ice and water. Algorithms differ due to the use of different frequencies, tie-points for ice and water, and are sensitive to changes in the physical temperature of the surface and weather filters (Comiso et al., 1997). Ice concentration products used in this study are based on 11 different algorithms and are listed in Table 2.

2.4 Snow depth

Our knowledge of snow depth on top of Arctic sea ice is limited. Snow depth can be measured directly in the field but these measurements are limited to field campaigns in a local area during a couple of weeks. The most comprehensive compilation of in-situ data so far is based on man-

Table 2: Different assumptions on sea ice density as used in this study to assess the possible range of sea ice thickness.

Acronym	Sea Ice Density [$\mathrm{kgm^{-3}}$]		Description	used e.g. in
D1	916		typical value found for FYI	similar to Laxon et al. (2003) and Alexandrov et al. (2010)
D2	925		density of ice containing brine inclusions	Kwok et al. (2009b) (JPL data set)
D3	882		density of ice containing air inclusions typical value found for MYI	Alexandrov et al. (2010)
D4	900		mean value	
	FYI	MYI		
D5	916	882		Laxon et al. (2013)
D6	916	882	weighted by MYI fraction in each pixel	

made observations taken during soviet drifting stations between 1954 and 1991. Warren et al. (1999, W99 here after) created a climatology of monthly snow depth by fitting a two-dimensional quadratic function for each month independently of the year. The mean winter (October–April) snow depth from W99 is shown in Fig. 1 as thin contour lines. Because MYI was the dominating ice type during those decades, the climatology represents snow depth on MYI.

Another way to obtain information about snow depth on a basin wide scale are retrievals from passive microwave sensors (Markus and Cavalieri, 1998). In this case snow depth is calculated using the spectral gradient ratio of the 18.7 GHz and 37 GHz vertical polarization channels. In our study we use the data sets based on AMSR-E (Markus and Cavalieri, 2008) for which the algorithm is applied over FYI. Evaluation studies found the retrieval to be accurate over smooth first year ice, while over rougher FYI or MYI it needs further development (Markus et al., 2006; Brucker and Markus, 2013).

In our freeboard estimates we require that the freeboard should always be positive. Negative freeboard, as a result of e.g. ice flooding is common in Antarctica due to the large snow fall in that region (Lytle and Ackley, 2001), but this has not been observed to a large degree in the Arctic. We therefore replaced the snow depth with the freeboard value in the cases where the snow depth was larger than the freeboard.

3 Methods

To combine the data sets we described above, we re-gridded them following a polar stereographic projection on a 25 km grid. For snow depth we used the mean value of the two periods, in fall and late winter (see Table 1) when freeboard measurements were available. For sea ice area we used the mean over each ICESat period and for the MYI fraction the mid-day of each ICESat period. As the export of MYI is only about 10 % each year (Smedsrud et al., 2011) we believe that the change in MYI fraction is slow enough to allow for this simplification.

ICESat has an orbit inclination of 94°, hence for a considerable percentage of the Arctic Ocean, no freeboard measurements are available. To fill this data gap we use the MYI fraction around the hole as a proxy for sea ice thickness. For each ICESat period, we fitted a 3rd order polynomial to the values of sea ice thickness and MYI fraction 2 degrees around the data hole, and used this function to derive information about sea ice thickness within the hole. A similar method has previously been used by Kwok et al. (2009b) and provides a simple way to get an estimate of sea ice thickness and volume on a basin-wide scale. Other data gaps, mostly occurring in the shelf areas, have been filled similarly, using the fraction of MYI in the adjacent pixels. As done in previous studies, all results presented in our analysis are restricted to the "ICESat domain" which does not include the Canadian Archipelago, Fram Strait, Bering, Barents and Kara Sea.

3.1 Sea ice thickness estimates

To convert sea ice freeboard measurements from ICESat into sea ice thickness a number of assumptions have to be made. The first major assumption is that sea ice floats in hydrostatic equilibrium, which results in the following equation for the sea ice thickness (SIT):

$$SIT = f_{is} \cdot \frac{\rho_\mathrm{w}}{\rho_\mathrm{w} - \rho_\mathrm{i}} + h_\mathrm{s} \cdot \frac{\rho_\mathrm{s} - \rho_\mathrm{w}}{\rho_\mathrm{w} - \rho_\mathrm{i}} \quad (1)$$

where f_{is} is the snow-ice freeboard as retrieved from ICESat, h_s is the snow depth, and ρ_w, ρ_s, and ρ_i are the densities of water, snow and ice, respectively. The thickness depends on the measured freeboard, and the snow and sea ice properties. For ρ_w we use a value of $1024\,\mathrm{kgm^{-3}}$ and for ρ_s $270\,\mathrm{kgm^{-3}}$ in October/November and $330\,\mathrm{kgm^{-3}}$ in February/March, following Warren et al. (1999). To investigate the influence of ρ_i and h_s on sea ice thickness estimates on a basin-wide scale we analyse a number of data sets for these two parameters as described below in Sects. 3.2 and 3.3.

Equation (1) describes the "true" sea ice thickness, which is the averaged thickness of the ice in a certain area. An observer on the ice would think this is the most meaningful

Table 3: Different assumptions on snow depth as used in this study to assess the possible range of sea ice thickness due to snow depth.

Acronym	Snow Depth FYI	Snow Depth MYI	Description	used e.g. in
S1	W99	W99	snow taken from climatology W99	Laxon et al. (2003), Giles et al. (2008)
S2	W99/2	W99		Laxon et al. (2013)
S3	W99/2	W99	weighted by MYI fraction in each pixel	
S4	AMSR-E	W99	snow depth retrieval from AMSR-E used over FYI	
S5	0	0	lowest possible value	

value of ice thickness. We also analyse the effective sea ice thickness, which is defined as the mean sea ice thickness including open water areas. We use the sea ice concentration to account for the open water in each pixel and compute the effective sea ice thickness as following:

$$SIT_{eff} = SIT \cdot SIC[0,1] \quad (2)$$

where SIT_{eff} is the effective sea ice thickness, SIT is the sea ice thickness as described in Eq. (1), and SIC is the sea ice concentration. This is the most common diagnostic in current sea ice models in which sea ice mainly grows thermodynamically and rather homogeneously over a grid cell.

3.2 Density scenarios

The density of sea ice depends on the amount of brine and air inclusions, and therefore on temperature and sea state during formation and the age of the ice. Ice containing no salt is expected to have a density of 916 kgm^{-3}. Newly frozen FYI, however, contains a substantial amount of salt water that increases the sea ice density. Concentrated sea water with a salinity higher than 35 is termed brine, and brine salinities can reach values up to 100 depending on the sea ice temperature. In course of time the brine drains out and is replaced by air. Density of MYI is thus expected to be lower than that of FYI, in particular in the freeboard part above water level, and values vary largely among sources (e.g Timco and Frederking, 1996; Kovacs, 1996; Alexandrov et al., 2010; Forström et al., 2011). To investigate and visualize the influence of sea ice density on sea ice thickness we explored different values ranging from 882 kgm^{-3} to 925 kgm^{-3} (see Table 2). We first assumed the sea ice density to be the same over the entire Arctic (D1–D4), and second we varied the sea ice density dependent on ice type (D5 and D6). For the second approach, we chose the ice type either by a binary classification (D5) or by accounting for the fraction of MYI per pixel (D6).

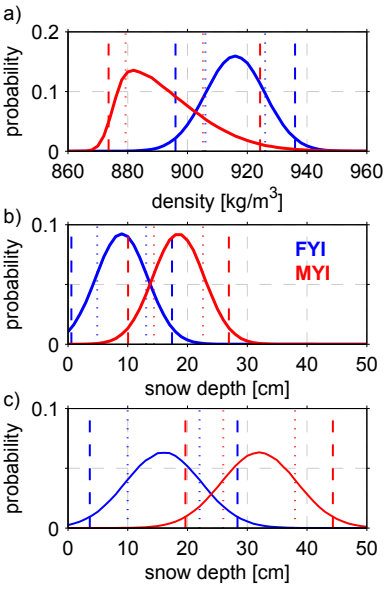

Fig. 2: Probability distributions for sea ice density and snow depth. Distributions are shown separately for First-Year-Ice (FYI) and Multi-Year-Ice (MYI). a) mean sea ice density, b) mean snow depth in October-November and c) mean snow depth in February-March. Snow depth over MYI is based on climatological values from W99, and 50% of these snow depth is used over FYI. Dotted lines indicate the first standard deviation (15 and 85 percentile) and dashed lines the second standard deviation from the mean (2.3 and 97.7 percentile).

3.3 Snow depth scenarios

To assess the influence of snow depth on sea ice thickness estimates we used the snow depth retrieval from AMSR-E, and the W99 climatology. Additionally we used a modification of W99 based on results from airborne measurements of

snow depth. Evaluating snow depth data from the Operation IceBridge campaigns, Kurtz and Farrell (2011a) found that snow load is reduced by 50 % over FYI compared to climatological values of W99. An overview of our selected values is presented in Table 3. As for the ice density we either used the same assumption over FYI and MYI (S1 and S5) or used different assumptions for the two ice types (S2–S4). Snow depth weighted by MYI fraction (S3) has been calculated as follows:

$$H_s = \mathrm{W99} \cdot (0.5 + 0.5 \cdot MYI_{fraction}) \quad (3)$$

where W99 is snow depth based on climatological values from Warren et al. (1999). The AMSR-E product is available over FYI but, the classification of sea ice type used is different from our approach. Therefore the pixels considered as FYI are slightly different than based on the MYI fraction derived from QuikSCAT.

3.4 Monte-Carlo approach to calculate uncertainty

The uncertainties of sea ice volume and thickness are calculated using a Monte-Carlo approach. This is a probabilistic method based on repeated calculations of the results, using input parameters changed by a random selection from their probability distributions. Parameters and their uncertainties are therefore not simply treated as a mean value and its standard deviation, but for each input parameter real data, algorithms and distributions are used. In our study the result is the effective sea ice thickness (or sea ice volume) and the input parameters are sea ice area, density and snow depth. For sea ice area we assume each of the eleven algorithms to be equally likely (distribution not shown). The assumed PDFs of snow depth and sea ice density are shown in Figure 2 and are described in detail in the paragraphs bellow. To calculate total uncertainties we iterate simultaneously through the PDFs of all three parameters accordingly to their respective PDF. To calculate the uncertainty coming from a single parameter we iterate through the PDF of this parameter and keep the other two fixed at the mean value. As the cross-correlation between the parameters is not well understood, it is not included in our approach. Spatial auto-correlation for each parameter is included by varying the parameters Arctic wide for each Monte Carlo run, or accordingly to its sea ice type.

The PDF of snow depth follows the W99 climatology over MYI and is reduced by 50 % over FYI. For the standard deviation of the distributions we use the reported inter-annual variability from the W99 climatology, of i.e. 4.3 cm in October/November and 6.2 cm in February/March. This is consistent with uncertainties found for the AMSR-E retrieval (Brucker and Markus, 2013), so we believe that our assumptions are still conservative. In Fig. 2 we show separate distributions for MYI and FYI for visualization, but in reality the correlation between snow depth on FYI and MYI has to be considered. For each Monte-Carlo calculation we therefore picked one random value from the MYI distribution and took half of this value for the FYI. For the campaign in spring 2007 we used a PDF which was one centimeter higher then shown in Fig. 2, because the campaign took place in March/April. Because snow depth can not be negative we set a lower bound at 0 cm.

For the PDF of sea ice density we also assumed different values for FYI and MYI. For FYI we assumed a mean value of 916 $\mathrm{kgm^{-3}}$ and a standard deviation of $\pm 10\,\mathrm{kgm^{-3}}$ which is smaller than reported in other studies (Alexandrov et al., 2010; Forström et al., 2011). For the Monte-Carlo-approach we seek a value that would correspond to a basin-wide average over a number of years, while the reported values are based on field observations from a local area and a given time. For the MYI density we assume a slightly skewed distribution as MYI generally includes areas of FYI, both from bottom freezing and refrozen leads, and literature values vary widely among sources. The mode of the density distribution is 882 $\mathrm{kgm^{-3}}$, while the mean is slightly higher, i.e. 890 $\mathrm{kgm^{-3}}$.

4 Results

In this section we first illustrate the influence of selected values for density and snow depth on the sea ice thickness estimates. We further show uncertainties in effective sea ice thickness due to sea ice area, density and snow depth, and how they are distributed over space and time. Finally we use these estimates to calculate the total sea ice volume and its uncertainties, and show implications for reported trends in sea ice volume.

4.1 Sea ice density influence on sea ice thickness

Mean sea ice thickness calculated over the whole Arctic basin using different assumptions on sea ice density is shown in Fig. 3. The assumptions are listed in Table 2. The same snow depth was used for all calculations, and corresponds to climatological values from W99 over MYI, and half of the values over FYI weighted by MYI fraction per pixel (S3 in Table 3).

We show that the mean sea ice thickness is strongly influenced by the choice of sea ice density, while the trend and the annual cycle are hardly affected. The resulting mean values in October/November range between 1.39 m and 2.00 m. At the end of winter, in February/March sea ice thickness has increased and ranges between 1.53 m and 2.20 m. Because the influence of sea ice density increases with sea ice thickness, we found the range to be smaller for FYI (about 55 cm), and larger for MYI (about 80 cm). The difference in sea ice density due to different sea ice classification methods, only influences the mean sea ice thickness by a few centimeters, and the difference between D5 and D6 in Fig. 3 is too small to be visible.

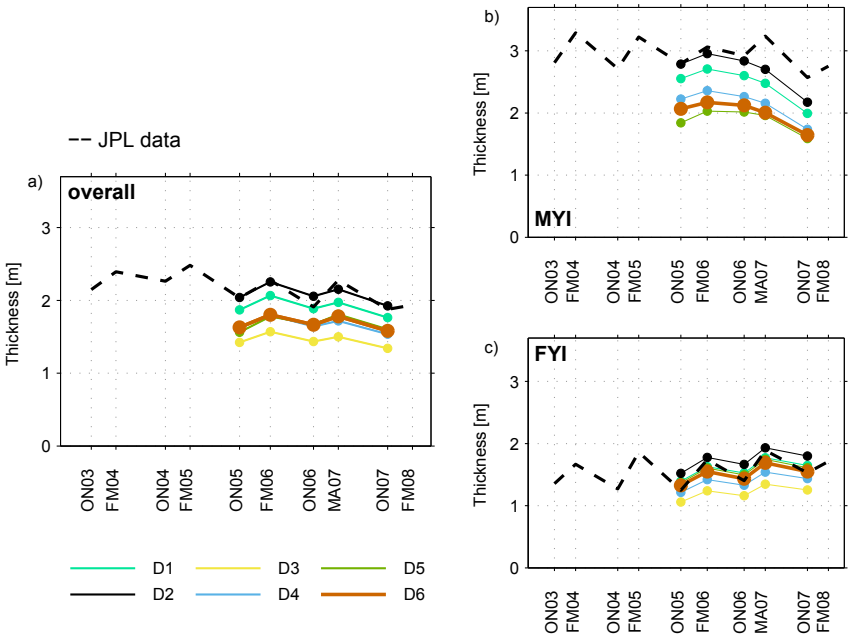

Fig. 3: Spatially averaged Arctic sea ice thickness calculated with different values for ice density. In a) the total mean thickness is shown, in b) the thickness of Multi-Year Ice (MYI) and in c) the thickness of First-Year Ice (FYI). Density values used are described in section 3.2 and can be found in table 2. The brown line (D6) is the same as S3 in Fig. 5.

The trend in FYI and MYI thickness is diametric: While thickness of MYI is decreasing over the period (Fig. 3b) the thickness of FYI is increasing (Fig. 3c). A number of processes could contribute to such an increase in thickness and we will come back to these in the discussion section.

From October/November to February/March the FYI thickness increases by about 0.25 m, representing "normal winter growth" over areas that were open water in the beginning of the freezing season. However it is surprising and rather counter-intuitive to see that the mean thickness of MYI does not increase between October/November 2006 and February/March 2007 (Fig. 3b). To get more insight into this peculiarity and the inter-annual variability we proceed with analyzing the impact of snow depth on the mean sea ice thickness estimates.

4.2 Snow depth estimates over Arctic sea ice

Figure 4 compares the climatology from W99 representing snow depth on MYI, and the snow depth retrieval from AMSR-E over FYI. Based on the W99 climatology the mean snow depth on the Arctic sea ice increases from near zero in August to a maximum in spring. The accumulation rate is as high as $5\,\mathrm{cm month}^{-1}$ from August to January, before lowering to about $2\,\mathrm{cm month}^{-1}$ until March. The snow increases somewhat further until May, before solar radiation is strong enough to melt the snow in June and July. At the end of summer only a few cm of snow are left. The inter-annual variability in the W99 climatology ranges from 3–8 cm, and is largest in the winter period.

Based on the AMSR-E snow depth retrieval the snow accumulation over the winter season has a similar shape, with a maximum in late winter, in phase with the W99 climatology. The accumulation rate, however, is much lower and the maximum value of about 19 cm is only 54 % of the climatological value from W99. One can speculate, that this is not only a result of snow falling into water, but is additionally caused by changed atmospheric conditions and a reduction in snow fall (Screen and Simmonds, 2012). These might also have influenced the snow depth on MYI and can explain some of the peculiarities mentioned in the previous section. The absence of MYI thickening between Oc-

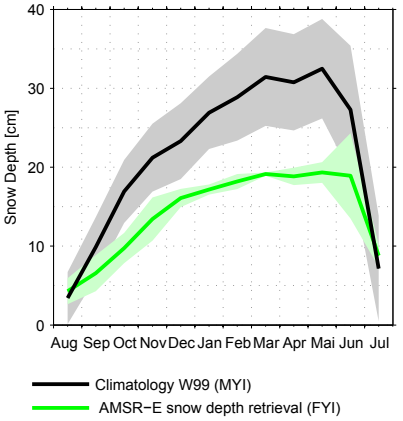

Fig. 4: Annual evolution of the spatially averaged snow depth on the Arctic sea ice. The spatial pattern is shown in Fig. 1, and the W99 climatology is based on observations between 1954 and 1991 on Multi-Year-Ice (MYI). The AMSR-E snow depth retrievals cover First-Year-Ice (FYI) and is averaged for the IceSat period between 2003 and 2008. For both data sets the standard deviation is plotted around the mean value of any given month.

tober/November 2006 and February/March 2007 (Fig. 3b) could partly be explained by an overestimation of snow depth in February/March, which results in an underestimation of sea ice thickness. More information about the influence of snow depth on sea ice thickness estimates is given in the next section.

4.3 Snow depth influence on sea ice thickness

Mean sea ice thickness calculated from ICESats' freeboard observations over the whole Arctic ocean using different assumptions on snow depth is shown in Fig. 5. The different assumptions are given in Table 3. For sea ice density we used the ice-type-dependent method (D6 in Table 2) weighted by MYI fraction per pixel.

Mean sea ice thickness in October/November ranges between 1.28 m and 2.45 m, but goes down to 1.62 m if we exclude the "no snow" assumption, which is unrealistic but still considered as a reference. In February/March the mean sea ice thickness ranges between 1.33 m and 3.00 m, or 1.79 m if the no-snow assumption is left out. The effect of sub-grid scale variability of snow depth due to sea ice type is about a few cm only (compare S2 and S3 in Fig. 5), which is similar to the results found for the sub-grid scale variability of ice density (Fig. 3).

Using climatological snow depth from W99 for FYI we found no increase in sea ice thickness in the winter season (S1 in Fig. 5). This is a counter intuitive and an unrealistic result, indicating that the W99 snow depth needs revision, as sea ice is indeed expected to increase in thickness during an Arctic winter. Reducing the climatological values from W99 by half or using available passive microwave retrievals from AMSR-E over FYI results in a increase of winter growth to about 40 cm (S2–S4 in Fig. 5).

For MYI we can only use the W99 climatology for snow depth as no other data sets are available. The resulting spread in Fig. 5b is due to the different MYI classifications in the retrievals. As mentioned above, the absence of MYI thickening between October/November 2006 and February/March 2007 (Fig. 3b), could be a result of an overestimation of snow depth in February/March.

4.4 Spatial distribution and absolute uncertainties

So far we have shown the range of spatially averaged sea ice thickness estimates over the Arctic Ocean as the results of different selected values for sea ice density and snow depth. To get more insight into how the uncertainties in ice density, snow depth and sea ice area contribute quantitatively to the total uncertainty in the sea ice thickness estimates, we introduce results from the Monte-Carlo approach. As the sea ice area is considered now, the results represent uncertainties in the effective sea ice thickness. The single uncertainties are calculated keeping two of the parameters fixed at the mean values, while varying the third according to the PDFs shown in Fig. 2. We used the MYI fraction in each pixel when calculating the ice type dependent values for sea ice density and snow depth (see Eq. 3).

Averaged absolute uncertainties and the contributions from sea ice density, snow depth, and sea ice are shown in Fig. 6. Mean absolute uncertainty of effective sea ice thickness is close to ± 0.25 m for each ICESat campaign. It is smaller in October/November (± 0.21 m) than in February/March (± 0.28 m), and we found snow depth to be the largest contributor to the total uncertainties with up to 70 %. Ice density contributes with 30–35 % with higher values in October/November due to the small snow cover at that time of year. The area contribution also increase in October/November but remains below 10 %.

The spatial distributions of these uncertainties in absolute values and their relative contribution to the total uncertainties are shown in the maps of Fig. 6. We show only results for October/November but the spatial distribution of uncertainties are very similar in winter. Overall, the absolute uncertainty resulting from sea ice density is around 0.1 m to 0.2 m for FYI, with uncertainties increasing for the thicker sea ice between the North Pole and Greenland (Fig. 6a). The transition from FYI to MYI also marks the transition from the smaller to the larger uncertainties, stemming from the larger uncertainty in density for MYI that we assumed in our analysis

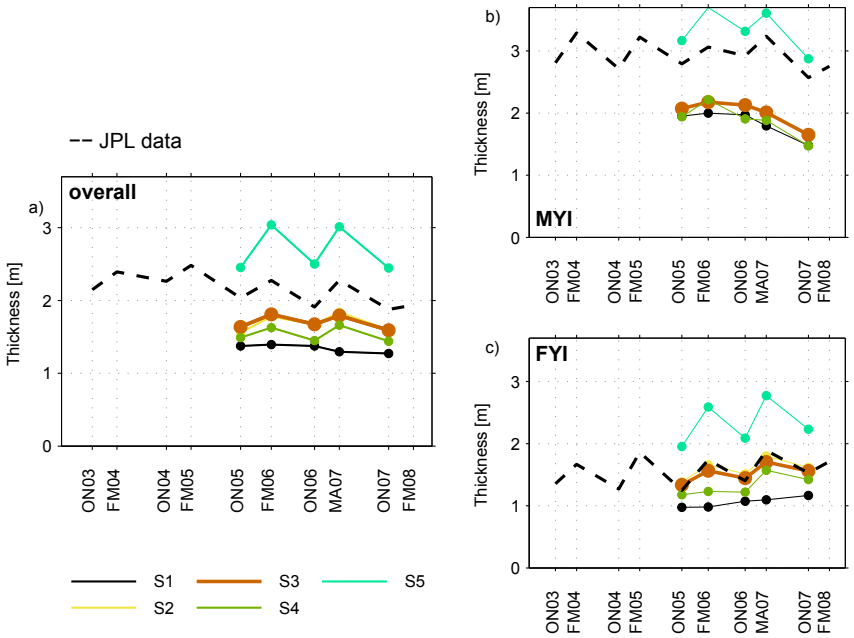

Fig. 5: Spatially averaged Arctic sea ice thickness calculated with different assumptions on snow depth. In a) the total mean thickness is shown, in b) the thickness of Multi-Year Ice (MYI) and in c) the thickness of First-Year Ice (FYI). Values are based on available data sets described in section 4.2, and can be found in table 3. The brown line (S3) is the same line as D6 in Fig. 3.

(see Fig. 2). For MYI the uncertainties in the sea ice thickness estimates resulting from sea ice density are therefore up to 70 %, while over FYI its relative contribution remains mostly below 40 %.

The absolute uncertainties resulting from uncertainties in snow depth show a similar pattern, with smaller values for thin FYI (from 0.1 m) and increasing for the thicker part between the North Pole and Greenland to 0.25 m. The relative contribution from uncertainties in snow depth accounts for only about 40 % of the total uncertainty for the MYI but up to more than 70 % for FYI.

Uncertainty in effective sea ice thickness resulting from the different sea ice area algorithms is less than 5 % or 10 cm (Fig. 6c). This is caused by the high ice concentrations inside our selected Arctic Ocean area of interest (Fig. 1). When ice concentrations approach 100 %, there is little difference between the algorithms, and the related uncertainties become small. Some larger values are visible in Fig. 6c in the marginal ice zone north of Svalbard and in the vicinity of the Bering Strait. In these locations the uncertainties in sea ice area drive the relative uncertainty in effective thickness up to 60 %. However, in this regions the sea ice is very thin and concentrations are low, the large values therefore hardly contribute to the uncertainty in mean effective sea ice thickness and volume (Fig. 7).

4.5 Sea ice volume uncertainties

The evolution of sea ice volume over time and the related uncertainties calculated using a Monte-Carlo approach are shown in Fig. 9. We estimate the mean Arctic sea ice volume between 2005 and 2007 to be $10120 \pm 1280\,\mathrm{km}^3$ in October/November, and to increase to $13250 \pm 1860\,\mathrm{km}^3$ in February/March (see green curve in Fig. 9).

The ice volume in October/November 2007 stands out as a major anomaly, following the steady reduction in MYI for the length of our record, and a large decrease in FYI volume since February/March 2007. The loss of FYI ice volume from February/March 2007 to October/November is more than 50 % or about $4700\,\mathrm{km}^3$. This is especially remarkable as FYI volume actually increased from October/November 2005 until February/March 2007. In Octo-

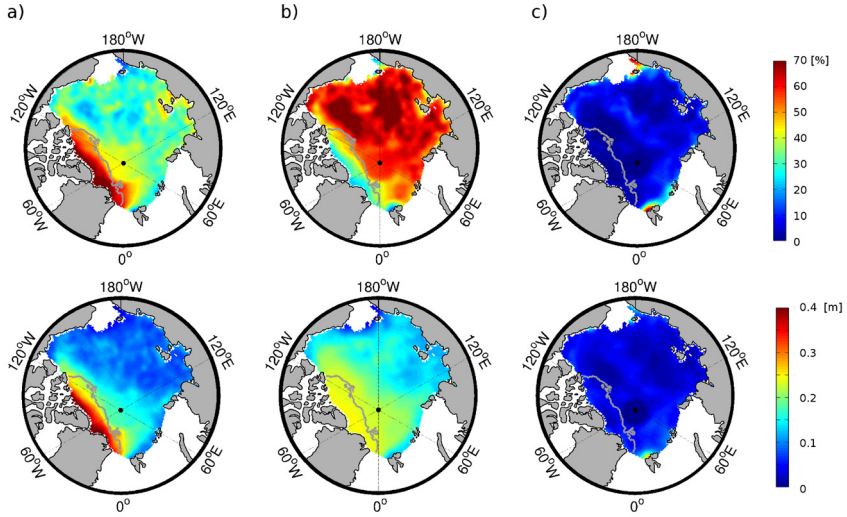

Fig. 6: Spatial distribution of uncertainties in effective sea ice thickness in October-November as a result of uncertainties in a) sea ice density b) snow depth and c) sea ice area. The gray contour line indicates 50 % Multi-Year-Ice fraction. In the upper line relative values of the total uncertainties are shown, and in the lower line absolute values of uncertainty.

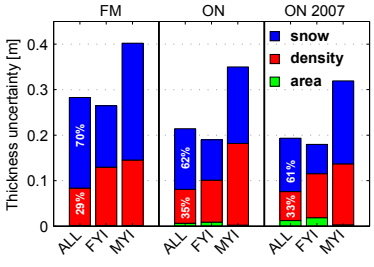

Fig. 7: Absolute uncertainties of the effective sea ice thickness. Contributions from uncertainties in sea ice density, snow depth, and sea ice area are included and given for the the mean in February-March (FM) and October-November (ON). Additionally October-November 2007 (ON07) is shown separately. Note that the distributions of sea ice density and snow depth are non-gaussian for the total sea ice (see PDFs in Fig. 2) and therefore the contributions from the three parameters over First-Year-Ice (FYI) and Multi-Year-Ice (MYI) do not sum up for the total sea ice thickness (ALL).

ber/November 2005 MYI was the dominant ice type, but has lost almost 50 %, or $\sim 3000\,\mathrm{km}^3$ of its volume until 2007. Because of this decrease, relative uncertainties in sea ice volume are increasing, and exceed 30 % at the end of the analysis period.

Absolute uncertainties and the relative contributions arising from uncertainties in sea ice density, snow depth and sea ice area are shown in Fig. 8. In February/March 73 % of the uncertainty is caused by uncertainties in snow depth. The snow contribution reduces to 55 % in October/November because of the thinner snow cover during this time of the year, similar to the absolute uncertainties for thickness (Fig. 7). Density thus plays a larger role during October/November but remains smaller than uncertainties resulting from uncertainties in snow depth. The sea ice area contribution is visible in October/November, but remains small throughout. This is however dependent on the area covered by sea ice, and particularly visible in October/November 2007 when it increases to around 5 %.

5 Discussion

We have calculated uncertainties in the estimates of Arctic sea ice thickness and volume. The uncertainties represented in this study arise from three different parameters that are set

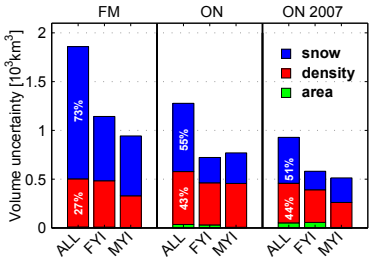

Fig. 8: Absolute uncertainties in Arctic sea ice volume. Contributions from uncertainties in sea ice density, snow depth, and sea ice area are included and given for the the mean in February-March (FM) and October-November (ON). Additionally October-November 2007 (ON07) is shown separately. Note that the distributions of sea ice density and snow depth are non-gaussian for the total sea ice (see PDFs in Fig. 2) and therefore the contributions from the three parameters over First-Year-Ice (FYI) and Multi-Year-Ice (MYI) do not sum up for the total sea ice volume (ALL).

up when estimating sea ice thickness and volume: sea ice density, snow depth and sea ice area. Below we will first discuss the findings for sea ice thickness and its uncertainties and then discuss our results for sea ice volume, its uncertainties, and implications for its recent trend.

5.1 Sea ice thickness

We found that the choice of sea ice density significantly changes the estimated mean sea ice thickness. Our mean sea ice thickness ranges from 1.45 m to 2.09 m using a range for sea ice density in accordance with the values seen in the literature. While the density affects the mean sea ice thickness, the snow depth affects its annual cycle and the inter-annual variability. The W99 snow depth climatology results in a underestimation of winter growth and indicates that the climatology is outdated, also over MYI.

The range of densities we used captures the real ice density, but it remains an unresolved issue whether the density has changed, or will be changing, due to a change in sea ice type over the Arctic Ocean, or due to changing weather conditions like warming temperatures and later ocean freeze-up. The snow depth has already been affected by these changes (Hezel et al., 2012; Kurtz and Farrell, 2011a), and our study confirms that the climatological values from W99 do not represent the current snow conditions over the Arctic sea ice.

Absolute changes in snow depth do not have to be considered solely, but to derive accurate estimates for sea ice thickness, it is additionally important to capture its inter-annual variability. Passive microwave retrievals seem to be reliable over smooth FYI and have been found to be within $\pm$ 0.05 m of snow depth measurements from the Operation Ice Bridge (Brucker and Markus, 2013). For large snow depths and rougher surfaces the uncertainties may however be larger (Markus et al., 2006). With thinning of the sea ice comes weakening and increased deformation (Rampal et al., 2009), so the retrievals may actually become less accurate in the future. Over MYI, the lack of more recent and accurate snow depth retrievals remains an issue, and explains why we have used the climatological values from W99 for this ice type in all our analysis. Recently, a new snow depth algorithm for thick ice has been developed (Maaß et al., 2013), based on brightness temperatures from the longwave passive microwave radiometer on-board SMOS. The algorithm requires more validation, but first results show very good agreement with airborne campaigns. The second way to retrieve information about snow depth on Arctic sea ice is to combine precipitation from atmospheric reanalysis and ice drift data from satellite products (used in e.g Kwok and Cunningham, 2008; Kurtz et al., 2011b). The accuracy of the reanalysis data depends on the model set up and the data assimilation method which is not always reliable over the Arctic ocean (Screen and Simmonds, 2011) and also varies significantly between different data sources (Bitz and Fu, 2008). Our results show that snow significantly affects the sea ice thickness estimates and an accurate method to retrieve snow depth will be essential to derive absolute values and trends in sea ice thickness in the future.

Using the Monte-Carlo approach we estimate the mean absolute uncertainty of effective sea ice thickness to be $\pm$0.21 m in October/November and $\pm$0.28 m in February/March. Previous studies estimate the uncertainty in sea ice thickness to be e.g. 0.5 m (Kwok et al., 2009b), 0.7 m (Kwok and Rothrock, 2009a), 0.76 m (Giles et al., 2007) or 0.93 m (Forström et al., 2011). In all these studies the uncertainty has been calculated with the variance formula, which is the common method to calculate uncertainties from uncorrelated parameters. The difference to our uncertainty estimates can be explained by two main reasons: Our uncertainty estimates are for effective sea ice thickness and we did not include uncertainties resulting from freeboard and snow density. Freeboard has been found to be the main source of uncertainty and by not including it we clearly underestimate the uncertainties in sea ice thickness. However, the results are consistent with our findings, that besides the freeboard, the snow depth is the main source of uncertainty. The different values found in the mentioned studies result from different assumptions made on the uncertainties of single parameters. In particular, there is large disagreement in the influence of snow density into the total uncertainty, ranging from 1 cm (Giles et al., 2007) to more then 20 cm (Kwok and Rothrock, 2009a).

Sea ice thickness can also be estimated with sea ice models, which are an important tool to understand and predict the state of Arctic sea ice. Evaluating results from the Pan-Arctic Ice-Ocean Modeling and Assimilation System (PI-

OMAS) Schweiger et al. (2011) found a bias to the ICESat derived sea ice thickness estimates from JPL of 0.26 m in fall and 0.1 m in spring. In spring this bias is within the range of our uncertainties while in fall it is slightly larger than uncertainties found in our study. Our analysis provides some possible explanation for the discrepancies found between the sea ice thickness estimates from ICESat and PIOMAS. Schweiger et al. (2011) found a larger difference between the two data sets north of Greenland and the Canadian Archipelago than in other areas, with ICESat giving values around 0.7 m larger than results from PIOMAS. As estimates from PIOMAS agree better with in-situ data in this area, they hypothesized that ICESat retrievals may overestimate the sea ice thickness in this area of the Arctic ocean. A part of this discrepancy could be explained by the choice of sea ice density. In the data set from JPL the sea ice density is chosen to be 925 kgm^{-3} and reducing it to 882 kgm^{-3} lowers the sea ice thickness about 0.5 m (see Fig. 3). This explanation is supported by the apparently lower difference between sea ice thickness estimates from PIOMAS and CryoSat-2 (Laxon et al., 2013), where the reduced value for sea ice density has been used to convert freeboard into thickness. More comparison, however, is needed for verification.

5.2 Sea ice volume

We calculated the sea ice volume for the three years between 2005 and 2007 with a Monte-Carlo approach using probability distribution functions for sea ice density, snow depth and area as described in Sect. 3.4. We estimate a mean sea ice volume of $10120 \pm 1280\,\mathrm{km}^3$ (12.7 %) in October/November, increasing to $13250 \pm 1860x\,\mathrm{km}^3$ (14 %) in February/March. In February/March snow depth accounts for more than 70 % of the uncertainty. In October/November, when snow depth is lower, the density becomes more important and accounts for 43 % of the total uncertainty.

These large uncertainties resulting from sea ice density can be illustrated using the selected values for the density as described in Sect. 3.2. Using a sea ice density of 925 kgm^{-3} as done in the JPL data set (see line 2 and 3 in Table 4 and green dashed line in Fig. 9) increases the sea ice volume by 15 % on a yearly average. Using values of 882 kgm^{-3} and 916.7 kgm^{-3}, as done in Laxon et al. (2013) for the CryoSat-2 data, produces a sea ice volume about 5 % smaller than our Monte-Carlo based volume estimates (see green dotted line in Fig. 9 and line 4 in Table 4).

ICESat data have been freely available and have therefore been analyzed in many studies (e.g. Spreen et al., 2006; Kwok and Cunningham, 2008; Farrell et al., 2009; Kurtz et al., 2011b; Schweiger et al., 2011). Only a minority of them, however, conducted detailed calculations of uncertainties and errors. A detailed but completely different approach to calculate the uncertainty in sea ice volume based on ICESat data was used by Kwok et al. (2009b). The uncertainty was calculated as the sum of uncorrelated errors for each pixel: $\sigma_\mathrm{T} = N^{1/2}(A_\mathrm{c}^2\sigma_\mathrm{h}^2 + h^2\sigma_{A_\mathrm{c}}^2)^{1/2}$, where σ_h and σ_{A_c} are the uncertainties in cell thickness (h) and cell area (A_c), σ_T uncertainties in total thickness, and N the number of grid cells. Assuming an error of 0.5 m for sea ice thickness, the resulting sea ice volume uncertainty in this study was given as 33 km^3. This approach is valid for uncertainties in sea ice thickness stemming from uncorrelated errors, and as stated by Kwok et al. (2009b), should be considered as best case scenario. In our analysis we did not account for such uncorrelated errors, but uncertainties resulting from the mean values of snow depth, sea ice density and area. The uncertainties in these geophysical parameters should be understood more as a bias - not as uncorrelated errors. This explains why our ice volume uncertainty becomes as high as $\pm 1860\,\mathrm{km}^3$ in February/March, a value 56 times higher than the uncertainty calculated by Kwok et al. (2009b). In the future more work needs to be done to analyse to which extent parameters and their uncertainties are correlated and to which extent retrieval errors are indeed random as assumed by Kwok et al. (2009b). Both would lower the estimates of uncertainty. However considering the lack of current knowledge on the absolute values, our uncertainty estimates can be assumed to be in the right range.

A bias in sea ice thickness as measure of uncertainty that propagates into the estimates of uncertainty in sea ice volume has been previously used to assess uncertainties in modeled Arctic sea ice volume with PIOMAS (Schweiger et al., 2011). This is comparable to the uncertainties in our studies, and the resulting uncertainties in sea ice volume of 6.3 % in spring and 10 % in fall are of the same order (14 % and 12.7 % in our study for the two season, respectively). While Schweiger et al. (2011) used the differences between model results and validation data to identify the bias, in this study we provide additional physical insight, quantifying uncertainties resulting from geophysical parameters such as area, snow depth and sea ice density.

5.3 Implications for trends in sea ice volume

The calculated uncertainties have implications on trends in sea ice volume. Our time series of ICESats' freeboard measurements from NSIDC is rather short, ranging from 2005 to 2007, which is admittedly too short to allow for robust calculations of trends. We therefore applied our calculated uncertainties of 12.7 % in February/March and 14 % in October/November to the longer time series processed at JPL (Kwok and Cunningham, 2008). Using a weighted regression to account for the obtained uncertainties (weighted by $1\,\mathrm{std}^{-2}$), we calculate a trend of $-1450 \pm 530\,\mathrm{km}^3\mathrm{a}^{-1}$ in October/November and $-880 \pm 260\,\mathrm{km}^3\mathrm{a}^{-1}$ in February/March. The calculated trends are close to previous findings from Kwok et al. (2009b) of $-1240\,\mathrm{km}^3\mathrm{a}^{-1}$ in October/November and $-860\,\mathrm{km}^3\mathrm{a}^{-1}$ and February/March, respectively.

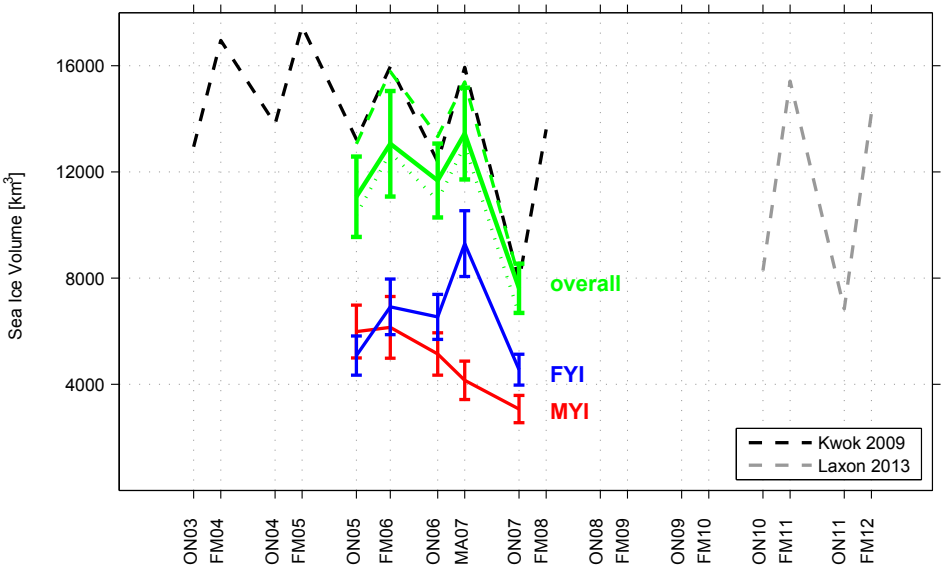

Fig. 9: Sea ice volume and its uncertainties calculated with different methods. For comparison ICESat results based on sea ice thickness data from JPL are included as a black dashed line, and CryoSat-2 values (Laxon et al., 2013) as the gray dashed line.

ICESat operated until 2008, and efforts to produce long-term trends by merging ICESat data with recent CryoSat-2 data is ongoing. Laxon et al. (2013) produced the first estimates and concluded on a loss of ice volume in October/November of 4290 km^3 between the mean of the ICESat period (2003–2008) and the CryoSat-2 period (2010–2012), which is a loss of about 36 %. In February/March they estimated a smaller loss of about 1480 km^3. In Table 4 we compare our results to the ICESat values from JPL (Kwok and Cunningham, 2008) and CryoSat-2 values from Laxon et al. (2013) illustrating the importance of the density estimate. Despite a consistent long-term change between ICESat and CryoSat-2 there are also differences that can be elucidated by our new results on uncertainties. The main difference is the high density of 925 kgm^{-3} in the JPL dataset used when converting freeboard measurements to thickness, compared to the values of 882 kgm^{-3} and 916 kgm^{-3} used by Laxon et al. (2013) for CryoSat-2. Adjusting the values for sea ice density in the ICESat period accordingly (see Table 4) allows for a more consistent comparison between the ICESat and CryoSat-2 periods. For the October/November this adjustment lowers the ice loss between the two periods considerably, and the ice loss becomes smaller than 2000 km^3, corresponding to a rate of $-390\,\mathrm{km}^3\mathrm{a}^{-1}$. For February/March we find that the Arctic ice volume has even increased from the end of the considered ICESat period 2007 up to March 2011.

Table 4: Sea ice volume as calculated in this study using different assumptions of the density in comparison with previous publications. Same values are given in Fig. 9.

Source	Volume [km^3] Oct–Nov	Feb–Mar
Monte-Carlo-Mean	**10 120**	**13 254**
JPL data 2005–2007[b]	**11 705**	**14 842**
$\rho_i = 925\,\mathrm{kgm}^{-3}$	**11 461**	**15 587**
$\rho_i = 916\,\mathrm{kgm}^{-3}$ & $882\,\mathrm{kgm}^{-3}$	**9312**	**12 870**
JPL data 2003–2008[b]	12 054	15 999
CryoSat 2010/11[a]	8283	15 424
CryoSat 2011/12[a]	6838	14 215

[a] Using $\rho_i = 916\mathrm{kgm}^{-3}$ for FYI and $882\,\mathrm{kgm}^{-3}$ for MYI.
[b] Using $\rho_i = 925\mathrm{kgm}^{-3}$.

The low loss, and in particular the increase, of sea ice volume between the ICESat and CryoSat-2 period is an interesting and somewhat surprising result, raising questions about the accuracy of our methods. Indeed, the increase in Febru-

ary/March may partly be an artifact due to the snow depth assumed and the differences in the measurement techniques. The ice freeboard from ICESat is measured using a laser whose signal is reflected from the snow–air interface, while the radar signal from CryoSat-2 is assumed to be reflected from the snow–ice interface. Hence for ICESat data, more snow results in thinner sea ice, while for CryoSat-2 more snow results in thicker sea ice estimate. As stated above, the W99 climatology is overestimating the snow depth on Arctic sea ice, not only over FYI (as previously found by Kurtz and Farrell, 2011a) but also over MYI. Therefore our estimates of ice thickness and volume from ICESat might be too low and estimates based on CryoSat-2 too high, which could artificially lead to the low loss, or increase, of ice volume between the two periods.

Sea ice thickness estimates from JPL (e.g. Kwok and Cunningham, 2008)) and Laxon et al. (2013) have been evaluated and agree well with independent in-situ data. Assuming that these data sets represent the real state of the Arctic sea ice it implies that there are large biases in the freeboard retrievals and these biases are mitigated by the choices made for sea ice density and snow depth. Biases can indeed be expected, in particular for CryoSat-2 due to preferential sampling of leads (Tonboe et al., 2010) or the unknown penetration depth of the radar signal into the snow layer (Willat et al., 2011). The evaluation data, however, are still highly limited in space and time, and do not cover all ice types and seasons. Therefore, more work is required to separate between the different, seasonally changing biases.

However, the moderate ice loss as found in our study in fall is consistent with synoptic airborne measurements during summer showing little change in sea ice thickness (Haas et al., 2010) and with satellite based retrievals showing a slight recovery of MYI fraction from 2008 till 2010 (Stroeve et al., 2012). On year-to-year timescales a temporal recovery of Arctic sea ice is indeed possible given e.g. an effective loss of insulation caused by the autumn snow ending in the ocean and not on the sea ice (Notz, 2009; Tietsche et al., 2011).

To get more robust results on long term trends, further evaluation of the freeboard retrievals, in particular from CryoSat-2, is needed and more reliable estimates of sea ice density and snow depth on the Arctic sea ice are necessary. Our results indicate a less dramatic decline of Arctic sea ice volume than reported in previous studies, but it is not possible to draw quantitative conclusions about changes in sea ice volume between the ICESat period (2003–2008) and the CryoSat-2 (2010–2012) period.

6 Conclusions

Remotely sensed observations of Arctic sea ice thickness and volume are available for the last decade. In accordance with documented loss of sea ice area over the last $30\,\mathrm{yr}$, available studies point to a dramatic loss of sea ice volume. We have shown here that such estimates of Arctic sea ice volume rest on a number of geophysical parameters that have influence on the overall mean, the year-to-year variability, and the trends. The overall uncertainties appear larger than previous studies suggest, and the dramatic ice loss appears smaller.

Despite the large number of algorithms available, and the associated uncertainties of ~ 1.3 million km^2, uncertainties in area do not carry on to the sea ice volume estimates in cold seasons over the Arctic Ocean. They become important when concentrations are well below $100\,\%$, like in the marginal ice zone, and may therefore become more important in the future, caused by the ongoing sea ice retreat in the Arctic.

The choice of the mean density used when converting ICESat derived freeboard measurements to sea ice thickness has a major influence on the resulting mean thickness, but does not alter the year-to-year variability. To obtain accurate estimates of changes in sea ice volume and thickness in the future, the change from mainly Multi-Year-Ice to First-Year-Ice and the corresponding changes in sea ice density also has to be considered.

The snow loading on top of Arctic sea ice greatly effects the estimated thickness and volume during the winter and is a likely driver for year-to-year variability. Our results indicate that climatological values from Warren et al. (1999) not only overestimate the snow load on First-Year-Ice compared to the present day climate, but also give incorrect values for Multi-Year-Ice.

The absolute uncertainty in mean effective sea ice thickness derived from the laser altimeter on-board ICESat is $0.28\,\mathrm{m}$ in February/March and 0.21 in October/November. The uncertainty in snow depth contributes up to $70\,\%$ of the total error, and the ice density 30–35 % with higher values in October/November.

We find large uncertainties in total sea ice volume and trend. For the total sea ice volume the mean is $10120 \pm 1280\,\mathrm{km}^3$ in October/November and $13250 \pm 1860\,\mathrm{km}^3$ in February/March for our time period from 2005 till 2007. We obtain a trend of $-880 \pm 260\,\mathrm{km}^3\,\mathrm{a}^{-1}$ in February/March and $-1450 \pm 530\,\mathrm{km}^3\,\mathrm{a}^{-1}$ in October/November in the ICESat period 2003–2008.

Our results still reveal a decline in sea ice volume between the ICESat (2003–2008) and the CryoSat-2 (2010–2012) periods, but less dramatic than reported in previous studies. However, final quantitative conclusions about a change of sea ice volume are hard to make, considering the large uncertainties and unresolved biases found in our study.

Acknowledgements. We thank the editor Ron Lindsay and two anonymous reviewers for their critical comments and suggestions which helped us to improve the quality of our paper. We also acknowledge Laurent Bertino for his help on the statistical methods used for this study and Timothy Williams for language corrections. We thank the National Snow and Ice Data Center, University of Colorado, Boulder, USA for providing the input data for the sea ice concentration algorithms. This work is supported by the Research

Council of Norway, through the projects CISAR no. 202313/V30 and the project ArcticSIV no. 207584.

References

Aagaard, K. and Carmack, E.: The role of sea ice and other fresh water in the Arctic circulation, J. Geophys. Res., 94, 14485–14498, 10.1029/JC094iC10p14485, 1989.

Alexandrov, V., Sandven, S., Wahlin, J., and Johannessen, O. M.: The relation between sea ice thickness and freeboard in the Arctic, The Cryosphere, 4, 373–380, 10.5194/tc-4-373-2010, 2010.

Bitz, C. M. and Fu, Q.: Arctic warming aloft is data set dependent, Nature, 455, 3–4, 10.1038/nature07258, 2008.

Brucker, L. and Markus, T.: Arctic-scale assessment of satellite passive microwave derived snow depth on sea ice using operation IceBridge airborne data, J. Geophys. Res., 118, 2892–2905, 10.1002/jgrc.20228, 2013.

Cavalieri, D. J., Gloersen, P., and Campbell, W. J.: Determination of sea ice parameters with the Nimbus 7 SMMR, J. Geophys. Res, 89, 5355–5369, 10.1029/JD089iD04p05355, 1984.

Cavalieri, D. J. and Parkinson, C. L.: Arctic sea ice variability and trends, 1979–2010, The Cryosphere, 6, 881–889, 10.5194/tc-6-881-2012, 2012.

Comiso, J.: Characteristics of Arctic winter sea ice from satellite multispectral microwave observations, J. Geophys. Res., 91, 975–994, 10.1029/JC091iC01p00975, 1986.

Comiso, J. C., Cavalieri, D. J., Parkinson, C. L., and Gloersen, P.: Passive microwave algorithms for sea ice concentration: a comparison of two techniques, Remote Sens. Environ., 60, 357–384, 10.1016/S0034-4257(96)00220-9, 1997.

Farrell, S., Laxon, S., McAdoo, D., Yi, D., and Zwally, H.: Five years of Arctic sea ice freeboard measurements from the Ice, Cloud and land Elevation Satellite, J. Geophys. Res., 114, C04008, 10.1029/2008JC005074, 2009.

Forström, S., Gerland, S., and Pedersen, C.: Thickness and density of snow-covered sea ice and hydrostatic equilibrium assumption from in situ measurements in Fram Strait, the Barents Sea and the Svalbard coast, Ann. Glaciol., 52, 261–271, 10.3189/172756411795931598, 2011.

Giles, K. and Hvidegaard, S.: Comparison of space borne radar altimetry and airborne laser altimetry over sea ice in the Fram Strait, Int. J. Remote Sens., 27, 3105–3113, 10.1080/01431160600563273, 2006.

Giles, K., Laxon, S., Wingham, D., Wallis, D., Krabill, W., Leuschen, C., McAdoo, D., Manizade, S., and Raney, R.: Combined airborne laser and radar altimeter measurements over the Fram Strait in May 2002, Remote Sens. Environ., 111, 182–194, 10.1016/j.rse.2007.02.037, 2007.

Giles, K., Laxon, S., and Ridout, A.: Circumpolar thinning of Arctic sea ice following the 2007 record ice extent minimum, Geophys. Res. Lett., 35, L22502, 10.1029/2008GL035710, 2008.

Haas, C., Hendricks, S., Eicken, H., and Herber, A.: Synoptic airborne thickness surveys reveal state of Arctic sea ice cover, Geophys. Res. Lett., 37, L09501, 10.1029/2010GL042652, 2010.

Hezel, P., Zhang, X., Bitz, C., Kelly, B., and Massonnet, F.: Projected decline in spring snow depth on Arctic sea ice caused by progressively later autumn open ocean freeze-up this century, Geophys. Res. Lett., 39, L17505, 10.1029/2012GL052794, 2012.

Kaleschke, L., Heygster, G., Lüpkes, C., Bochert, A., Hartmann, J., Haarpaintner, J., and Vihma, T.: SSM/I sea ice remote sensing for mesoscale ocean-atmosphere interaction analysis: ice and icebergs, Can. J. Remote Sens., 27, 526–537, 2001.

Kattsov, V. M., Ryabinin,V. E., Overland,J. E., Serreze,M. C, Visbek, Walsh, M., Meier, W. and Zhang, X.: Arctic sea-ice change: a grand challenge of climate science, Journal of Glaciology, 56, 1115–1121, 2010

Kloster, K.: Ice type concentration by microwave radiometry, Earth Observation Compendium for course AGF-207, Tech. rep., Norwegian Space Center, 1996.

Kovacs, A.: Sea Ice, Part 1, Bulk Salinity Versus Ice Floe Thickness, Tech. rep., DTIC Document, 1996.

Kurtz, N. and Farrell, S.: Large-scale surveys of snow depth on Arctic sea ice from operation IceBridge, Geophys. Res. Lett., 38, L20505, 10.1029/2011GL049216, 2011a.

Kurtz, N., Markus, T., Farrell, S., Worthen, D., and Boisvert, L.: Observations of recent Arctic sea ice volume loss and its impact on ocean-atmosphere energy exchange and ice production, J. Geophys. Res., 116, C04015, 10.1029/2010JC006235, 2011b.

Kwok, R.: Annual cycles of multiyear sea ice coverage of the Arctic Ocean: 1999–2003, J. Geophys. Res., 109, C11004, 10.1029/2003JC002238, 2004a.

Kwok, R. and Cunningham, G.: ICESat over Arctic sea ice: estimation of snow depth and ice thickness, J. Geophys. Res., 113, C08010, 10.1029/2008JC004753, 2008.

Kwok, R. and Rothrock, D.: Decline in Arctic sea ice thickness from submarine and ICESat records: 1958–2008, Geophys. Res. Lett., 36, L15501, 10.1029/2009GL039035, 2009a.

Kwok, R., Zwally, H., and Yi, D.: ICESat observations of Arctic sea ice: a first look, Geophys. Res. Lett, 31, L16401, 10.1029/2004GL020309, 2004b.

Kwok, R., Cunningham, G., Zwally, H., and Yi, D.: Ice, Cloud, and land Elevation Satellite (ICESat) over Arctic sea ice: retrieval of freeboard, J. Geophys. Res, 112, C12013, 10.1029/2006JC003978, 2007.

Kwok, R., Cunningham, G., Wensnahan, M., Rigor, I., Zwally, H., and Yi, D.: Thinning and volume loss of the Arctic Ocean sea ice cover: 2003–2008, J. Geophys. Res, 114, C07005, 10.1029/2009JC005312, 2009b.

Laxon, S., Peacock, N., and Smith, D.: High interannual variability of sea ice thickness in the Arctic region, Nature, 425, 947–950, 10.1038/nature02050, 2003.

Laxon, S. W., Giles, K. A., Ridout, A. L., Wingham, D. J., Willatt, R., Cullen, R., Kwok, R.,Schweiger, A., Zhang, J., Haas, C., Hendricks, S., Krishfield, R., Kurtz, N., Farrell, S., and Davidson, M.: CryoSat-2 estimates of Arctic sea ice thickness and volume, Geophys. Res. Lett., 40, 732–737, 10.1002/grl.50193, 2013.

Lytle, V. and Ackley, S. F.: Snow-ice growth: a fresh water flux inhibiting deep convection in the Weddell Sea, Antarctica, Ann. Glaciol., 33, 45–50, 10.3189/172756401781818752, 2001.

Maaß, N., Kaleschke, L., Tian-Kunze, X., and Drusch, M.: Snow thickness retrieval over thick Arctic sea ice using SMOS satellite data, The Cryosphere, 7, 1971–1989, 10.5194/tc-7-1971-2013, 2013.

Markus, T. and Cavalieri, D. J.: Snow depth distribution over sea ice in the Southern Ocean from satellite passive microwave data, Antarct. Res. Ser., 74, 19–39, 10.1029/AR074p0019, 1998.

Markus, T. and Cavalieri, D. J.: An enhancement of the NASA Team sea ice algorithm, IEEE T. Geosci. Remote, 38, 1387–1398, 2000.

Markus, T. and Cavalieri, D. J.: AMSR-E Algorithm Theoretical Basis Document: Sea Ice Products, NASA, Greenbelt, MD, USA, 2008.

Markus, T., Cavalieri, D. J., Gasiewski, A. J., Klein, M., Maslanik, J. A., Powell, D. C., Stankov, B. B., Stroeve, J. C., and Sturm, M.: Microwave signatures of snow on sea ice: observations, IEEE T. Geosci. Remote, 44, 3081–3090, 10.1109/TGRS.2006.883134, 2006.

Maslanik, J. and Stroeve, J.: DMSP SSM/I-SSMIS Daily Polar Gridded Brightness Temperatures, version 4, October 2005–November 2007, NASA DAAC at the National Snow and Ice Data Center, Boulder, Colorado USA, 2004, updated 2012.

McPhee, M., Proshutinsky, A., Morison, J., Steele, M., and Alkire, M.: Rapid change in freshwater content of the Arctic Ocean, Geophys. Res. Lett., 36, L10602, 10.1029/2009GL037525, 2009.

Notz, D.: The future of ice sheets and sea ice: between reversible retreat and unstoppable loss, P. Natl. Acad. Sci. USA, 106, 20590–20595, 10.1073/pnas.0902356106, 2009.

Outten, S. and Esau, I.: A link between Arctic sea ice and recent cooling trends over Eurasia, Climatic Change, 110, 1069–1075, 10.1007/s10584-011-0334-z, 2012.

Parkinson, C. L., Cavalieri, D. J., Gloersen, P., Zwally, H. J., and Comiso, J. C.: Arctic sea ice extents, areas, and trends, 1978–1996, J. Geophys. Res.-Oceans, 104, 20837–20856, 10.1029/1999jc900082, 1999.

Pedersen, L. T.: Improved spatial resolution of SSM/I products, development of new satellite ice data products, Tech. rep., Nansen Environmental and Remote Sensing Center, Bergen, Norway, 1998.

Perovich, D., Jones, K., Light, B., Eicken, H., Markus, T., Stroeve, J., and Lindsay, R.: Solar partitioning in a changing Arctic sea-ice cover, Ann. Glaciol., 52, 192–196, 10.3189/172756411795931543, 2011.

Polyakov, I., Kwok, R., and Walsh, J.: Recent changes of arctic multiyear sea-ice coverage and the likely causes, B. Am. Meteorol. Soc., 93, 145–151, 10.1175/BAMS-D-11-00070.1, 2011.

Rampal, P., Weiss, J., and Marsan, D.: Positive trend in the mean speed and deformation rate of Arctic sea ice, 1979–2007, J. Geophys. Res., 114, C05013, 10.1029/2008JC005066, 2009.

Ramseier, R.: Sea Ice Validation, DMSP special sensor microwave/imager calibration/validation, Tech. Rep., Final Report Volume II, Naval Research Laboratory, Washington, DC, 1991.

Rothrock, D., Yu, Y., and Maykut, G.: Thinning of the Arctic sea-ice cover, Geophys. Res. Lett., 26, 3469–3472, 1999.

Schweiger, A., Lindsay, R., Zhang, J., Steele, M., Stern, H., and Kwok, R.: Uncertainty in modeled Arctic sea ice volume, J. Geophys. Res, 116, C00D06, 10.1029/2011JC007084, 2011.

Screen, J. and Simmonds, I.: The central role of diminishing sea ice in recent Arctic temperature amplification, Nature, 464, 1334–1337, 10.1038/nature09051, 2010.

Screen, J. A. and Simmonds, I.: Erroneous Arctic temperature trends in the ERA-40 reanalysis: a closer look, J. Climate, 24, 2620–2627, 10.1175/2010JCLI4054.1, 2011.

Screen, J. A. and Simmonds, I.: Declining summer snowfall in the Arctic: Causes, impacts and feedbacks, Climate Dynamics, 38, 2243–2256, 10.1007/s00382-011-1105-2, 2012.

Serreze, M. C., Maslanik, J. A., Key, J. R., Kokaly, R. F., and Robinson, D. A.: Diagnosis of the record minimum in Arctic sea ice area during 1990 and associated snow cover extremes, Geophys. Res. Lett., 22, 2183–2186, 10.1029/95GL02068, 1995.

Smedsrud, L. H., Sirevaag, A., Kloster, K., Sorteberg, A., and Sandven, S.: Recent wind driven high sea ice area export in the Fram Strait contributes to Arctic sea ice decline, The Cryosphere, 5, 821–829, 10.5194/tc-5-821-2011, 2011.

Smith, D. M. and Barrett, E. C.: Satellite mapping and monitoring of sea ice, unpublished final report to the Defence Research Agency, RSU, University of Bristol, 1994.

Spreen, G., Kern, S., Stammer, D., Forsberg, R., and Haarpaintner, J.: Satellite-based estimates of sea-ice volume flux through Fram Strait, Ann. Glaciol., 44, 321–328, 10.3189/172756406781811385, 2006.

Stroeve, J., Serreze, M., Holland, M., Kay, J., Malanik, J., and Barrett, A.: The Arctic's rapidly shrinking sea ice cover: a research synthesis, Climatic Change, 110, 1005–1027, 10.1007/s10584-011-0101-1, 2012.

Svendsen, E., Kloster, K., Farrelly, B., Johannessen, O., Johannessen, J., Campbell, W., Gloersen, P., Cavalieri, D., and Mätzler, C.: Norwegian remote sensing experiment: Evaluation of the Nimbus 7 scanning multichannel microwave radiometer for sea ice research, J. Geophys. Res., 88, 2781–2791, 10.1029/JC088iC05p02781, 1983.

Svendsen, E., Matzler, C., and Grenfell, T.: A model for retrieving total sea ice concentration from a spaceborne dual-polarized passive microwave instrument operating near 90 GHz, Int. J. Remote Sens., 8, 1479–1487, 1987.

Swift, C., Fedor, L., and Ramseier, R.: An algorithm to measure sea ice concentration with microwave radiometers, J. Geophys. Res., 90, 1087–1099, 1985.

Tonboe, R.T., Pedersen, L.T. and Haas, C.: Simulation of the CryoSat-2 satellite radar altimeter sea ice thickness retrieval uncertainty, Canadian Journal of Remote Sensing, 36,55–67, 2010.

Tietsche, S., Notz, D., Jungclaus, J., and Marotzke, J.: Recovery mechanisms of Arctic summer sea ice, Geophys. Res. Lett., 38, L02707, 10.1029/2010GL045698, 2011.

Timco, G. and Frederking, R.: A review of sea ice density, Cold Reg. Sci. Technol., 24, 1–6, 1996.

Warren, S., Rigor, I., Untersteiner, N., Radionov, V., Bryazgin, N., Aleksandrov, Y., and Colony, R.: Snow depth on Arctic sea ice, J. Climate, 12, 1814–1829, 10.1175/1520-0442(1999)012<1814:SDOASI>2.0.CO;2, 1999.

Willat, R., Laxon, S., Giles, K., Cullen, R., Haas, C., and Helm, V.: Ku-band radar penetration into snow cover on Arctic sea ice using airborne data, Ann. Glaciol., 52, 197–205, 10.3189/172756411795931589, 2011.

Yi, D. and Zwally, J.: Arctic Sea Ice Freeboard and Thickness, National Snow and Ice Data Center, Boulder, Colorado, USA, 2009.

Zwally, H. J., Schutz, B., Abdalati, W., Abshire, J., Bentley, C., Brenner, A., Bufton, J., Dezio, J., Hancock, D., Harding, D., Herring, T., Minster, B., Quinn, K., Palm, S., Spinhirne, J., and Thomas, R.: ICESat's laser measurements of polar ice, atmosphere, ocean, and land, J. Geodyn., 34, 405–445, 10.1016/S0264-3707(02)00042-X, 2002.

Paper II

Waveform classification of synthetic aperture radar altimeter over Arctic sea ice

Zygmuntowska, M.; Khvorostovsky, K.; Helm, V. and Sandven, S.

The Cryosphere, **7**, 1315-1324, 2013

II

The Cryosphere, 7, 1315–1324, 2013
www.the-cryosphere.net/7/1315/2013/
doi:10.5194/tc-7-1315-2013

The Cryosphere Open Access

Waveform classification of airborne synthetic aperture radar altimeter over Arctic sea ice

M. Zygmuntowska[1], K. Khvorostovsky[1], V. Helm[2], and S. Sandven[1]

[1]Nansen Environmental and Remote Sensing Center, Bergen, Norway
[2]Alfred Wegener Institute, Bremerhaven, Germany

Correspondence to: M. Zygmuntowska (marta.zygmuntowska@nersc.no)

Received: 4 February 2013 – Published in The Cryosphere Discuss.: 22 March 2013
Revised: 12 July 2013 – Accepted: 15 July 2013 – Published: 19 August 2013

Abstract. Sea ice thickness is one of the most sensitive variables in the Arctic climate system. In order to quantify changes in sea ice thickness, CryoSat-2 was launched in 2010 carrying a Ku-band radar altimeter (SIRAL) designed to measure sea ice freeboard with a few centimeters accuracy. The instrument uses the synthetic aperture radar technique providing signals with a resolution of about 300 m along track. In this study, airborne Ku-band radar altimeter data over different sea ice types have been analyzed. A set of parameters has been defined to characterize the differences in strength and width of the returned power waveforms. With a Bayesian-based method, it is possible to classify about 80 % of the waveforms from three parameters: maximum of the returned power waveform, the trailing edge width and pulse peakiness. Furthermore, the maximum of the power waveform can be used to reduce the number of false detections of leads, compared to the widely used pulse peakiness parameter. For the pulse peakiness the false classification rate is 12.6 % while for the power maximum it is reduced to 6.5 %. The ability to distinguish between different ice types and leads allows us to improve the freeboard retrieval and the conversion from freeboard into sea ice thickness, where surface type dependent values for the sea ice density and snow load can be used.

1 Introduction

While Arctic sea ice extent and its changes have been studied widely in the last decades (Kwok, 2002; Comiso et al., 2007; Stroeve et al., 2012), sea ice thickness and its decrease remain one of the least observed variables of the Arctic climate system (Laxon et al., 2003; Maslanik et al., 2007; Giles et al., 2008; Kwok and Rothrock, 2009). Ice thickness data are sparse and only available from a few campaigns with upward-looking sonar on submarines and moorings (Rothrock et al., 1999, 2008) or helicopter surveys using electro-magnetic induction (Haas et al., 1997, 2010, 2011; Hendricks et al., 2011). Satellite laser and radar altimeters have provided large-scale coverage of ice thickness data in the Arctic, but the operations were limited to certain periods and regions. ICESat's high-resolution laser altimeter, with a footprint of 70 m, covered the area up to 86° N, while its temporal coverage was limited to two five-week operation periods per year from 2003 to 2009 (Kwok et al., 2004; Kwok and Untersteiner, 2011). Conventional radar altimeters on board ERS-1/2 and Envisat provided continuous high-density measurements from 1992 to 2012, but have a relatively coarse resolution, with a footprint of several kilometers, and only cover the polar regions up to 81.6° N (Laxon et al., 2003). In 2010 CryoSat-2 was launched addressing the shortcomings of previous altimeter missions (Wingham et al., 2006; Laxon et al., 2013). CryoSat's payload instrument is the SAR/Interferometric Radar Altimeter (SIRAL), which uses the synthetic aperture radar (SAR) technique to enhance the resolution along track. When operating in SAR mode over sea ice, CryoSat-2 has a footprint of about 270 m × 1000 m, which is a significant improvement compared to the previous ERS and Envisat altimeters. CryoSat-2 orbits the earth with an inclination of 92°, which enables the measurement of sea ice thickness at high latitudes.

Radar altimeter signals from sea ice have been analyzed in many studies since the 1980s (Dwyer and Godin, 1980; Onstott et al., 1987). Dwyer and Godin (1980) published the

first analysis of radar altimeter waveform signals over sea ice using data from the GEOS-3 satellite. They found altimeter power waveforms over smooth sea ice to rise to a higher value than over the rough open ocean. Drinkwater (1991) and Ulander (1987) found correlations between radar backscatter in SAR images and radar altimeter echo strength and width. Fedor et al. (1989) observed a reduction of the signal response from flat to ridged sea ice. The strongest return signal has been found to come from leads with calm, open water or thin ice, producing specular echo power waveforms (Fetterer, 1992). Encouraged by these findings, the possibility for sea ice classification based on radar altimeter data alone has been discussed in several studies (Chase and Holyer, 1990; Drinkwater, 1991; Laxon, 1994a). Even though the results were promising, the methods have not been developed any further. The current Envisat algorithm for example only distinguishes between leads and ice floes, and large open water areas are masked out by the use of passive microwave data (Laxon et al., 2003; Giles et al., 2008; Ridout et al., 2012). Leads are most commonly identified by the pulse peakiness parameter – the ratio of signal maximum and accumulated power (Peacock and Laxon, 2004; Giles et al., 2007). Sea ice thickness is calculated using prescribed values for ice density and climatological snow depth (Warren et al., 1999).

All the assumptions used in this algorithm are based on conventional altimeters where the waveform is essentially a step function. Once the power has reached the maximum, it remains there for many delay intervals as the area contributing to the power echo is constant over time (Brown, 1977). For synthetic aperture radar altimeters, the signal decays more rapidly after the peak as the area contributing to the response signal decreases with the square root of time (Raney, 1998). The different sampling techniques, and the resulting different echo shape, suggest that a classification of different sea ice types using only waveform data from synthetic aperture radar altimeters may be possible.

In this paper we present a method to distinguish between first-year ice and multi-year ice based on the shape of the radar echo waveform alone. The data used in the study were obtained by an airborne synthetic aperture radar altimeter, ASIRAS, during pre-launch calibration and validation campaigns for CryoSat-2. Different parameters to describe the returned signal and techniques for classification have been explored. The paper contains the following sections: in Sect. 2 we describe the radar altimeter ASIRAS as well as the validation data sets used. Parametrization of the echo power waveforms is described in Sect. 2.2 and the used classification methods in Sect. 2.3. The distribution of each parameter for different surface types and the resulting classification rates are given in Sect. 3. In Sect. 4 our results are compared to previous findings, and perspectives for further applications are discussed.

2 Data and methods

2.1 Instrument and data campaigns

To examine the possibilities of surface classification based on radar altimeter data, measurements from ESA's CryoSat calibration and validation experiments CryoVEx 2007 and CryoVEx 2008 have been used. Both airborne operations were coordinated by the National Space Institute, Danish Technical University (DTU Space) and the Alfred Wegener Institute (AWI). In 2007 the campaign took place from April 15 to April 25 while in 2008 it lasted from April 15 until May 8. In this study we mainly use data from the Airborne Synthetic Aperture and Interferometric Radar Altimeter System (ASIRAS). The instrument operates at a center frequency of 13.5 GHz (Ku-band) and features along-track resolution enhancement by using the synthetic aperture radar technique like its satellite counterpart SIRAL on board CryoSat-2. ASIRAS operates with an antenna beam pattern of 10 degrees along track and 2.5 degrees across track. The footprint size depends on flight altitude but can be considered to be around 10 m × 50 m at a flight altitude of 300 m. Synthetic aperture radar processing is used to increase the resolution along track, which results in a sampling resolution of 3 m. The return echo power for each data point is recorded with a vertical resolution of approximately 0.095 m and sampled in a 24 m range window, corresponding to 256 bins.

Since CryoSat-2 was primarily designed to measure trends in perennial sea ice, the main validation campaigns took place north of Greenland and Canada, which is an area known to be mostly covered by this type of ice. Single flights have also been performed in areas covered by first-year ice such as Baffin Bay and around the Svalbard archipelago. Therefore we were able to analyze the returned signal waveform over different surfaces such as leads, first-year ice (FYI) and multi-year ice (MYI) (see Table 1). In the area of acquisition, surface types have been identified on contemporary Envisat ASAR wide-swath images (see Fig. 2). In some of the areas, as in the first-year and multi-year ice cases north of Alert, detailed in situ measurements were also available. The area has also been surveyed by an airborne electromagnetic induction device (EM-Bird), which measures the combined snow and ice thickness. Additionally, data from downward-looking optical cameras on board the airplanes were available. The combination of these data sets gives an excellent knowledge of the ice conditions and allows for a detailed study of the waveform signal over different surface regimes. More information about the campaigns can be found in technical reports (Helm and Steinhage, 2008; Hvidegaard et al., 2009). An overview of the location of the cases analyzed is given in Fig. 1. Further details of the study areas are provided in Table 1.

Table 1. Overview of the study areas and numbers of available echo waveforms for each case. We evaluated nine cases: two for leads (L), four for first-year ice (FYI) and three for multi-year ice (MYI), each containing several hundred waveforms. Additional data sets, which have been used for obtaining information about the surface type, are listed in the right column. ASAR indicates that an Envisat ASAR wide-swath image was available.

Cases	Date	Description	No. of echoes	Additional data sets
L1	27.04.2008	Leads northeast of Greenland	566	ASAR, photo camera
L2	01.05.2008	Leads north of Alert	1635	ASAR, photo camera
FYI 1	21.04.2007	Svalbard Walenbergfjorden, fast ice	3273	ASAR
FYI 2	06.05.2008	Baffin Bay	10755	ASAR
FYI 3	01.05.2008	Thin, flat, snow-covered ice north of Alert	5248	ASAR, in situ, EM-Bird, photo camera
FYI 4	01.05.2008	Validation area north of Alert	513	ASAR, photo camera
MYI 1	27.04.2008	Big ice field northeast of Greenland	7223	ASAR, photo camera
MYI 2	01.05.2008	Sea ice field north of Alert	7205	ASAR, photo camera
MYI 3	01.05.2008	Validation area north of Alert	796	ASAR, in situ, EM-Bird, photo camera

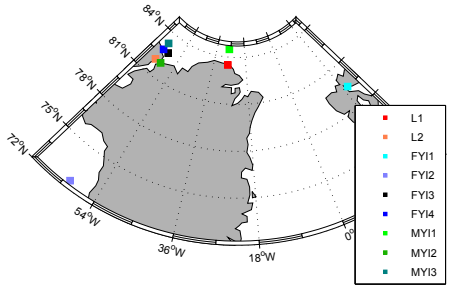

Fig. 1. Map showing the approximate location for each of the evaluated cases (see detailed description in Table 1). Cases with leads (L) are marked in red colors, first-year ice (FYI) in blue and multi-year ice (MYI) in green.

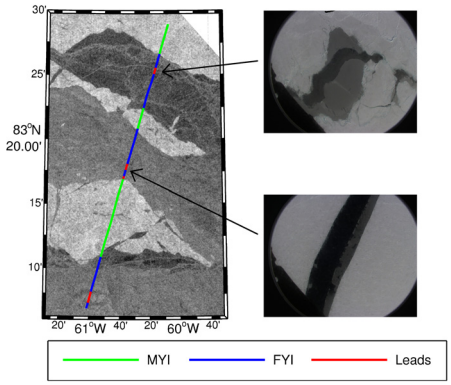

Fig. 2. Example of background information available to retrieve sea ice type north of Alert. Left: Envisat ASAR wide-swath image overlaid with contemporary ASIRAS track from 1 May 2008. In green the ASIRAS track over MYI is shown, in blue FYI and in red the leads. Right: example of camera images used for identifying leads within the ice.

2.2 Parametrization of waveform shape

The return signal from the airborne radar altimeter is sampled in a range window of 256 bins, each with a size of about 0.095 m. The signal is usually referred to as power echo waveform or simply waveform. To be able to describe the shape of the waveform quantitatively and account for the differences in strength and width of the signal, the following parameters have been used (see Fig. 3):

- *Maximum (Max)* value of the power echo.
- *Pulse peakiness (PP)* is the ratio of the maximum power to the accumulated echo power (first defined by Laxon, 1994b).

$$\mathrm{PP} = \frac{\max(\mathrm{power})}{\sum_{i=1}^{256} \mathrm{power(i)}} \quad (1)$$

- *Leading edge width (LeW)* is obtained by fitting a Gaussian curve to the leading edge (starting at the bin containing an echo power larger than 1 % of the power maximum and ending two bins after the bin with the maximum value). The distance between 1 % and 99 % of maximum power echo is defined as the leading edge width (e.g., Legresy et al., 2005).
- *Trailing edge width (TeW)* is obtained by fitting an exponential decay function to the trailing edge starting with the bin containing the maximum power. The trailing edge width is the distance between the 99 % and 1 % of the power maximum.

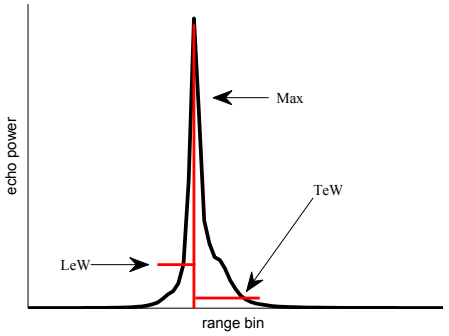

Fig. 3. Subset of the averaged waveform for first-year ice, calculated as the mean of all waveforms retrieved over first-year ice (specified in Table 1). The approximate width of the leading edge and trailing edge are indicated for visualization of these two waveform parameters.

– *Trailing edge slope (TeS)* is the decay factor for the exponential fit (e.g., Legresy et al., 2005).

2.3 Classification parameters and methods

To evaluate which parameters are most distinct for each surface type, and therefore suitable to distinguish between surface classes, the Kolmogorov–Smirnov test (KS test) has been applied. In statistics, the KS test makes it possible to determine if two data sets differ significantly by quantifying the distance between the empirical cumulative distribution functions of two samples. No assumption about the distribution of the two data samples is made, but the test is sensitive to differences in location and shape of the distribution functions.

After analyzing the probability distributions and finding the parameters that are most suitable for classification, two different classification methods have been explored: (1) rule-based threshold method and (2) Bayesian classifier. The threshold method is the one most commonly applied to detect leads within sea ice. The Bayesian classifier is a simple and robust classification method based on supervised learning that formulates the classification problem in probabilistic terms.

2.3.1 Rule-based threshold

By analyzing the distribution functions for different surface classes and waveform parameters, it seems straightforward to base a classification on simple thresholds between the classes. This is a widely used method to identify leads, and usually the pulse peakiness parameter or the Maximum are used (Peacock and Laxon, 2004; Giles et al., 2007; Röhrs et al., 2012). We selected an equal number of waveforms from each surface class and set the threshold by maximizing the number of correct classified waveforms from this selection. To minimize the number of false detections, a margin was set around the threshold. The size of the margin equals approximately 2 % of the range of each parameter. Waveforms with classification parameters within this margin are labeled as not classified. The advantages of this rule-based threshold method are that no assumption on the distribution is made and, after setting the threshold, it is very easy to implement.

2.3.2 Bayesian classifier

For the classification with the Bayesian approach, our data set has been divided into two different parts: a learning data set with 40 % of all available waveforms and a testing set with 60 %. The Bayesian classifier is based on Bayes' theorem (Hanson et al., 1991), which formulates the classification problem in probabilistic terms: based on the probabilities of each surface class and probabilities of the waveform parameters for each class, a probability calculation is used to make a classification decision. The used parameters are PP, Max, TeW, TeS and LeW, and the classes are the three surface types, FYI, MYI and leads. In our study we used Gaussian kernel density estimates to model the parameter densities for each class. It is assumed that parameters are conditionally independent and their class distributions are calculated independently. This is a simplification but as the parameters are partly depending on different surface properties, it is reasonable for our purpose. To reduce the number of wrong classifications, we added the requirement that the probability belonging to one class has to be higher than 70 %; otherwise waveforms were labeled as not classified.

3 Results

3.1 Typical waveform

As a first qualitative analysis we show mean waveforms for different surface types in Fig. 4. To account for the difference in surface elevation, all waveforms have been moved so that their maximum values are located in the same sampling bin. The mean of the maximum echo power resulting from reflection over leads is more than 8 times higher than from those coming from sea ice; and even 4 times higher than the mean maximum coming from flat first-year ice (Fig. 4a). The difference in the maximum from the waveforms coming from first-year ice and multi-year ice is less distinct. In Fig. 4b normalized waveforms are shown in order to visualize the difference in the width of the power echo.

Based on the visual analysis of the waveforms, there is a clear difference in the decay after the peak, with multi-year ice having a lower decay rate and a wider trailing edge than

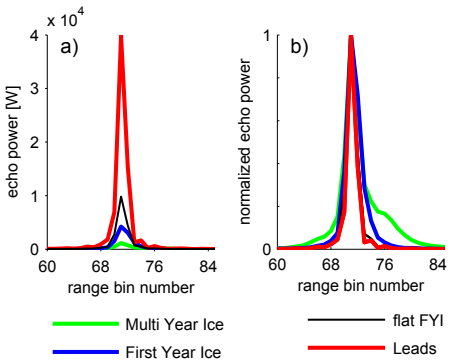

Fig. 4. Averaged waveforms for the three evaluated surface types: leads (red), FYI (blue) and MYI (green). Additionally the mean waveform over flat FYI is shown (black). The waveforms have been calculated as a mean of all available measurements for these surface type as listed in Table 1. **(a)** Mean reflected waveform for each surface type. **(b)** Normalized mean waveform to show the difference in the width of the reflected signal.

first-year ice and leads. Reflection over flat FYI (black line) does not result in a wider signal than over leads.

3.2 Distribution of the parameters

For each of the waveforms for the analyzed cases, we calculated the five parameters PP, Max, TeW, TeS and LeW. The cumulative probability distributions for each parameter and case are shown in Fig. 5. The more separated the distributions are from one surface type to another, the easier it is to classify the surface type.

For all parameters the spread of the distributions coming from FYI is quite large. Since the term first-year ice refers to a wide range of conditions – ranging from undeformed thin ice to ice that has undergone a high rate of deformation – this is in accordance to our expectations.

The spread of the Max parameter for the FYI distributions is very wide and reaches both extremes: distributions are observed with much smaller and higher values than coming from the MYI cases. The two cases of sea ice with the strongest signal are flat new ice (FYI3) and fast ice (FYI1). In all cases the distributions differ substantially from those obtained over leads (L1 and L2).

The distributions for PP coming from MYI and leads closely resemble each other within these classes. The distributions for FYI in turn largely differ from case to case. The PPs resulting from the power echo waveforms of flat thin ice (FYI3) are almost as high as those resulting from the waveform of leads, while all other cases clearly show smaller PP values. On average, reflection from FYI results in higher PP values than from MYI, but the cumulative probability distributions from FYI and MYI largely overlap. For all cases a clear difference between the distributions from MYI and leads can be found.

The distributions of the parameters related to the leading and trailing edge (the TeW, LeW and TeS) look much alike. We find narrow and similar distributions for the two evaluated cases of leads: a wide spread in the distributions for FYI and wide distributions with long tails for the MYI.

However, even though we found a large spread in the distributions for each class and sometimes large overlaps between single cases from different classes, the KS test shows the averaged distributions for each class are significantly different at a 5 % level for each of the five parameters. To find the parameters best suitable for surface classification, we analyzed the difference between the waveform shapes coming from different surface types more quantitatively. We calculated the mean difference in the cumulative probability distributions for each parameter (Table 2). The difference between the distributions is much larger between leads and sea ice (0.72) than between FYI and MYI (0.52), making it much easier to detect leads within the ice than to distinguish between the two sea ice classes. Differences between the parameters are very small, but they might be large enough to increase the rate of correct classification.

The largest difference between leads and sea ice can be found for the distribution of the Max and the LeW and TeW. Since flat ice is the biggest challenge for the lead detection – flat ice results in a waveform similar to that obtained over leads – we analyzed the difference in the distributions from leads and flat first-year ice (FYI3) more closely (right column in Table 2). We found the larger difference for the Max and TeW and selected these two parameters for lead detection within the ice. Together with the Max and the TeW, we found the TeS to be an adequate parameter to distinguish between MYI and FYI (Table 2). However, as the TeW and TeS are highly correlated, the TeS has been excluded from further analysis.

3.3 Detection of surface types

Results from the two classification methods based on PP, Max and TeW are shown in Table 3. A simple threshold method based on PP is the approach used in the Envisat processing chain (Ridout et al., 2012). Therefore, PP has been included in the analysis for comparison. In Table 3 we do not show all possible parameter combinations but present only those leading to the best classification rates. Our classification rates are calculated as described in the following paragraphs.

The rates of correct classification for the different surface classes are the percentage of the waveforms coming from one class that have been correctly classified:

$$\text{correct classification}_{\text{class1}} = \frac{\#(\text{class}_{\text{class1}} \cap \text{known}_{\text{class1}})}{\#\text{known}_{\text{class1}}}. \quad (2)$$

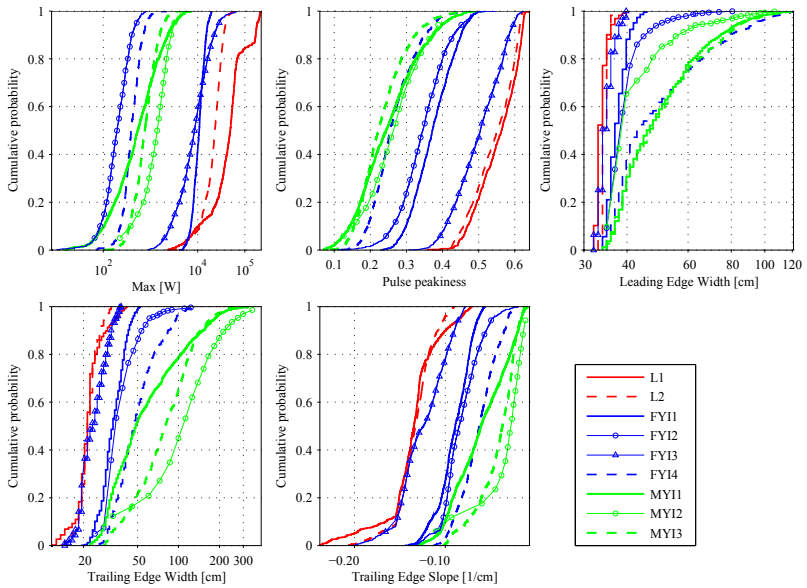

Fig. 5. Cumulative probability distributions for the nine cases (see Table 1) for the five waveform parameters: Max, PP, LeW, TeW and TeS. Distributions obtained from waveforms resulting from leads are shown in red colors, from first-year ice in blue and multi-year ice in green colors.

The rates of false detection are the percentage of waveforms classified as one class while actually belonging to another one:

$$\text{false classification}_{\text{class1}} = \frac{\#(\text{class}_{\text{class2}} \cap \text{known}_{\text{class1}})}{\#\text{class}_{\text{class2}}}. \quad (3)$$

As we selected and divided our waveforms by random choice (for the threshold method we selected an equal number of waveforms of each class, and for the Bayesian approach our data set has been divided into a learning and testing data set), each method has been performed 100 times. The presented classification rates are mean values, and the standard deviation of our results did not exceed 2 %.

Almost 95 % of the leads can be identified correctly based on the PP (Table 3). We found a lower average rate of correct classification of 87 % and a detection rate for leads around 83.8 % based on the Max. The percentage of waveforms reflected from sea ice, but falsely classified as a lead, is strongly reduced for the Max parameter (6.5 %) compared to results obtained with the PP (12.6 %). Our Bayesian approach does not significantly increase the detection rate of leads, but does lead to a decrease in false classifications for both leads and sea ice. The advantage of the Bayesian method can also be shown by analyzing the critical case of flat first-year ice (FYI3 in Fig. 5 and Table 1). For the basic threshold method based on the PP parameter, more than 97 % of the waveforms coming from flat ice have been classified as leads, while for the Bayesian approach combining TeW and PP only 87 % are (not shown in the Table).

Results for the two methods for the classification of FYI and MYI are shown in Table 3. Here the use of the Bayesian

Table 2. Mean distances between the empirical cumulative distribution functions of the five parameters determined from KS test: pulse peakiness (PP), trailing edge slope (TeS), leading edge width (LeW), trailing edge width (TeW), and the power maximum (Max).

	Leads vs. sea ice	FYI vs. MYI	Leads vs. flat FYI
PP	0.718	0.518	0.236
TeS	0.716	0.523	0.250
LeW	0.721	0.511	0.251
TeW	0.720	0.527	0.269
Max	0.737	0.521	0.307

Table 3. Results for the two different classification methods: rule-based threshold and Bayesian classifier. The overall classification rates, the probabilities of correct and false detection for ice and leads (left) and for first-year ice and multi-year ice (right) are presented. The classification rates are defined in Eqs. (2) and (3). The used parameters are the pulse peakiness (PP), the power maximum (Max) and the trailing edge width (TeW).

Method	Threshold		Bayes'	Method	Threshold	Bayes'	
Parameter	PP	Max	TeW and max	Parameter	PP	TeW and Max	TeW and PP
Correct classifications [%]				Correct classifications [%]			
All	88.0	87.3	91.3	all	72.4	80.3	79.9
Leads	94.2	83.8	94.9	FYI	72.6	78.7	80.5
Ice	79.5	90.8	89.1	MYI	68.6	81.7	75.5
False classifications [%]				False classifications [%]			
Leads	12.6	6.5	6.2	FYI	26.0	10.4	23.7
Ice	5.6	12.0	2.3	MYI	19.2	9.1	15.7
Not classified	4.6	3.7	6.9	not classified	6.2	11.3	12.8

method allows for a strong improvement of the classification by about 8 %, resulting in an average detection rate of almost 80 %. The rate of false classification can be lowered to about 10 % by using a combination of TeW and Max. The simple threshold method results not only in a poor classification rate but also in a high rate of false classification, where 26 % of the waveforms classified as FYI are actually MYI.

4 Discussion

In this study we present a method to distinguish between different sea ice types and leads using airborne Ku-band radar altimeter power waveforms. A method to distinguish between FYI and MYI is presented based on the waveform parameters PP and TeW. With a Bayesian-based method, we were able to classify around 80 % of the waveforms correctly. We can further confirm that a simple threshold method based on the PP parameter is a sufficient method to detect leads. Adding more parameters or using a more advanced method such as the Bayesian classifier does not significantly improve the rate of correct classification. Using Max instead of PP can increase the accuracy in distinguishing leads from undeformed first-year ice, but it also leads to a reduction in the detection rate of leads.

A related analysis was performed by Drinkwater (1991), who analyzed data from a conventional pulse-limited radar altimeter in the marginal ice zone. He found similar results to ours: bare first-year ice results in a high peak value of backscatter and a steep decay; deformed first-year ice results in a lower backscatter and a lower decay gradient; and multi-year ice results in a low peak and a low decay gradient. Despite these findings and even some clustering results that show a clear separation between FYI and MYI, he was skeptical about the possibilities of sea ice classification. In contrast to our study, his analysis was performed in the marginal ice zone where ice floes were smaller than the footprint size. Fedor et al. (1988, 1989) also published sea ice classification results based on conventional airborne radar altimeter waveforms in the Beaufort Sea. They showed that the returned signal decreases from dark nilas over gray ice to more deformed ice types such as rough first-year ice and multi-year ice. Laxon (1994a) presented a method for sea ice classification based on the ERS data by parameterizing the waveform shape, but the method has only been used to distinguish between leads and sea ice. In addition to a qualitative analysis, as done in previous studies, the classification method presented here provides quantitative results. We show that the selected waveform parameters differ significantly for various surface classes and present a method where a combination of waveform parameters leads to a correct classification of 80 % of the waveforms.

Numerous studies have been performed to understand the shape of the radar altimeter waveform and its sensitivity to surface conditions. Laboratory experiments have shown that close to nadir the influence of electrical properties can be neglected (Beaven et al., 1995). The influence of surface roughness has been described by Brown (1977) and Raney (1998). Based on the same laboratory experiments, Beaven et al. (1995) showed that the radar return originates at the snow/ice interface, and snow influence – as long as the snow is dry and cold – can be neglected. Dielectric properties of water have been found to dominate over those of dry snow for volumetric water contents of 1 % (Howell et al., 2005), which can occur at temperatures above −5 °C (Garrity, 1992). Based on forward modeling of the reflected radar signal, Makynen and Hallikainen (2009) found that this wet snow cannot be neglected because it alters the waveform shape substantially by adding more volume scattering to the power echo. Willat et al. (2011) confirmed the influence of snow on the radar signal based on data from a dedicated field campaign. The

influence of surface roughness cannot be separated from the influence of snow properties in the analysis presented. We can only conclude that the combination of difference in ice and snow properties is sufficient to generate a significant difference in the waveform shape.

Therefore more analyses are required to test how our findings can be adapted to satellite-borne altimeter systems. The main difference between the ASIRAS data used in this study and CryoSat-2 data is the resolution. While ASIRAS has a bin width of 9 cm and a footprint of tens of meters, SIRAL on board CryoSat-2 has a bin width of 45 cm and a resolution ranging from hundreds to thousands of meters. With this large footprint size, it is more likely that a mixture of different sea ice types occurs within each footprint, which makes a clear separation more difficult. The narrow bin width in the ASIRAS data allows for a detailed record of the returned power. For CryoSat-2 the wide bin width only allows for a detection of large-scale changes in surface structure and signal strength. This further limits the possibility of distinguishing between surface types. A more detailed study is needed to analyze the impact of the different resolutions as well as the influence of snow and roughness on the SIRAL waveform. This has to include measurements from radar and laser altimeters, snow radar, and EM measurements, as well as large-scale information about surface roughness (e.g., ASCAT scatterometer data Andersen et al., 2007) and snow retrievals from passive microwave measurements.

As with any other sea ice classification technique based on remote sensing, the method presented here might be limited to the central Arctic in cold seasons (e.g., Kwok et al., 1992; Zakhvatkina, 2012), where ice types are more distinct and a sufficient area of the radar footprint is covered by ice. The possibility of distinguishing FYI from MYI by radar altimeter data alone is not intended to replace well-established large-scale classification methods based on scatterometer or passive microwave data (Fetterer et al., 1994; Fowler et al., 2004; Andersen et al., 2007; Maslanik et al., 2011). The main benefit of ice classification from radar altimeter data is for improvement of freeboard retrieval and sea ice thickness calculation. Freeboard, the height of the ice above the water level, is retrieved by detecting leads between the ice and finding the difference in elevation of ocean and ice floes. To retrieve the elevation, a re-tracker needs to be applied to determine the position on the leading edge belonging to the surface. For the current Envisat algorithm, different methods are applied for waveforms from sea ice and leads (Ridout et al., 2012). In our study we found the shape of the radar echo waveform to differ significantly between first- and multi-year ice. Therefore we suggest that the identification of different sea ice types can be used to develop a more accurate re-tracker. This could be done by using different fitting procedures to the waveforms depending on surface type. More work is required to test this possibility. The calculation of sea ice thickness from the freeboard measurements is based on the assumption of hydrostatic equilibrium

$$h_{\mathrm{i}} = \frac{f_{\mathrm{i}}\rho_{\mathrm{w}}}{\rho_{\mathrm{w}} - \rho_{\mathrm{i}}} + \frac{h_{\mathrm{s}}\rho_{\mathrm{s}}}{\rho_{\mathrm{w}} - \rho_{\mathrm{i}}}, \tag{4}$$

where f_{i} is the ice freeboard, ρ_{i} the ice density, ρ_{w} the density of water, ρ_{s} density of snow and h_{s} the snow load. The highest uncertainties in sea ice thickness have been found to come from the freeboard retrieval itself, the snow load and from the density of the ice (Forström et al., 2011; Alexandrov et al., 2010). So far snow load has been taken from climatologies (Warren et al., 1999) that are based on measurements on multi-year ice. Recent results from IceBridge laser data over Arctic sea ice reveal a significantly smaller snow load on first-year ice compared to multi-year ice where the snow accumulates over the entire season (Kurtz and Farrell, 2011). Therefore the method presented allows not only the possibility of improving the freeboard retrieval but also using ice type dependent values for the sea ice density and snow load. Previously this has been done by using large-scale sea ice classification retrievals based on scatterometer or passive microwave retrievals. Our method has the benefit of not being dependent on other instruments and providing synchronous information about the surface type. It can improve the sea ice thickness estimates, both on regional and Arctic-wide scales, and improve our knowledge about changes in sea ice thickness.

5 Conclusions

In this study, airborne Ku-band radar altimeter data over different sea ice types have been analyzed. It was found that the radar altimeter waveforms retrieved over first-year ice and multi-year ice differ significantly. Various parameters to describe the shape of the radar echo waveforms coming from first-year ice, multi-year ice and leads were evaluated. The maximum of the returned power echo and the trailing edge width were selected as the most suitable ones for sea ice classification. A Bayesian approach used in combination with the waveform parameters was found to be a successful method to distinguish between first-year ice and multi-year ice. With this method it was possible to detect 80 % of the waveforms correctly. In addition, a simple threshold method based on the pulse peakiness parameter was used for lead detection. It was shown that the use of the maximum parameter could lower the rate of false detection of leads. For the pulse peakiness parameter, the false classification rate is 12.6 % while for the power maximum it is reduced to 6.5 %. More analyses are required to test the presented method for satellite-based altimeters. The method has the potential to improve the freeboard retrieval by developing a more accurate re-tracker algorithm and improve the conversion of freeboard into sea ice thickness by applying surface-dependent values for sea ice density and snow load.

Acknowledgements. This work is supported by the Research Council of Norway through the ROMFORSK program (project no. 202313/V30) and ESA PRODEX contract no. 4200090318 CN1. We thank the CryoVEx teams from the Alfred Wegener Institute and the Danish National Space Institute, Danish Technical University (DTU Space), for their work during the campaigns and the data processing. The work from Alfred Wegener Institute was funded by the German Ministry of Economics and Technology (Grant 50EE1008). We gratefully acknowledge the comments from Kjell Kloster and Natalia Ivanova on our manuscript and Laurent Bertino's advice on the statistical methods. The shown SAR image from 1 May 2008 was obtained from the European Space Agency.

Edited by: J. L. Bamber

References

Alexandrov, V., Sandven, S., Wahlin, J., and Johannessen, O. M.: The relation between sea ice thickness and freeboard in the Arctic, The Cryosphere, 4, 373–380, doi:10.5194/tc-4-373-2010, 2010.

Andersen, S., Breivik, L., Eastwood, S., Godøy, Ø., Lind, M., Porcires, M., and Schyberg, H.: OSI SAF Sea Ice Product Manual–v3. 5, EUMETSAT OSI SAF–Ocean and Sea Ice Sattelite Application Facility, Tech. Rep. SAF/OSI/met. no/TEC/MA/125, 2007.

Beaven, S., Lockhart, G., Gogineni, S., Hossetnmostafa, A., Jezek, K., Gow, A., Perovich, D., Fung, A., and Tjuatja, S.: Laboratory measurements of radar backscatter from bare and snow-covered saline ice sheets, Int. J. Remote Sens., 16, 851–876, 1995.

Brown, G.: The average impulse response of a rough surface and its applications, IEEE T. Antenn. Propag., 25, 67–74, 1977.

Chase, J. and Holyer, R.: Estimation of sea ice type and concentration by linear unmixing of Geosat altimeter waveforms, J. Geophys. Res., 95, 18015–18018, 1990.

Comiso, J. C., Parkinson, C. L., Gersten, R., and Stock, L.: Accelerated decline in the Arctic sea ice cover, Geophys. Res. Lett., 34, L01703, doi:10.1029/2007GL031972, 2007.

Drinkwater, M.: Ku band airborne radar altimeter observations of marginal sea ice during the 1984 marginal ice zone experiment, J. Geophys. Res., 96, 4555–4572, 1991.

Drinkwater, M., Francis, R., Ratier, G., and Wingham, D.: The European Space Agency's earth explorer mission CryoSat: measuring variability in the cryosphere, Ann. Glaciol., 39, 313–320, 2004.

Dwyer, R. and Godin, R.: Determining sea-ice boundaries and ice roughness using GEOS-3 altimeter data, 1980.

Fedor, L., Hayne, G., and Walsh, E.: Airborne pulse-limited radar altimeter return waveform characteristics over ice in the Beaufort Sea, in: OCEANS'88: a Partnership of Marine Interests, Proceedings, 1704–1710, IEEE, 1988.

Fedor, L., Hayne, G., and Walsh, E.: Ice-type Classifications From Airborne Pulse-limited Radar Altimeter Return Waveform Characteristics, in: Geoscience and Remote Sensing Symposium, 1989, IGARSS'89, 12th Canadian Symposium on Remote Sensing, 1989 International, vol. 3, 1949–1952, IEEE, 1989.

Fetterer, F.: Sea ice altimetry, Tech. rep., DTIC Document, 1992.

Fetterer, F., Gineris, D., and Kwok, R.: Sea ice type maps from Alaska synthetic aperture radar facility imagery: an assessment, J. Geophys. Res., 99, 22–22, 1994.

Forström, S., Gerland, S., and Pedersen, C.: Thickness and density of snow-covered sea ice and hydrostatic equilibrium assumption from in situ measurements in Fram Strait, the Barents Sea and the Svalbard coast, Ann. Glaciol., 52, 261–271, 2011.

Fowler, C., Emery, W., and Maslanik, J.: Satellite-derived evolution of Arctic sea ice age: October 1978 to March 2003, IEEE Geosci. Remote S., 1, 71–74, 2004.

Garrity, C.: Characterization of snow on floating ice and case studies of brightness temperature changes during the onset of melt, Geoph. Monog. Ser., 68, 313–328, 1992.

Giles, K., Laxon, S., Wingham, D., Wallis, D., Krabill, W., Leuschen, C., McAdoo, D., Manizade, S., and Raney, R.: Combined airborne laser and radar altimeter measurements over the Fram Strait in May 2002, Remote Sens. Environ., 111, 182–194, 2007.

Giles, K., Laxon, S., and Ridout, A.: Circumpolar thinning of Arctic sea ice following the 2007 record ice extent minimum, Geophys. Res. Lett., 35, L22502, doi:10.1029/2008GL035710, 2008.

Haas, C., Gerland, S., Eicken, H., and Miller, H.: Comparison of sea-ice thickness measurements under summer and winter conditions in the Arctic using a small electromagnetic induction device, Geophysics, 62, 749–757, 1997.

Haas, C., Hendricks, S., Eicken, H., and Herber, A.: Synoptic airborne thickness surveys reveal state of Arctic sea ice cover, Geophys. Res. Lett., 37, L09501, doi:10.1029/2010GL042652, 2010.

Haas, C., Goff, H., Audrain, S., Perovich, D., and Haapala, J.: Comparison of seasonal sea-ice thickness change in the Transpolar Drift observed by local ice mass-balance observations and floe-scale EM surveys, Ann. Glaciol., 52, 97–102, 2011.

Hanson, R., Stutz, J. and Cheeseman, P.: Bayesian classification theory, NASA Ames Research Center, Artificial Intelligence Research Branch, 1991.

Helm, V. and Steinhage, D.: CryoVEx 2007-Data Acquisition and Final Processing Report, Tech. rep., 2008.

Hendricks, S., Gerland, S., Smedsrud, L., Haas, C., Pfaffhuber, A., and Nilsen, F.: Sea-ice thickness variability in Storfjorden, Svalbard, Ann. Glaciol., 52, 61–68, 2011.

Howell, S., Yackel, J., De Abreu, R., Geldsetzer, T., and Breneman, C.: On the utility of SeaWinds/QuikSCAT data for the estimation of the thermodynamic state of first-year sea ice, IEEE T. Geosci. Remote, 43, 1338–1350, 2005.

Hvidegaard, S. M., Forsberg, R., Helm, V., Hendricks, S., Skourup, H., Stenseng, L., Hanson, S., and Haas, C.: CryoVEx 2008 Final Report, Tech. rep., Dansh National Space Institute, DTU Space, 2009.

Kurtz, N. and Farrell, S.: Large-scale surveys of snow depth on Arctic sea ice from operation IceBridge, Geophys. Res. Lett., 38, L20505, doi:10.1029/2011GL049216, 2011.

Kwok, R.: The RADARSAT geophysical processor system, 1996.

Kwok, R.: Sea ice concentration estimates from satellite passive microwave radiometry and openings from SAR ice motion, Geophys. Res. Let., 29, 25-1–25-4, 2002.

Kwok, R. and Rothrock, D.: Decline in Arctic sea ice thickness from submarine and ICESat records: 1958–2008, Geophys. Res. Lett., 36, L15501, doi:10.1029/2009GL039035, 2009.

Kwok, R. and Untersteiner, N.: The thinning of Arctic sea ice, Phys. Today, 64, 36–41, 2011.

Kwok, R., Rignot, E., Holt, B., and Onstott, R.: Identification of sea ice types in spaceborne synthetic aperture radar data, J. Geophys. Res., 97, 2391–2402, 1992.

Kwok, R., Zwally, H., and Yi, D.: ICESat observations of Arctic sea ice: a first look, Geophys. Res. Lett, 31, L16401, doi:10.1029/2004GL020309, 2004.

Laxon, S.: Sea ice altimeter processing scheme at the EODC, Int. J. Remote Sens., 15, 915–924, 1994a.

Laxon, S.: Sea ice extent mapping using the ERS-1 radar altimeter, EARSeL Adv. Remote Sens., 3, 112–116, 1994b.

Laxon, S., Peacock, N., and Smith, D.: High interannual variability of sea ice thickness in the Arctic region, Nature, 425, 947–950, 2003.

Laxon, S. W., Giles, K. A., Ridout, A. L., Wingham, D. J., Willatt, R., Cullen, R., Kwok, R., Schweiger, A., Zhang, J., Haas, C., Hendricks, S., Krishfield, R., Kurtz, N., Farrell, S., and Davidson, M.: CryoSat-2 estimates of Arctic sea ice thickness and volume, Geophys. Res. Lett, 40, 732–737, doi:10.1002/grl.50193, 2013.

Legresy, B., Papa, F., Remy, F., Vinay, G., van den Bosch, M., and Zanife, O.: ENVISAT radar altimeter measurements over continental surfaces and ice caps using the ICE-2 retracking algorithm, Remote Sens. Environ., 95, 150–163, 2005.

Makynen, M. and Hallikainen, M.: Simulation of ASIRAS altimeter echoes for snow-covered first-year sea ice, IEEE Geosci. Remote S., 6, 486–490, 2009.

Maslanik, J., Fowler, C., Stroeve, J., Drobot, S., Zwally, J., Yi, D., and Emery, W.: A younger, thinner Arctic ice cover: Increased potential for rapid, extensive sea-ice loss, Geophys. Res. Lett., 34, L24501, doi:10.1029/2007GL032043, 2007.

Maslanik, J., Stroeve, J., Fowler, C., and Emery, W.: Distribution and trends in Arctic sea ice age through spring 2011, Geophys. Res. Lett., 38, L13502, doi:10.1029/2011GL047735, 2011.

Onstott, R., Grenfell, T., Matzler, C., Luther, C., and Svendsen, E.: Evolution of microwave sea ice signatures during early summer and midsummer in the marginal ice zone, J. Geophys. Res., 92, 6825–6835, 1987.

Peacock, N. and Laxon, S.: Sea surface height determination in the Arctic Ocean from ERS altimetry, J. Geophys. Res, 109, C07001, doi:10.1029/2001JC001026, 2004.

Polyakov, I., Kwok, R., and Walsh, J.: Recent changes of arctic multiyear sea-ice coverage and the likely causes, B. Am. Meteorol. Soc., 92, 145–151, doi:10.1175/BAMS-D-11-00070.1, 2011.

Raney, R.: The delay/Doppler radar altimeter, IEEE T. Geosci. Remote, 36, 1578–1588, 1998.

Ridout, A., Ivanova, N., Tonboe, R., Laxon, S., Timms, G., and Kern, S. Kloster, K.: Algorithm Theoretical Basis Document SICCI-ATBDv0-07-12 Version 1.1./03Sept 2012, Tech. rep., ESA, 2012.

Röhrs, J. and Kaleschke, L.: An algorithm to detect sea ice leads by using AMSR-E passive microwave imagery, The Cryosphere, 6, 343–352, doi:10.5194/tc-6-343-2012, 2012.

Rothrock, D., Yu, Y., and Maykut, G.: Thinning of the Arctic sea-ice cover, Geophys. Res. Lett., 26, 3469–3472, 1999.

Rothrock, D., Percival, D., and Wensnahan, M.: The decline in arctic sea-ice thickness: Separating the spatial, annual, and interannual variability in a quarter century of submarine data, J. Geophys. Res., 113, C05003, doi:10.1029/2007JC004252, 2008.

Stroeve, J., Serreze, M., Holland, M., Kay, J., Malanik, J., and Barrett, A.: The Arctic's rapidly shrinking sea ice cover: a research synthesis, Climatic Change, 110, 1005–1027, 2012.

Ulander, L.: Interpretation of Seasat radar-altimeter data over sea ice using near-simultaneous SAR imagery, Int. J. Remote Sens., 8, 1679–1686, 1987.

Warren, S., Rigor, I., Untersteiner, N., Radionov, V., Bryazgin, N., Aleksandrov, Y., and Colony, R.: Snow depth on Arctic sea ice, J. Climate, 12, 1814–1829, 1999.

Willat, R., Laxon, S., Giles, K.and Cullen, R., Haas, C., and Helm, V.: Ku-band radar penetration into snow cover on Arctic sea ice using airborne data, Ann. Glaciol., 52, 197–205, 2011.

Wingham, D.; Francis, C.; Baker, S.; Bouzinac, C.; Brockley, D.; Cullen, R.; de Chateau-Thierry, P.; Laxon, S.; Mallow, U.; Mavrocordatos, C. and others:CryoSat: A mission to determine the fluctuations in Earth's land and marine ice fields, Adv. Space Res., Elsevier, 37, 841–871, 2006.

Zakhvatkina, N.: Classification of Sea Ice Types in ENVISAT Synthetic Aperture Radar Images, IEEE ASSP Magazine, 2012.

Paper III

Analysis of CryoSats radar altimeter waveforms over different Arctic sea ice regimes

Zygmuntowska, M. and Khvorostovsky, K.

manuscript to be submitted, 2014

III

Analysis of CryoSat's radar altimeter waveforms over different Arctic sea ice regimes

Marta Zygmuntowska, Kirill Khvorostovsky

Nansen Environmental and Remote Sensing Center

Abstract

Satellite altimetry has been used to derive information about sea ice thickness in the Arctic already for several decades. As part of the algorithms applied the shape of the radar signal is used to identify leads, the open water between ice floes. Analysis of airborne altimeter data reveals that the waveform shape can additionally be used to identify different sea ice types. In this study we analyze signal waveforms from ESA's CryoSat-2 satellite, to test the possibility of sea ice classification based on radar altimeter waveforms on an Arctic wide scale. We define six parameters to account for the difference in the shape of the radar waveforms obtained over First- and Multi-Year-Ice and find significant differences for several of these parameters. The Pulse Peakiness, Stack Standard Deviation and Leading Edge Width show the largest difference. These waveform parameters can thus be used to classify First- and Multi-Year-Ice over large areas of the Arctic Ocean. However, analyzing the spatial distribution we find some discrepancies compared to other retrievals of sea ice type. CryoSat waveform parameters have values typical for Multi-Year-Ice over large areas classified as First-Year-Ice. These areas are co-located with strong gradients in drift speed, indicating, that the radar signal is mainly sensitive to surface roughness. Potentially this information could be used to reduce biases in the freeboard retrievals and to improve estimates of sea ice thickness.

I. Introduction

Decline in sea ice thickness is one of the main indicators of climate change (Stocker et al., 2013), and radar altimetry is one of the main tools used to measure this decline (Giles et al., 2008; Laxon et al., 2013). Consequently in the last decade, many attempts have been made to improve the algorithms used to derive sea ice thickness from radar altimetry. Algorithms have to consider how to detect open water between ice floes (Laxon, 1994; Laxon et al., 2013; Armitage and Davidson, 2013), retrieve freeboard, and then convert these measurements into an estimate of sea ice thickness (Wadhams et al., 1992; Giles et al., 2007). Sea ice thickness is then assumed to be around 10 times the sea ice freeboard (Wadhams et al., 1992). With the launch of CryoSat-2 in 2010 (Drinkwater et al., 2004) a new generation of radar altimeters is utilized (Wingham et al., 2006). The synthetic aperture approach used for the SAR/Interferometric Radar ALtimeter (SIRAL) onboard CryoSat-2 enhances the resolution along track (Raney, 1998; Wingham et al., 2006) and thus provides more detailed information about the surface properties.

Already for conventional altimeters it is well known, that the returned signal waveforms are sensitive to surface properties (Fetterer, 1992). Over oceans it is thus a well established method to use the shape and strength of the signal to retrieve information about wave height or wind speed (e.g. Fedor and Brown, 1982; Gourrion et al., 2002). Over sea ice it has been found that the strongest return comes from leads (Fetterer, 1992) and the signal strength is decreasing from flat to ridged sea ice (Fedor et al., 1989). Ulander (1987) and Drinkwater (1991) additionally found a correlation between radar backscatter from SAR images and the radar altimeter signal strength and width. Even though these results indicated that a distinction between ice types is possible based on the shape of the radar altimeter signal waveform, the methods have not been developed any further for a long time . Just recently, encouraged by the new capabilities resulting from the SAR technique used for CryoSat-2, Zygmuntowska et al. (2013a) presented a classification method based on measurements from an airborne synthetic aperture radar altimeter. The method is able to distinguish between First- and Multi-Year-Ice, using only the characteristics of the radar altimeter signal waveforms. They were able to classify 80% of the waveforms correctly using a combination of different waveform characteristics and applying a Bayesian based approach.

For satellite-based altimeters there is so far no algorithm that is able to distinguish between different sea ice types. The current algorithms for Envisat and CryoSat-2 use the waveform shape only to distinguish between leads and ice floes (Laxon et al., 2003, 2013; Hendricks et al., 2013). However, for accurate retrieval of sea ice thickness from freeboard data, information about sea ice type is needed. The type of sea ice determines the snow and ice properties which can highly influence the estimates of sea ice thickness (Alexandrov et al., 2010; Zygmuntowska et al., 2013b). In this study we therefore analyze waveform characteristics over different sea ice regimes, to check if sea ice classification is possible based on signal waveforms from CryoSat's radar altimeter SIRAL. We analyze one winter of CryoSat-2 data over the entire Arctic ocean, and compare waveform characteristics to other retrievals of sea ice type.

This paper is outlined as follows: First we describe the CryoSat-2 data, and the parameters used to characterize the shape of the radar signal waveforms. We compare our results to other satellite retrievals of sea ice type and discuss the ice properties which influence the different instruments used. Finally we discuss the potential applications and limitations of this work.

II. Data

In this section we describe the radar waveform parameters analyzed over different surface regimes in the Arctic. Additionally we describe different data sets used for comparison with our results, such as other ice type retrievals, and sea ice drift.

1. CryoSat-2 waveform parameters

The primary data set in this study is from ESA's CryoSat-2 satellite. CryoSat-2 was launched in 2010 and was ESAs first satellite mission specifically designed to measure changes in the Earth's cryosphere. The satellite orbit has an inclination of 92 degrees, and a repeat cycle of 369 days. Additional sub-cycles every 30 days enable to monitor the Arctic on a regular grid on a monthly basis. CryoSat's payload instrument, the SAR/Interferometric Radar Altimeter (SIRAL), operates with center frequency of 13.575 GHz and has a receiving bandwidth of 360 MHz. After processing the footprint size is around 1700 m across track and 300 m along track. The returning echo is sampled in 128 bins each 1.563 ns resulting in a range resolution of 0.486 m.

For this study we use baseline B Level 1b (SIR_SAR_L1B) and Level 2 (SIR_SAR_L2) SAR mode data for the winter 2012/2013 (November - March). Level 1b data, containing the radar altimeter signal waveforms, can be used to retrieve quantities such as surface elevation, freeboard or thickness. Based on the waveforms in the level 1b data set we calculate the following parameters:

- *Maximum (Max)* value of the waveform power.
- *Leading Edge Width (LeW)* is obtained by fitting a cubic spline to each waveform and calculating the distance between the first bins containing a signal strength above 5% and 99% of the maximum power.
- *Trailing Edge Width (TeW)* is obtained by fitting a cubic spline to each waveform and calculating the distance between the last bins containing a signal strength above 99% and 5% of the maximum power.

Level 2 data does not yet contain information about freeboard, but contains some parameters which give information about the returned signal waveform. From the level 2 data set we analyse the following parameters:

- *Pulse Peakiness (PP)* is the ratio of the maximum power and the accumulated signal power (first defined by Laxon (1994)):

$$\mathrm{PP} = \frac{\max(\mathrm{power})}{\sum_{i=1}^{128} \mathrm{power(i)}} \tag{1}$$

- *Stack Standard Deviation (SSD)* is the standard deviation of the multi-looked waveforms used at each location.
- $Sigma_0$ is the radar backscatter coefficient.

The objective of the study is to analyze waveform characteristics over sea ice, so waveforms reflected from leads are excluded from further analysis. We identify leads using the Pulse Peakiness and the Stack Standard Deviation as done previously by Laxon et al. (2013) and Hendricks

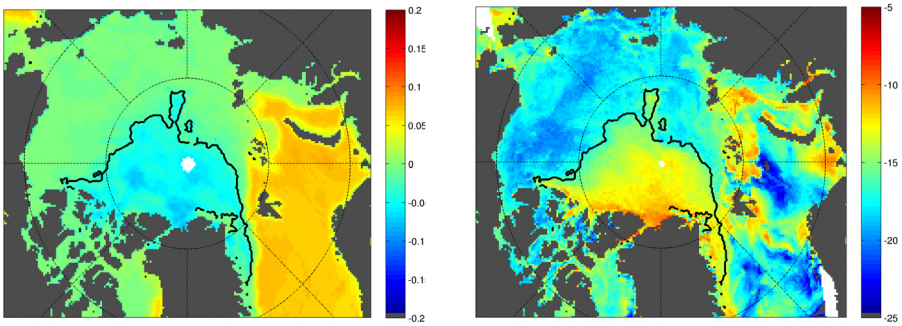

(a) *GR(19,37,V)* **(b)** *ASCAT Backscatter [dbz]*

Figure 1: *Spatial distribution of remote sensing retrievals used to identify sea ice type (December 2012). a) Gradient of vertically polarized 19 and 37 GHz brightness temperatures GR(19,37,V). b) ASCAT sigma$_0$ backscatter. Black contour line in both plots shows the border of First and Multi-Year-Ice (based on the OSI SAF retrieval) with Multi-Year-Ice north of Greenland.*

et al. (2013). Waveforms are rejected if the Pulse Peakiness is larger than 15 or the Stack Standard Deviation smaller than 4.

All parameters are averaged and gridded to a polar stereographic projection on a 25 km grid. Outliers, defined by a distance of more than 3 standard deviations from the mean, are removed to reduce noise. So far we only use data retrieved in SAR mode. Thus a data gap occurs north of Greenland in the so-called 'Wingham Box' (see https://earth.esa.int/web/guest/-/geographical-mode-mask-7107 for updated mode map). SARIn mode is originally designed for operations over ice caps and ice sheet margins but is also used for algorithm testing over this area of the Arctic ocean (e.g. Armitage and Davidson, 2013).

2. Other data

A. Sea ice type

For comparison we use the binary sea ice classification (First-Year-Ice vs. Multi-Year-Ice) available from the EUMETSAT Ocean and Sea Ice Satellite Application Facility (OSI SAF, www.osi-saf.org). Ice classes are based on SSMIS and ASCAT measurements, using a Bayesian approach. From SSMIS data the algorithm uses the gradient ratio of the 19 and 37 GHz vertically polarized channels GR(19,37,V) = (Tb37v - Tb19v) / (Tb37v + Tb19v), and from ASCAT the sigma$_0$ backscatter. The signal from the two instruments and the resulting sea ice type is visualized in Figure 1. More information about this product can be found in Eastwood (2012) and in Breivik and Eastwood (2009). In all Figures the sea ice type is given as black contour line for each respective month.

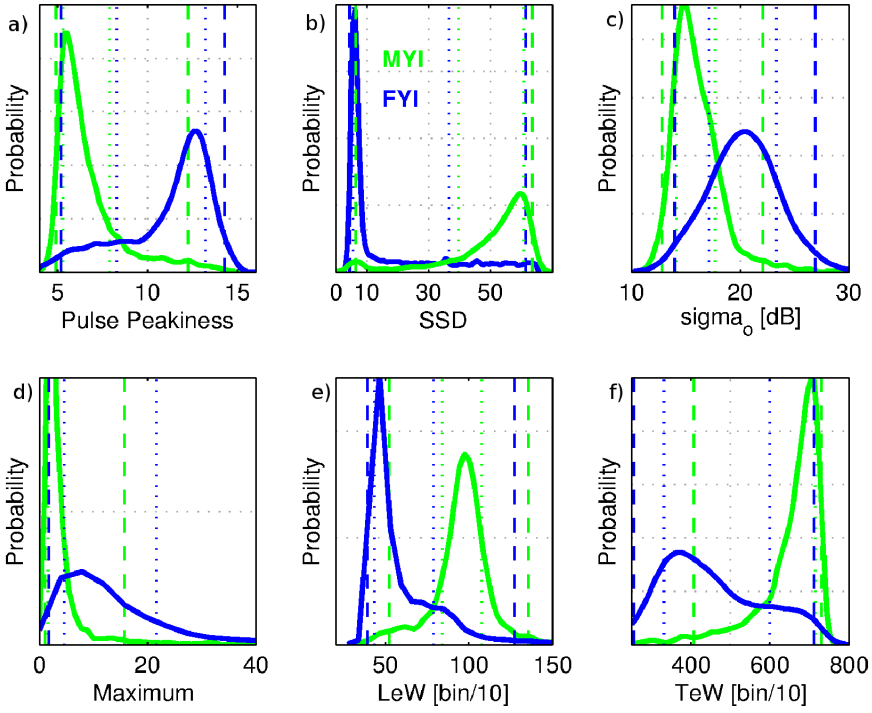

Figure 2: *Probability distribution functions (PDF) for different CryoSat-2 SIRAL parameters: a) Pulse Peakiness b) Stack Standard Deviation and c) sigma$_0$ d) Maximum e) Leading Edge Width f) Trailing Edge Width. Green lines show distributions for Multi-Year-Ice (MYI) and blue lines for First-Year-Ice (FYI). Dashed and dotted lines in all 6 figures correspond to 15.9th and 84.13th percentile and 2.3th and 97.7th percentile which are the 1st and 2nd standard deviation in a normal distribution. Distributions are smoothed for visualization with gaussian kernel functions.*

B. Sea ice drift

We use the low resolution sea ice drift product from the EUMETSAT Ocean and Sea Ice Satellite Application Facility (OSI SAF, www.osi-saf.org). It is a two day ice drift product, processed every day and provided as gridded data set on a 62 km polar stereographic grid. The multi-sensor data set is again based on data from ASCAT and SSMIS instruments, using a continuous Maximum-Cross-Correlation method for motion tracking. More information about the product can be found in Lavergne and Eastwood (2010) and Lavergne et al. (2010).

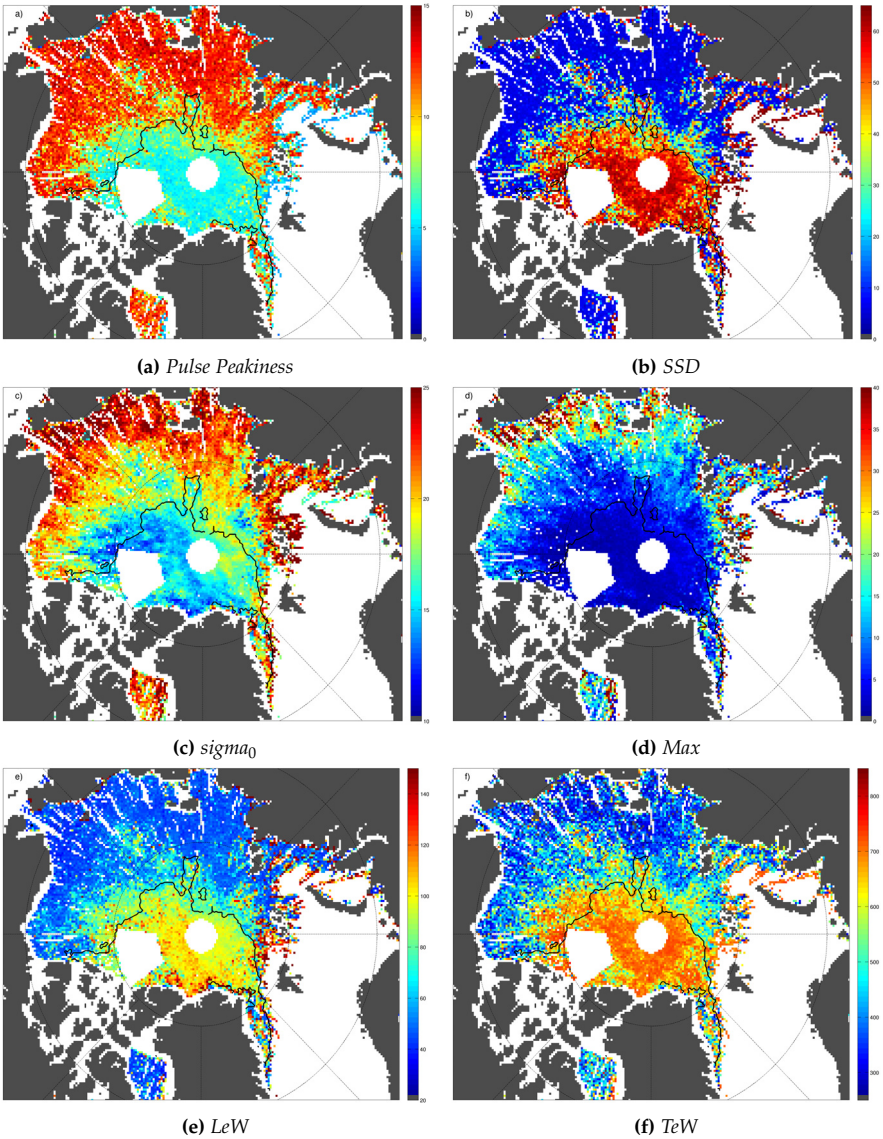

(a) *Pulse Peakiness* **(b)** *SSD*

(c) *sigma*$_0$ **(d)** *Max*

(e) *LeW* **(f)** *TeW*

Figure 3: *Spatial distribution of the different CryoSat-2 SIRAL parameters in December 2012: a) Pulse Peakiness, b) Stack Standard Deviation, c) sigma*$_0$*, d) Max), e) Leading Edge Width f) Trailing Edge Width. Black contour line shows the border of First and Multi-Year-Ice (based on the OSI SAF retrieval) with Multi-Year-Ice north of Greenland.*

III. Results

The probability distributions of the six analyzed parameters - Pulse Peakiness, Stack Standard Deviation, Simga$_0$, Maximum, Leading Edge Width and Trailing Edge Width - is shown in Figure 2. Distributions are calculated separately for First-Year-Ice and Multi-Year-Ice using the sea ice type retrieval from OSI SAF for classification. The PDFs are shown for December 2012 but results are similar for the other months.

For the Pulse Peakiness (Fig. 2 a) a clear difference can be found in the distributions from the two ice types, with waveforms reflected from First-Year-Ice having larger values of Pulse Peakiness than from Multi-Year-Ice. Also for the Stack Standard Deviation (Fig. 2 b) a clear difference in the distributions can be found, but waveforms reflected from First-Year-Ice have smaller values than from Multi-Year-Ice. For both parameters the distribution are not only different visually but also statistically: The null hypothesis, that measurements over First-Year-Ice and Multi-Year-Ice are from the same continuous distribution, can be rejected at 5% significance level (2 sided Kolmogorov-Smirnov test). The Leading and Trailing Edge width are larger from waveforms reflected from Multi-Year-Ice than First-Year-Ice, and show significantly different distributions over these two ice types (5% significance level) (Fig. 2 e & f). The distributions of backscatter sigma$_0$ are closer to each other but have a tendency towards higher values for First-Year-Ice (Fig. 2 c). The maximum of the signal waveform is larger for waveforms reflected over First-Year-Ice but the distribution from First- and Multi-Year-Ice overlap to a large extent (Fig. 2 d).

The spatial distributions of the six CryoSat-2 parameters for December 2012 are shown in Figure 3. In particular the Pulse Peakiness, Stack Standard Deviation, Leading and Trailing Edge have a similar spatial pattern. For the Pulse peakiness clearly smaller values can be found in the western part of the Arctic Ocean north of Greenland and the Canadian Archipelago, and higher values towards the southern part of the Beaufort see, the Chuckchi, Siberian and Laptev Sea. For the other three parameters Stack Standard Deviation, Leading and Trailing Edge the same pattern can be found, but higher values are observed in the western part of the Arctic Ocean. The spatial distribution of the Maximum power and the sigma$_0$ backscatter show a more blurry distributions (Fig. 3 c) & d)), with no clear borders between different surface regimes.

In Figure 3 we also show the border of Multi-Year-Ice and First-Year-Ice based on the sea ice type retrieval from OSI SAF. In the Beaufort Sea for all parameters a clear discrepancy can be found with respect to the border of the two expected sea ice types. To analyze this in more detail, Figure 4 shows the spatial distribution of the Pulse Peakiness for the months November 2012 until March 2013. While in autumn the largest discrepancy can be found in the Beaufort Sea, in February 2013 a difference mainly occurs north of Svalbard. In March, this pattern disappears, but the values of Pulse Peakiness from CryoSat-2 are lower in the swath from the North Pole to the East Siberian Sea than previously found over the First-Year-Ice in this region. For the other

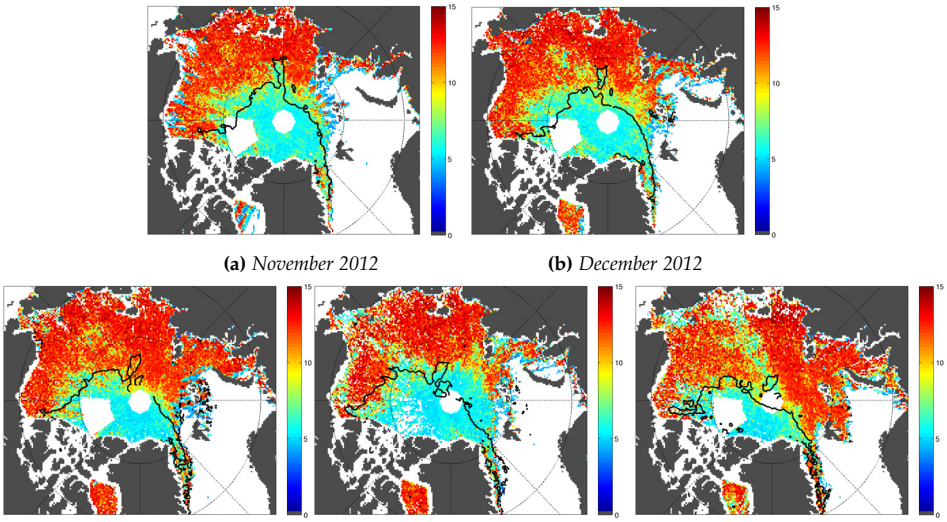

(a) *November 2012* **(b)** *December 2012*

(c) *January 2012* **(d)** *Februray 2013* **(e)** *March 2013*

Figure 4: *Spatial distribution of Pulse Peakiness for different months. Black contour line shows the border of First and Multi-Year-Ice (based on the OSI SAF retrieval) with Multi-Year-Ice north of Greenland.*

parameters we found a very similar pattern for each month (not shown).

IV. Discussion

We have analyzed different waveform characteristics from CryoSat's synthetic aperture radar altimeter SIRAL over Arctic sea ice. To be able to quantify the waveform characteristics over different surface regimes we used the following parameters: Pulse Peakiness, Stack Standard Deviation and sigma$_0$, Maximum, Leading Edge Width and Trailing Edge Width. Below we will first discuss our findings with respect to the physical and dynamical properties of sea ice and further discuss how our results can be used in future studies.

We found a statistically significant difference between the waveform parameters Pulse Peakiness and Stack Standard Deviation, Leading Edge Width and Trailing Edge Width from the waveform signal reflected from First- and Multi-Year-Ice (Figure 2). For sigma$_0$ the difference is not that distinct, but larger values can be found for waveforms coming from First-Year-Ice. For the power Maximum the distributions are even closer but smaller values are found for Multi-Year-Ice.

Our results are consistent with previous studies (Ulander, 1987; Fedor et al., 1989; Drinkwater,

1991; Fetterer, 1992) showing that the radar signal decreases and becomes wider from First- to Multi-Year-Ice. However, in their analysis of airborne synthetic aperture radar waveforms, Zygmuntowska et al. (2013a) concluded that the power Maximum and the Trailing Edge Width are the most suitable parameters to use for sea ice classification. In our study, based on the waveform shape from satellite based altimeters, we identified the Stack Standard Deviation, Leading Edge Width and Pulse Peakiness as the best parameters to distinguish between First- and Multi-Year-Ice. The power Maximum could not be confirmed as a reliable parameter for sea ice classification.

The spatial distribution generally shows a pattern that is consistent with the ice type retrieval from OSI SAF. However, we find discrepancies over large regions, which differ over the winter season (see Figure 4). In autumn the discrepancy is largest in the Beaufort Sea and in February 2013 it mainly occurs north of Svalbard. In March, this pattern disappears, but the values of Pulse Peakiness from CryoSat-2 are lower along the swath from the North Pole to the East Siberian Sea than previously found over the First-Year ice in this region.

To understand the inconsistencies found it is important to understand the physical properties of the surface that influence the sensors or algorithms. As shown in Figure 1 the sea ice type dataset from OSI SAF is driven by backscatter from ASCAT and brightness temperatures measured by SSMIS. For ASCAT a difference in sea ice types can be expected from a combination of dielectric properties of the surface and the roughness of the surface. Dielectric properties are dominated by relative proportions of ice, brine and air in the ice, as well as the shapes and spatial arrangements of brine and salt inclusions (Weeks, 2010). The roughness is driven by deformation and is thus often associated with the age of sea ice. For First-Year-Ice, the dielectric properties do not allow the signal to penetrate. Thus mainly surface scattering occurs and the returned signal is highly sensitive to surface roughness. Multi-Year-Ice in turn has survived one summer and is more porous and less saline. The signal can penetrate in the upper layer of the ice and so in addition to surface scattering, volume scattering also occurs. Brightness temperature from passive microwave measurements is defined by the physical temperature and the dielectric properties of the surface, as described above. The physical temperature is higher for thicker snow and thinner ice (Perovich and Elder, 2001) but it is hard to quantify a difference between ice types. However, the dependency of the brightness temperature on these properties varies for different frequencies, and the gradient between different frequencies can be used to derive information about the sea ice type (Steffen et al., 1992, also visualized in Fig. 1a) for December 2012).

The radar signal waveform from CryoSat-2 is dependent on the properties of sea ice and snow (Fetterer, 1992). The snow properties that most influence the signal are snow depth and snow density. Besides the snow fall that determines the snow depth, the atmospheric temperature influences the snow via two different mechanism: 1) Warm temperatures lead to melt and higher density of snow, 2) Extreme warm events, that caused surface melting followed by a freeze up, result in internal ice layers within the snow. The first effect changes the speed with which the

signal penetrates through the layer, and the second changes the scattering surface. Both effects have been found to influence significantly the scattering surface and the shape of the radar waveform (Tonboe et al., 2006), in particular the Leading Edge. From the sea ice itself no volume scattering occurs and mainly the surface roughness influences the returned signal waveform. The dependency of backscatter on surface roughness has previously been found to be non-linear and highly variable (Fetterer, 1992).

Due to a lack of data we are neither able to perform a detailed analysis of the snow properties nor the actual surface roughness. To get more information about the snow properties, we analyzed surface temperatures from ERA-Interim. We checked if the monthly mean of the daily maximum temperature and the monthly maximum vary for the regions where discrepancies occur, but did not find any anomalies (not shown). To get information about sea ice roughness we analyzed sea ice drift in different months. We found areas with values more typical for Multi-Year-Ice for the CryoSat-2 parameters over regions with First-Year-Ice, where a strong gradient in the ice drift can be observed (see Fig. 5 for examples and Figure and 4). This indicates that the waveform characteristics from CryoSat's radar altimeter SIRAL are dependent on the surface 'type' but hereby meaning flat and deformed ice. As long as this surface properties go together with sea ice age (meaning First-Year-Ice and Multi- Year-Ice) a classification of these two ice types is possible. In some areas, however, this is not the case, which makes a definite classification with respect to sea ice age difficult.

The discrepancy found in the Beaufort Sea region in November occurs only over a small area. One could thus argue that the binary classification from OSI SAF provides a simplified picture, while CryoSat-2 parameters provide more details about the fraction of each ice type. However, the underlying, non-binary retrievals used for the classification from OSI SAF (see Figure 1 for December) do not resemble the spatial distribution of the CryoSat-2 parameters. Thus we can refute the hypothesis that discrepancies are only due to the difference between a binary and fractional classification (compare Figure 4 b and Figure 1 for December).

A limitation of our work is the lack of a reliable information about the sea ice type. The large scale pattern is the same for the two instruments OSI SAF is based on, but on a basin or sub basin scale quite a few discrepancies can be found. Another widely used sea ice type retrieval is the ice age retrieval developed by Fowler et al. (2004) and Maslanik et al. (2011). The retrieval is based on a completely different approach, identifying sea ice with radiometers (AVHRR, SSMIS) and tracking its movement on a weekly basis. As the method is so different, it could provide an independent evaluation. However, the distribution of sea ice age neither corresponds to ASCAT backscatter, nor the gradient from the brightness temperatures nor the different surface regimes found from CryoSat-2 parameters (comparison not shown). As the data set is based on a Lagrangian tracking approach, errors in sea ice drift may accumulate and potentially introduce large errors in the final retrieval. In our analysis we therefore use the well validated retrieval from OSI SAF as ground

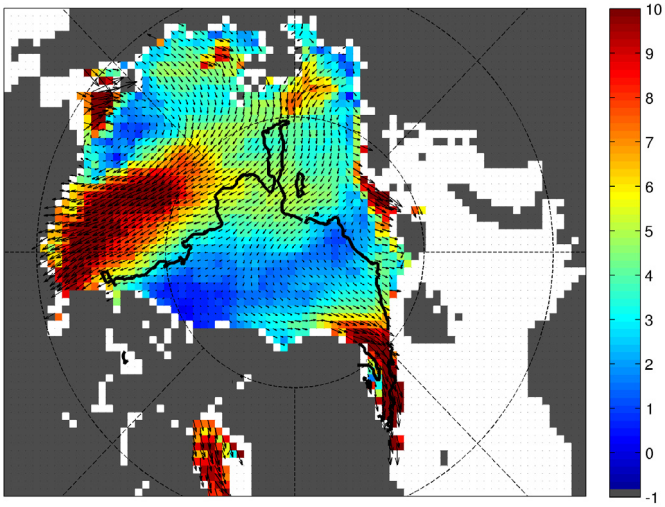

(a) *November 2012*

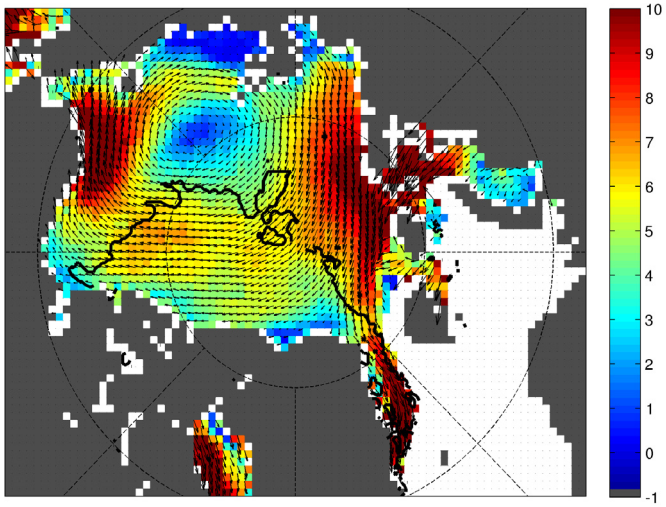

(b) *February 2013*

Figure 5: *Sea ice drift from OSI SAF for a) November, 20th 2012 and b) February, 10th 2013. Colour gives the drift 'speed' in km per two days. Black contour line in both plots shows the border of First and Multi-Year-Ice (based on the OSI SAF retrieval) with Multi-Year-Ice north of Greenland. Areas of First-Year-Ice (from OSI SAF classification) with high gradients in drift velocity correspond to areas with values typical for Multi-Year-ice for the CryoSat-2 parameters shown in Figure 3. In a) this is particularly the case in the Beaufort Sea and in b) north of Svalbard.*

truth, and believe, that, on large scales, this is currently the best available product.

Our findings regarding sea ice type and roughness could be evaluated using SAR images. SAR images are limited in their coverage over the Arctic ocean, but when available, they can provide information about ice type and deformation. The SAR signal is highly sensitive to the dielectric properties of sea ice, as described for ASCAT, and deformation and roughness are well captured due to its high resolution.

The information about surface roughness based on the radar signal waveform is a valuable piece of information in itself. Above all, it can be used to reduce biases in current freeboard retrievals. The current 'operational' algorithms (Ridout et al., 2013; Hendricks et al., 2013; Laxon et al., 2013) use fixed thresholds to derive the position along the leading edge corresponding to the surface elevation. The use of a fixed threshold, however, can generate a positive bias for the freeboard retrieval, since with increasing roughness, the selected threshold should be closer to the waveform peak. This theoretical argument has been recently confirmed by Kurtz et al. (2014). They found a positive bias of almost 45 cm using freeboard estimates from a fixed threshold re-tracker comapared to estimates based on an empirical model for re-tracking that takes into account for surface roughness, incidence angle and backscatter coefficient. Hendricks et al. (2013) found indeed a positive bias comparing freeboard estimates based on a fixed re-tracker to in-situ data. They argued that this bias results from an incomplete penetration of the radar signal into the snow pack. More work is required to test these two assumptions and to improve the final freeboard estimates.

V. Conclusions

We analyze the distributions of the parameters describing the shape of altimeter waveform from CryoSat-2 and find them to be significantly different over Arctic First and Multi-Year-Ice. The parameters with the largest difference between the two ice types are the Pulse Peakiness, Stack Standard Deviation and Leading Edge Width. These waveform parameters can be used to classify First- and Multi-Year-Ice over large areas of the Arctic Ocean, but in some regions clear discrepancies occur. These regions of First-Year-Ice are co-located with areas of strong gradients in drift speed, which are associated with a high rate of deformation. We find waveform parameters typical for Multi-Year-Ice in these areas and thus conclude that the radar signal is mainly sensitive to surface roughness. The information about surface roughness from radar altimeters can potentially be used to reduce biases in the freeboard retrievals.

Acknowledgment

We would like to thank the European Space Agency for processing and providing CryoSat-2 data, the National Snow and Ice Data Center (NSIDC) for providing the brightness temperatures (used

to calculate the gradient ratio GR(19,37,V) in Figure 1a), and the Brigham Young University (BYU) for proving gridded ASCAT backscatter data. We further acknowledge the EUMETSAT Ocean and Sea Ice Satellite Application Facility for providing data for sea ice type, edge and drift.

References

Alexandrov, V., Sandven, S., Wahlin, J., and Johannessen, O. (2010). The relation between sea ice thickness and freeboard in the Arctic. *The Cryosphere*, 4:641–661.

Armitage, T. and Davidson, M. (2013). Using the Interferometric Capabilities of ESA CryoSat-2 Mission to Improve the Accuracy of Sea Ice Freeboard Retrievals. *IEEE Transactions on Geoscience and Remote Sensing*, 52(1):529–536.

Breivik, L.-A. and Eastwood, S. (2009). Upgrade of the OSI SAF Sea Ice Edge and Sea Ice Type products âĂŞ Introduction of ASCAT. Technical report, Norwegian Meteorological Institute.

Drinkwater, M. (1991). Ku-Band Airborne Radar Altimeter Observations of Marginal Sea Ice During the 1984 Marginal Ice Zone Experiment. *Journal of Geophysical Research*, 96(C3):4555–4572.

Drinkwater, M., Francis, R., Ratier, G., and Wingham, D. (2004). The European Space Agency's earth explorer mission CryoSat: measuring variability in the cryosphere. *Annals of Glaciology*, 39(1):313–320.

Eastwood, S. (2012). Ocean & Sea Ice SAF Sea Ice Product Manual–v3.8. Technical report, EUMETSAT OSI SAF.

Fedor, L. and Brown, G. (1982). Waveheight and wind speed measurements from the Seasat radar altimeter. *Journal of Geophysical Research: Oceans (1978–2012)*, 87(C5):3254–3260.

Fedor, L., Hayne, G., and Walsh, E. (1989). Ice-type classifications from airborne pulse-limited radar altimeter return waveform characteristics. In *International Geoscience and Remote Sensing Symposium, 1989. IGARSS'89. 12th Canadian Symposium on Remote Sensing., 1989*, volume 3, pages 1949–1952. IEEE.

Fetterer, F. (1992). *Microwave remote Sensing of Sea Ice*, volume 68 of *Geophysical Monograph Series*, chapter 7: Sea ice altimetry, pages 111–135. American Geophysical Union.

Fowler, C., Emery, W., and Maslanik, J. (2004). Satellite-derived evolution of Arctic sea ice age: October 1978 to March 2003. *IEEE Geoscience and Remote Sensing Letters*, 1(2):71–74.

Giles, K., Laxon, S., and Ridout, A. (2008). Circumpolar thinning of Arctic sea ice following the 2007 record ice extent minimum. *Geophysical Research Letters*, 35(22):L22502.

Giles, K., Laxon, S., Wingham, D., Wallis, D., Krabill, W., Leuschen, C., McAdoo, D., Manizade, S., and Raney, R. (2007). Combined airborne laser and radar altimeter measurements over the Fram Strait in May 2002. *Remote Sensing of Environment*, 111(2-3):182–194.

Gourrion, J., Vandemark, D., Bailey, S., Chapron, B., Gommenginger, G., Challenor, P., and Srokosz, M. (2002). A two-parameter wind speed algorithm for Ku-band altimeters. *Journal of Atmospheric and Oceanic technology*, 19(12):2030–2048.

Hendricks, S., Ricker, R., and Helm, V. (2013). AWI CryoSat-2 Sea Ice Thickness Data Product. Technical report, Alfred Wegener Institute.

Kurtz, N. T., Galin, N., and Studinger, M. (2014). An improved CryoSat-2 sea ice freeboard and thickness retrieval algorithm through the use of waveform fitting. *The Cryosphere Discussions*, 8(1):721–768.

Lavergne, T. and Eastwood, S. (2010). Low Resolution Sea Ice drift Product User's Manual –V. 1.4. Technical Report PGL LR SID - OSI 405, EUMETSAT OSI SAF.

Lavergne, T., Eastwood, S., Teffah, Z., Schyberg, H., and Breivik, L.-A. (2010). Sea ice motion from low-resolution satellite sensors: An alternative method and its validation in the Arctic. *Journal of Geophysical Research: Oceans (1978–2012)*, 115(C10).

Laxon, S. (1994). Sea ice altimeter processing scheme at the EODC. *International Journal of Remote Sensing*, 15(4):915–924.

Laxon, S., Peacock, N., and Smith, D. (2003). High interannual variability of sea ice thickness in the Arctic region. *Nature*, 425(6961):947–950.

Laxon, S. W., Giles, K. A., Ridout, A. L., Wingham, D. J., Willatt, R., Cullen, R., Kwok, R., Schweiger, A., Zhang, J., Haas, C., Hendricks, S., Krishfield, R., Kurtz, N., Farrell, S., and Davidson, M. (2013). CryoSat-2 estimates of Arctic sea ice thickness and volume. *Geophysical Research Letters*, 40(4):732–737.

Maslanik, J., Stroeve, J., Fowler, C., and Emery, W. (2011). Distribution and trends in Arctic sea ice age through spring 2011. *Geophysical Research Letters*, 38(13):L13502.

Perovich, D. K. and Elder, B. C. (2001). Temporal evolution of Arctic sea-ice temperature. *Annals of Glaciology*, 33(1):207–211.

Raney, R. (1998). The delay/Doppler radar altimeter. *IEEE Transactions on Geoscience and Remote Sensing*, 36(5):1578–1588.

Ridout, A., Ivanova, A., Tonboe, R., and E., R. (2013). D2.6: Algorithm Theoretical Basis Document (ATBDv1). Technical report, ESA; NERSC.

Steffen, K., Key, J., Cavalieri, D. J., Comiso, J., Gloersen, P., Germain, K. S., and Rubinstein, I. (1992). *Microwave Remote Sensing of Sea Ice*, volume 68 of *Geophysical Monograph Series*, chapter 10: The estimation of geophysical parameters using passive microwave algorithms, pages 201–231. American Geophysical Union.

Stocker, T. F., Dahe, Q., and Plattner, G.-K. (2013). *Climate Change 2013: The Physical Science Basis*. Intergovernmental Panel on Climate Change 2013.

Tonboe, R., Andersen, S., and Pedersen, L. (2006). Simulation of the Ku-band Radar altimeter sea ice effective scattering surface. *Geoscience and Remote Sensing Letters, IEEE*, 3(2):237–240.

Ulander, L. (1987). Interpretation of Seasat radar-altimeter data over sea ice using near-simultaneous SAR imagery. *International Journal of Remote Sensing*, 8(11):1679–1686.

Wadhams, P., Tucker III, W., Krabill, W., Swift, R., Comiso, J., and Davis, N. (1992). Relationship between sea ice freeboard and draft in the Arctic Basin, and implications for ice thickness monitoring. *Journal of geophysical research*, 97(C12):20325–20.

Weeks, W. F. (2010). *On Sea Ice*. University of Alaska Press.

Wingham, D., Francis, C., Baker, S., Bouzinac, C., Brockley, D., Cullen, R., de Chateau-Thierry, P., Laxon, S., Mallow, U., Mavrocordatos, C., et al. (2006). CryoSat: A mission to determine the fluctuations in Earth's land and marine ice fields. *Advances in Space Research*, 37(4):841–871.

Zygmuntowska, M., Khvorostovsky, K., Helm, V., and Sandven, S. (2013a). Waveform classification of airborne synthetic aperture radar altimeter over Arctic sea ice. *The Cryosphere*, 7(4):1315–1324.

Zygmuntowska, M., Rampal, P., Ivanova, N., and Smedsrud, L. (2013b). Uncertainties in Arctic sea ice thickness and volume: new estimates and implications for trends. *Cryosphere Discussions*, 7(5). Revised paper accepted for publication in TC 2014.

References

Aagaard, K and Carmack, E. (1989). The role of sea ice and other fresh water in the Arctic circulation. *Journal of Geophysical Research*, 94(C10):14485–14498. doi: 10.1029/JC094iC10p14485. 1.1

AICA. (2005), *Arctic climate impact assessment*. Cambridge University Press Cambridge. 1.1

Andersen, S, Tonboe, R, Kaleschke, L, Heygster, G, and Pedersen, L. T. (2007). Intercomparison of passive microwave sea ice concentration retrievals over the high-concentration Arctic sea ice. *Journal of Geophysical Research*, 112(C8):C08. doi: 10.1029/2006JC003543. 1.2

Armitage, T and Davidson, M. (2013). Using the Interferometric Capabilities of ESA CryoSat-2 Mission to Improve the Accuracy of Sea Ice Freeboard Retrievals. *IEEE Transactions on Geoscience and Remote Sensing*, 52(1):529–536. doi: 10.1109/TGRS.2013.2242082. 1b

Arrhenius, S. (1896). On the influence of carbonic acid in the air upon the temperature of the ground. *The London, Edinburgh, and Dublin Philosophical Magazine and Journal of Science*, 41(251):237–276. 1.1

Beaven, S, Lockhart, G, Gogineni, S, Hossetnmostafa, A, Jezek, K, Gow, A, Perovich, D, Fung, A, and Tjuatja, S. (1995). Laboratory measurements of radar backscatter from bare and snow-covered saline ice sheets. *International Journal of Remote Sensing*, 16 (5):851–876. doi: 10.1080/01431169508954448. 1.3, 2

Brucker, l and Markus, T. (2013). Arctic-Scale Assessment of Satellite PassiveMicrowave Derived Snow Depth on Sea Ice using Operation IceBridge Airborne Data. *Journal of Geophysical Research*, 118(6):2892–2905. doi: 10.1002/jgrc.20228. 3

Cavalieri, D. J, Gloersen, P, and Campbell, W. J. (1984). Determination of sea ice parameters with the Nimbus 7 SMMR. *Journal of Geophysical Research*, 89(D4): 5355–5369. doi: 10.1029/JD089iD04p05355. 1.2

Cavalieri, D. J, Gloersen, P, Parkinson, C. L, Comiso, J. C, and Zwally, H. J. (1997). Observed hemispheric asymmetry in global sea ice changes. *Science*, 278(5340):1104–1106. doi: 10.1126/science.278.5340.1104. 1.1

Chapman, W. L and Walsh, J. E. (1993). Recent variations of sea ice and air temperature in high latitudes. *Bulletin of the American Meteorological Society*, 74(1):33–47. doi: 10.1175/1520-0477(1993)074<0033:RVOSIA>2.0.CO;2. 1.1

Colony, R and Thorndike, A. (1984). An estimate of the mean field of Arctic sea ice motion. *Journal of Geophysical Research*, 89(C6):10623–10629. 1.2

Comiso, J. C, Parkinson, C. L, Gersten, R, and Stock, L. (2007). Accelerated decline in the Arctic sea ice cover. *Geophys.Res.Lett.*, 34:L01703. doi: 10.1029/2007GL031972. 1.2

Connor, L. N, Farrell, S. L, McAdoo, D. C, Krabill, W. B, and Manizade, S. (2013). Validating icesat over thick sea ice in the northern canada basin. *IEEE Transactions on Geoscience and Remote Sensing*, 51:2188–2200. doi: 10.1109/TGRS.2012.2211603. 1a

Curry, J. A, Schramm, J. L, and Ebert, E. E. (1995). Sea ice-albedo climate feedback mechanism. *Journal of Climate*, 8(2):240–247. doi: 10.1175/1520-0442(1995)008<0240:SIACFM>2.0.CO;2. 1.1

Eastwood, S. Ocean & Sea Ice SAF Sea Ice Product Manual–v3.8. Technical report, EUMETSAT OSI SAF, (2012). 2

Farrell, S, Markus, T, Kwok, R, and Connor, L. (2011). Laser altimetry sampling strategies over sea ice. *Annals of Glaciology*, 52(57):69–76. 1a

Fedor, L and Brown, G. (1982). Waveheight and wind speed measurements from the Seasat radar altimeter. *Journal of Geophysical Research: Oceans (1978–2012)*, 87 (C5):3254–3260. doi: 10.1029/JC087iC05p03254. 1.4

Fetterer, F. *Microwave remote Sensing of Sea Ice*, vol. 68 of *Geophysical Monograph Series*, chapter 7: Sea ice altimetry, p. 111–135. American Geophysical Union, (1992). 1.3

Fowler, C, Emery, W, and Maslanik, J. (2004). Satellite-derived evolution of Arctic sea ice age: October 1978 to March 2003. *IEEE Geoscience and Remote Sensing Letters*, 1(2):71–74. doi: 10.1109/LGRS.2004.824741. 1.1, 1.2, 3.1, 2

Francis, J and Vavrus, S. (2012). Evidence linking arctic amplification to extreme weather in mid-latitudes. *Geophysical Research Letters*, 39(6):L06801. doi: 10.1029/2012GL051000. 1.1

Giles, K, Laxon, S, Wingham, D, Wallis, D, Krabill, W, Leuschen, C, McAdoo, D, Manizade, S, and Raney, R. (2007). Combined airborne laser and radar altimeter measurements over the Fram Strait in May 2002. *Remote Sensing of Environment*, 111(2-3):182–194. doi: 10.1016/j.rse.2007.02.037. 1.4

Giles, K, Laxon, S, and Ridout, A. (2008). Circumpolar thinning of Arctic sea ice following the 2007 record ice extent minimum. *Geophysical Research Letters*, 35(22): L22502. doi: 10.1029/2008GL035710. 1.2

Gourrion, J, Vandemark, D, Bailey, S, Chapron, B, Gommenginger, G, Challenor, P, and Srokosz, M. (2002). A two-parameter wind speed algorithm for Ku-band altimeters. *Journal of Atmospheric and Oceanic technology*, 19(12):2030–2048. 1.4

Haas, C, Gerland, S, Eicken, H, and Miller, H. (1997). Comparison of sea-ice thickness measurements under summer and winter conditions in the Arctic using a small electromagnetic induction device. *Geophysics*, 62(3):749–757. doi: 10.1190/1.1444184. 1b

Haas, C, Hendricks, S, Eicken, H, and Herber, A. (2010). Synoptic airborne thickness surveys reveal state of Arctic sea ice cover. *Geophysical Research Letters*, 37(09): L09501. doi: 10.1029/2010GL042652. 1

Haas, C, Goff, H, Audrain, S, Perovich, D, and Haapala, J. (2011). Comparison of seasonal sea-ice thickness change in the Transpolar Drift observed by local ice mass-balance observations and floe-scale EM surveys. *Annals of Glaciology*, 52(57):97–102. doi: 10.3189/172756411795931778. 1b

Hendricks, S, Ricker, R, and Helm, V. AWI CryoSat-2 Sea Ice Thickness Data Product. Technical report, Alfred Wegener Institute, (2013). 1.2, 1.3, 1.4, 1.4, 2, 1b

Holland, M, Bitz, C, and Tremblay, B. (2006). Future abrupt reductions in the summer Arctic sea ice. *Geophysical Research Letters*, 33(5):L23503. doi: 10.1029/2006GL028024. 1.2

Ivanova, N, Johannessen, O. M, Pedersen, L. T, and Tonboe, R. T. (2014). Retrieval of arctic sea ice parameters by satellite passive microwave sensors: A comparison between eleven sea ice algorithms. *IEEE Transactions on Geoscience and Remote Sensing*, 52. doi: 10.1109/TGRS.2014.2310136. 1.1, 1.2

Johannessen, O, Bengtsson, L, Miles, M, Kuzmina, S, Semenov, V, Alekseev, G, Nagurnyi, A, Zakharov, V, Bobylev, L, Pettersson, L, et al. (2004). Arctic climate change: observed and modelled temperature and sea-ice variability. *Tellus A*, 56(4): 328–341. doi: 10.1111/j.1600-0870.2004.00060.x. 1.1

Kattsov, V. M, Ryabinin, V. E, Overland, J. E, Serreze, M. C, Visbeck, M, Walsh, J. E, Meier, W, and Zhang, X. (2010). Arctic sea-ice change: a grand challenge of climate science. *Journal of Glaciology*, 56(200):1115–1121. doi: 10.3189/002214311796406176. 1.2

Kay, J and L'Ecuyer, T. (07()2013). Observational constraints on arctic ocean clouds and radiative fluxes during the early 21st century. *Journal of Geophysical Research*, 118:7219–7236. doi: 10.1002/jgrd.50489. 1.1

Kay, J and Gettelman, A. (2009). Cloud influence on and response to seasonal Arctic sea ice loss. *Journal of Geophysical Research*, 114(D18):D18204. doi: 10.1029/2009JD011773. 1.1

Kay, J, L'Ecuyer, T, Gettelman, A, and Stephens, C, G O'Dell. (2008). The contribution of cloud and radiation anomalies to the 2007 Arctic sea ice extent minimum. *Geophysical Research Letters*, 35(8):L08503. doi: 10.1029/2008GL033451. 1.1

Kay, J. E, Holland, M. M, and Jahn, A. (2011). Inter-annual to multi-decadal arctic sea ice extent trends in a warming world. *Geophysical Research Letters*, 38(15):L15708. doi: 10.1029/2011GL048008. 1.1, 1.2

Kurtz, N. T, Farrell, S. L, Studinger, M, Galin, N, Harbeck, J. P, Lindsay, R, Onana, V. D, Panzer, B, and Sonntag, J. G. (2013). Sea ice thickness, freeboard, and snow depth products from operation icebridge airborne data. *The Cryosphere*, 7 (4):1035–1056. doi: 10.5194/tc-7-1035-2013. 1b

Kurtz, N. T, Galin, N, and Studinger, M. (2014). An improved CryoSat-2 sea ice freeboard and thickness retrieval algorithm through the use of waveform fitting. *The Cryosphere Discussions*, 8(1):721–768. doi: 10.5194/tcd-8-721-2014. 1.4, 1, 1b

Kurtz, N and Farrell, S. (2011b). Large-scale surveys of snow depth on arctic sea ice from operation icebridge. *Geophysical Research Letters*, 38(20):L20505. doi: 10.1029/2011GL049216. 3

Kwok, R. (2011). Satellite remote sensing of sea-ice thickness and kinematics: a review. *Journal of Glaciology*, 56(200):1129. doi: 10.3189/002214311796406167. 1.2

Kwok, R and Cunningham, G. (2008). ICESat over Arctic sea ice: Estimation of snow depth and ice thickness. *Journal of Geophysical Research*, 113(C8):C08010. doi: 10.1029/2008JC004753. 1b

Kwok, R and Untersteiner, N. (2011). The thinning of Arctic sea ice. *Physics Today*, 64 (4):36–41. 1.1, 1.3, 1.2

Kwok, R, Cunningham, G, Zwally, H, and Yi, D. (2006). ICESat over Arctic sea ice: Interpretation of altimetric and reflectivity profiles. *Journal of Geophysical Research*, 111(C6):C06006. doi: 10.1029/2005JC003175. 1.2, 1.3

Kwok, R, Cunningham, G, Zwally, H, and Yi, D. (2007). Ice, Cloud, and land Elevation Satellite (ICESat) over Arctic sea ice: Retrieval of freeboard. *J. Geophys. Res*, 112: C12013. doi: 10.1029/2006JC003978. 1.3, 1a

Kwok, R, Cunningham, G, Wensnahan, M, Rigor, I, Zwally, H, and Yi, D. (2009). Thinning and volume loss of the Arctic Ocean sea ice cover: 2003–2008. *Journal of Geophysical Research*, 114(C7):C07005. doi: 10.1029/2009JC005312. 1.1, 1.2, 1.2, 1a, 1b

Kwok, R, Spreen, G, and Pang, S. (2013). Arctic sea ice circulation and drift speed: Decadal trends and ocean currents. *Journal of Geophysical Research*, 118:2408–2425. doi: 10.1002/jgrc.20191. 1.2

Laxon, S. (1994)a. Sea ice extent mapping using the ERS-1 radar altimeter. *EARSeL Advances in Remote Sensing*, 3:112–116. 1.2, 1.3

Laxon, S. (1994)b. Sea ice altimeter processing scheme at the EODC. *International Journal of Remote Sensing*, 15(4):915–924. doi: 10.1080/01431169408954124. 1.2, 1.3, 1.4

Laxon, S, Peacock, N, and Smith, D. (2003). High interannual variability of sea ice thickness in the Arctic region. *Nature*, 425(6961):947–950. doi: 10.1038/nature02050. 1.2

Laxon, S. W, Giles, K. A, Ridout, A. L, Wingham, D. J, Willatt, R, Cullen, R, Kwok, R, Schweiger, A, Zhang, J, Haas, C, Hendricks, S, Krishfield, R, Kurtz, N, Farrell, S, and Davidson, M. (2013). CryoSat-2 estimates of Arctic sea ice thickness and volume. *Geophysical Research Letters*, 40(4):732–737. doi: 10.1002/grl.50193. 1.1, 1.2, 1.4, 1

Lenton, T. M. (2012). Arctic climate tipping points. *Ambio*, 41(1):10–22. doi: 10.1007/s13280-011-0221-x. 1.2

Liu, Y, Key, J. R, Liu, Z, Wang, X, and Vavrus, S. J. (2012). A cloudier Arctic expected with diminishing sea ice. *Geophysical Research Letters*, 39(5):L05705. doi: 10.1029/2012GL051251. 1.1

Maaß, N, Kaleschke, L, Tian-Kunze, X, and Drusch, M. (2013). Snow thickness retrieval over thick Arctic sea ice using SMOS satellite data. *The Cryosphere*, 7(4):1971–1989. doi: 10.5194/tc-7-1971-2013. 3

Manabe, S and Stouffer, R. J. (1980). Sensitivity of a global climate model to an increase of CO2 concentration in the atmosphere. *Journal of Geophysical Research*, 85(C10): 5529–5554. doi: 10.1029/JC085iC10p05529. 1.1

Markus, T and Cavalieri, D. J. (1998). Snow depth distribution over sea ice in the Southern Ocean from satellite passive microwave data. *Antarctic Research Series*, 74: 19–39. doi: 10.1029/AR074p0019. 3

Markus, T and Cavalieri, D. J. (2008). AMSR-E Algorithm Theoretical Basis Document: Sea Ice Products. *NASA: Greenbelt, MD, USA*. 3

Maslanik, J, Stroeve, J, Fowler, C, and Emery, W. (2011). Distribution and trends in Arctic sea ice age through spring 2011. *Geophysical Research Letters*, 38(13):L13502. doi: 10.1029/2011GL047735. 1.1, 1.2

Maslanik, J, Fowler, C, Stroeve, J, Drobot, S, Zwally, J, Yi, D, and Emery, W. (2007). A younger, thinner Arctic ice cover: Increased potential for rapid, extensive sea-ice loss. *Geophysical Research Letters*, 34(24):L24501. doi: 10.1029/2007GL032043. 1.1, 1.2

Maslowski, W, Clement Kinney, J, Higgins, M, and Roberts, A. (2012). The future of Arctic sea ice. *Annual Review of Earth and Planetary Sciences*, 40:625–654. doi: 10.1146/annurev-earth-042711-105345. 1.2

Massonnet, F, Fichefet, T, Goosse, H, Bitz, C. M, Philippon-Berthier, G, Holland, M. M, and Barriat, P.-Y. (2012). Constraining projections of summer Arctic sea ice. *The Cryosphere*, 6(4):1383–1394. doi: 10.5194/tc-6-1383-2012. 1.2

McPhee, M, Proshutinsky, A, Morison, J, Steele, M, and Alkire, M. (2009). Rapid change in freshwater content of the Arctic Ocean. *Geophysical Research Letters*, 36 (10):L10602. doi: 10.1029/2009GL037525. 1.1

McPhee, M. G, Stanton, T. P, Morison, J. H, and Martinson, D. G. (1998). Freshening of the upper ocean in the Arctic: Is perennial sea ice disappearing? *Geophysical Research Letters*, 25(10):1729–1732. doi: 10.1029/98GL00933. 1.1

Meier, W and Notz, D. A note on the accuracy and reliability of satellite-derived passive microwave estimates of sea-ice extent, CliC Arctic Sea Ice Working Group Consensus Document. In *The 2nd meeting of the CliC Arctic Sea Ice Working Group (ASWG2)*, (2010). 1.2

Meier, W. N, Stroeve, J, Barrett, A, and Fetterer, F. (2012). A simple approach to providing a more consistent Arctic sea ice extent time series from the 1950s to present. *The Cryosphere*, 6(6):1359–1368. doi: 10.5194/tc-6-1359-2012. 1.2

Morison, J, Kwok, R, Peralta-Ferriz, C, Alkire, M, Rigor, I, Andersen, R, and Steele, M. (2012). Changing Arctic Ocean freshwater pathways. *Nature*, 481(7379):66–70. doi: 10.1038/nature10705. 1.1

Nansen, F. (1897), *Fram over Polhavet: Den norske polarfærd 1893–1896 Vol I & II*. Aschehoug. 1.2

Notz, D. (2009). The future of ice sheets and sea ice: Between reversible retreat and unstoppable loss. *Proceedings of the National Academy of Sciences*, 106(49):20590–20595. doi: 10.1073/pnas.0902356106. 1.2

Ogi, M and Wallace, J. (2007). Summer minimum Arctic sea ice extent and the associated summer atmospheric circulation. *Geophysical Research Letters*, 34(12):3247–3259. doi: 10.1029/2007GL029897. 1.1

Olason, E and Notz, D. (2014). Drivers of variability in Arctic sea-ice drift speed. *in review for Journal of Geophysical Research*. 1.2

Outten, S and Esau, I. (2012). A link between Arctic sea ice and recent cooling trends over Eurasia. *Climatic Change*, 110(3-4):1069–1075. doi: 10.1007/s10584-011-0334-z. 1.1

Overland, J. E and Wang, M. (2013). When will the summer Arctic be nearly sea ice free? *Geophysical Research Letters*, 40:2097–2101. doi: 10.1002/grl.50316. 1.2

Overland, J and Wang, M. (2010). Large-scale atmospheric circulation changes are associated with the recent loss of Arctic sea ice. *Tellus A*, 62(1):1–9. doi: 10.1111/j.1600-0870.2009.00421.x. 1.1

Parkinson, C. L and Comiso, J. C. (2013). On the 2012 record low arctic sea ice cover: Combined impact of preconditioning and an august storm. *Geophysical Research Letters*, p. 1–6. doi: 10.1002/grl.50349. 1.1

Perovich, D. K, Light, B, Eicken, H, Jones, K. F, Runciman, K, and Nghiem, S. V. (2007). Increasing solar heating of the Arctic Ocean and adjacent seas 1979–2005: Attribution and role in the ice-albedo feedback. *Geophys.Res.Lett.*, 34:L19505. doi: 10.1029/2007GL031480. 1.1

Pithan, F and Mauritsen, T. (2014). Arctic amplification dominated by temperature feedbacks in contemporary climate models. *Nature Geoscience*. doi: 10.1038/NGEO2071. 1.1

Polyakov, I, Kwok, R, and Walsh, J. (2011). Recent Changes of Arctic Multiyear Sea-Ice Coverage and the Likely Causes. *Bulletin of the American Meteorological Society*, 93: 145–151. doi: 10.1175/BAMS-D-11-00070.1. 1.1

Rampal, P, Weiss, J, and Marsan, D. (2009). Positive trend in the mean speed and deformation rate of Arctic sea ice, 1979–2007. *Journal of Geophysical Research*, 114 (C5):C05013. doi: 10.1029/2008JC005066. 1.2

Raney, R. (1998). The delay/Doppler radar altimeter. *IEEE Transactions on Geoscience and Remote Sensing*, 36(5):1578–1588. 1.6, 1.7, 1.4

Renner, A, Hendricks, S, Gerland, S, Beckers, J. M, Haas, C, and Krumpen, T. (2013). Large-scale ice thickness distribution of first-year sea ice in spring and summer north of Svalbard. *Annals of Glaciology*, 54(62). doi: 10.3189/2013AoG62A146. 1b

Richter-Menge, J. A and Farrell, S. L. (2013). Arctic sea ice conditions in spring 2009–2013 prior to melt. *Geophysical Research Letters*, 40(22):5888–5893. doi: 10.1002/2013GL058011. 1

Schweiger, A, Lindsay, R, Zhang, J, Steele, M, Stern, H, and Kwok, R. (2011). Uncertainty in modeled Arctic sea ice volume. *Journal of Geophysical Research*, 116: C00D06. doi: 10.1029/2011JC007084. 1.2

Schweiger, A, Zhang, J, Lindsay, R, and Steele, M. (2008). Did unusually sunny skies help drive the record sea ice minimum of 2007? *Geophysical Research Letters*, 35(10): L10503. doi: 10.1029/2008GL033463. 1.1

Screen, J and Simmonds, I. (2010). The central role of diminishing sea ice in recent Arctic temperature amplification. *Nature*, 464(7293):1334–1337. doi: 10.1038/nature09051. 1.1

Serreze, M. C and Barry, R. G. (2005), *The Arctic climate system*, vol. 22. Cambridge University Press. 1.1

Serreze, M. (2011). Climate change: Rethinking the sea-ice tipping point. *Nature*, 471 (7336):47–48. doi: 10.1038/471047a. 1.2

Serreze, M and Francis, J. (2006). The arctic amplification debate. *Climate Change*, 76: 241–264. doi: 10.1007/s10584-005-9017-y. 1.1

Serreze, M, Holland, M, and Stroeve, J. (2007). Perspectives on the Arctic's shrinking sea-ice cover. *Science*, 16(5818):1533–1536. doi: 10.1126/science.1139426. 1.1

Shimada, K, Komashida, T, Itoh, M, Nishino, S, Carmack, E, McLaughlin, F, Zimmermann, S, and Proshutinsky, A. (2006). Pacific Ocean inflow: Influence on catastrophic reduction of sea ice-covered cover in the Arctic Ocean. *Geophysical Research Letters*, 33:L08605. doi: 10.1029/2005GL025624. 1.1

Spreen, G, Kwok, R, and Menemenlis, D. (2011). Trends in Arctic sea ice drift and role of wind forcing: 1992–2009. *Geophysical Research Letters*, 38(19):L19501. doi: 10.1029/2011GL048970. 1.2

Stephenson, S. R, Smith, L. C, Brigham, L. W, and Agnew, J. A. (2013). Projected 21st-century changes to Arctic marine access. *Climatic Change*, 118:885–899. doi: 10.1007/s10584-012-0685-0. 1.1

Stern, D. I and Kaufmann, R. K. (2014). Anthropogenic and natural causes of climate change. *Climatic Change*, 122(1-2):257–269. doi: 10.1007/s10584-013-1007-x. 1.1

Stocker, T. F, Dahe, Q, and Plattner, G.-K. (2013), *Climate Change 2013: The Physical Science Basis*. Intergovernmental Panel on Climate Change 2013. 1.1

Stroeve, J, Holland, M, Meier, W, Scambos, T, and M.Serreze. (2007). Arctic sea ice decline: Faster than forecast. *Geophysical Research Letters*, 34:L09501. doi: 10.1029/2007GL029703. 1.2

Stroeve, J, Kattsov, V, Barrett, A, Serreze, M, Pavlova, T, Holland, M, and Meier, W. (2012)a. Trends in Arctic sea ice extent from CMIP5, CMIP3 and observations. *Geophysical Research Letters*, 39(16):L16502. doi: 10.1029/2012GL052676. 1.2

Stroeve, J, Serreze, M, Holland, M, Kay, J, Malanik, J, and Barrett, A. (2012)b. The arctic's rapidly shrinking sea ice cover: a research synthesis. *Climatic Change*, 1005–1027:1–23. doi: 10.1007/s10584-011-0101-1. 1.1

Tietsche, S, Notz, D, Jungclaus, J, and Marotzke, J. (2011). Recovery mechanisms of Arctic summer sea ice. *Geophysical Research Letters*, 38(2):L02707. doi: 10.1029/2010GL045698. 1.2

Tilling, R, Ridout, A, Wingham, J, Shepherd, A, Haas, C, Farrell, S, Schweiger, A, Zhang, J, Giles, K, and Laxon, S. Trends in arctic sea ice volume 2010-2013 from cryosat-2. In *AGU*, (2013). 3

Tiuri, M. E, Sihvola, A. H, Nyfors, E, and Hallikaiken, M. (1984). The complex dielectric constant of snow at microwave frequencies. *IEEE Journal of Oceanic Engineering*, 9 (5):377–382. doi: 10.1109/JOE.1984.1145645. 1

Tonboe, R, Pedersen, L, and Haas, C. (2010). Simulation of the CryoSat-2 satellite radar altimeter sea ice thickness retrieval uncertainty. *Canadian Journal of Remote Sensing*, 36(1):55–67. 1b

Vavrus, S. J, Holland, M. M, Jahn, A, Bailey, D. A, and Blazey, B. A. (2012). Twenty-First-Century Arctic Climate Change in CCSM4. *Journal of Climate*, 25(8):2696–2710. doi: 10.1175/JCLI-D-11-00220.1. 1.2

Vihma, T. (2014). Effects of arctic sea ice decline on weather and climate: A review. *Surveys in Geophysics*, p. 1–40. doi: 0.1007/s10712-014-9284-0. 1.1

Vihma, T, Tisler, P, and Uotila, P. (2012). Atmospheric forcing on the drift of arctic sea ice in 1989–2009. *Geophysical Research Letters*, 39(2):L02501. doi: 10.1029/2011GL050118. 1.2

Wadhams, P. (2012). Arctic ice cover, ice thickness and tipping points. *Ambio*, 41(1): 23–33. doi: 10.1007/s13280-011-0222-9. 1.2

Wang, M and Overland, J. (2009). A sea ice free summer Arctic within 30 years. *Geophysical Research Letters*, 36(7):L07502. doi: 10.1029/2009GL037820. 1.2

Warren, S, Rigor, I, Untersteiner, N, Radionov, V, Bryazgin, N, Aleksandrov, Y, and Colony, R. (1999). Snow depth on Arctic sea ice. *Journal of Climate*, 12:1814–1829. doi: 10.1175/1520-0442(1999)012<1814:SDOASI>2.0.CO;2. 3

Weeks, W. F and Ackley, S. F. (1986), *The growth, structure, and properties of sea ice*. Springer. 1.2

Willat, R, Laxon, S, Giles, K, Cullen, R, Haas, C, and Helm, V. (2011). Ku-band radar penetration into snow cover on Arctic sea ice using airborne data. *Annals of Glaciology*, 52(57):197–205. doi: 10.3189/172756411795931589. 2

Wingham, D, Francis, C, Baker, S, Bouzinac, C, Brockley, D, Cullen, R, de Chateau-Thierry, P, Laxon, S, Mallow, U, Mavrocordatos, C, et al. (2006). CryoSat: A mission to determine the fluctuations in Earth's land and marine ice fields. *Advances in Space Research*, 37(4):841–871. doi: 10.1016/j.asr.2005.07.027. 1.4

Wood, K. R and Overland, J. E. (2006). Climate Lessons from the First International Polar Year. *Bulletin of the American Meteorological Society*, 87(12):1685–1697. doi: 10.1175/BAMS-87-12-1685. 1.2

Yi, D, Zwally, H, and Robbins, J. (2011). ICESat observations of seasonal and interannual variations of sea-ice freeboard and estimated thickness in the Weddell Sea, Antarctica (2003-2009). *Annals of Glaciology*, 52(57):43–51. doi: 10.3189/172756411795931480. 1a

Zwally, H, Schutz, B, Abdalati, W, Abshire, J, Bentley, C, Brenner, A, Bufton, J, Dezio, J, Hancock, D, Harding, D, Herring, T, Minster, B, Quinn, K, Palm, S, Spinhirne, J, and R., T. (2002). ICESat's laser measurements of polar ice, atmosphere, ocean, and land. *Journal of Geodynamics*, 34(3-4):405–445. doi: 10.1016/S0264-3707(02)00042-X. 1.2, 1.3

Zygmuntowska, M, Mauritsen, T, Quaas, J, and Kaleschke, L. (2012). Arctic Clouds and Surface Radiation - a critical comparison of satellite retrievals and the ERA-Interim reanalysis. *Atmospheric Chemistry and Physics*, 12:6667–6677. doi: 10.5194/acp-12-6667-2012. 1.1